FINAL COURSE ASSIGNMENT

THEORETICAL AND EXPERIMENTAL CONTRIBUTIONS FOR MODELING WIRELESS CHANNELS

CONTRIBUIÇÕES TEÓRICAS E EXPERIMENTAIS PARA MODELAGEM DE CANAIS SEM FIO

Letícia Moreira Valle

Brasília, December 2017

UNIVERSITY OF BRASÍLIA
TECHNOLOGY COLLEGE
DEPARTMENT OF ELECTRICAL ENGINEERING

UNIVERSITY OF BRASÍLIA
TECHNOLOGY COLLEGE

FINAL COURSE ASSIGNMENT

THEORETICAL AND EXPERIMENTAL CONTRIBUTIONS FOR MODELING WIRELESS CHANNELS

CONTRIBUIÇÕES TEÓRICAS E EXPERIMENTAIS PARA MODELAGEM DE CANAIS SEM FIO

Letícia Moreira Valle

Final course assignment submitted to the Department of Electrical Engineering in partial fulfillment of the requirements for the degree of Network Communication Engineer

Examination Board

Prof. Ugo Silva Dias, Dr., EnE/UnB _____
Supervisor

Prof. Georges D. Amvame Nze, Dr., EnE/UnB _____
Faculty examiner

Prof. Leonardo R.A.X. Menezes, Dr., EnE/UnB _____
Faculty examiner

Acknowledgments

First of all, I would like to express my gratitude to all the teaching team of the University of Brasilia and ENSEIRB-MATMECA for having assured the theoretical part of it.
I would like to thanks equally my supervisor Professor Ugo Dias for all his patience and motivation throughout this work and for guiding and supporting me over the undergraduate course. Your advices not only helped me grow professionally but also personally.
Furthermore, I also thank my friends and classmates who have always been present for the past six years, making me smile and relax during times of difficulty. I would especially like to thank my friends Bruna Maria and Lucas Lobão for their support and companionship, always encouraging me.
Lastly and most importantly, I would like to thank God for giving me the strength, knowledge, ability and opportunity to perform this work and my parents Francisco and Valeria Valle and my brother Fernando Valle for the invaluable love and support they have given me throughout my life.

Letícia Moreira Valle

RESUMO

Este trabalho de conclusão de curso visa agregar contribuições teóricas e experimentais para a modelagem de redes sem fio à partir de quatro projetos realizados durante um estágio supervisionado entre a Universidade de Brasília e a escola francesa de engenharia ENSEIRB-MATMECA durante o ano de 2017. Todos os projetos desse trabalho giram em torno do tema "desafios atuais nas comunicações sem fio" e tem como objetivo a apresentação de tais desafios através de uma breve introdução teórica seguida da realização de simulações, análises estatísticas ou medições em campo. O primeiro projeto propõem um estudo teórico e a validação experimental da distribuição de desvanecimento α-μ/Γ generalizada, usada nesse trabalho para caracterizar ambientes realistas que experimentam desvanecimento composto. Ainda no escopo de análises estatísticas, o segundo projeto propõe uma caracterização da qualidade do sinal celular à partir de dados de potência medidos usando um aplicativo Android de analise de qualidade de redes móveis. As análises estatísticas realizadas poderão auxiliar operadoras de telefonia móvel à parametrizar suas redes e contribuir para o melhoramento da cobertura celular no pais. Em seguida, o terceiro projeto desenvolvido nesse trabalho de conclusão de curso propõe estudos práticos e teóricos de interferência entre os sistema LTE 700MHz e TV digital em Brasília na região da Asa Norte, um tema recente de grande importância dada a desconexão da TV analógica no Brasil até 2018. Por fim, o quarto projeto, realizado em parceria com a Agência Nacional de Telecomunicações (ANATEL) propõe contribuições para o desenvolvimento de um simulador de rede IMT para uso em estudos de compartilhamento e compatibilidade proposto para ajudar na identificação de novas faixas de frequência para o IMT-2020. Os projetos propostos nesse trabalho focam na caracterização e modelagem de canais sem fio à partir do levantamento de estatísticas de primeira ordem, na análise de qualidade das redes celulares no país com base nas informações sobre a cobertura celular experimentada pelos usuários de telefonia móvel e na análise da interferência entre sistemas à partir de estudos entre o LTE e a TV digital e da busca de novas possíveis frequências para o 5G. A realização do estágio supervisionado e desse trabalho de conclusão de curso é um requerimento oficial para a obtenção do título de "Engenheiro diplomado do Instituto politécnico de Bordeaux, especialidade Engenharia eletrônica" pela ENSEIRB-MATMECA e para a obtenção do titulo de "Engenheiro de redes de comunicação" pela Universidade de Brasília.

Palavras-chave: Canal sem fio, desvanecimento, análises estatísticas do canal, qualidade do sinal celular, sistemas LTE 700MHz, TV digital, relação de proteção, IMT-2020

ABSTRACT

This final course assignment aims to add theoretical and experimental contributions to the modeling of wireless networks from four different projects carried out over an supervised internship held between the University of Brasília and the french school of engineering ENSEIRB-MATMECA during the year of 2017. All projects revolve around the central theme "current challenges in wireless communications" and aims to present such challenges through a brief theoretical introduction followed by simulations, statistical analyzes or field measurements. The first project proposes a theoretical study and the experimental investigation of the α-μ/Γ generalized fading distribution, used in this work to characterize realistic environments that experience composite fading. A second project, also based on statistical analysis, proposes a characterization of the mobile phone signal quality from power data measured using an Android application of mobile network quality analysis. Statistical analyzes can help mobile operators to parameterize their network and contribute to the improvement of cellular coverage in the country. Next, the third project developed in the internship proposes practical and theoretical studies of interference between the LTE 700MHz system and digital TV in Brasília in the region of Asa Norte, a recent topic of great importance given the analogue TV disconnection in Brazil until 2018. Finally, the fourth project, carried out in partnership with the National Telecommunications Agency (ANATEL), proposes contributions for the development of an IMT network simulator for use in sharing and compatibility studies to help in the identification of new frequency bands for the IMT-2020. The projects proposed in this work focus on the characterization and modeling of wireless channels from first order statistics, on the analysis of the quality of cellular networks in the country based on the information collected from the App about the network coverage experienced by final users and on the analysis of interference between systems based on studies between LTE and digital TV and on the search for new possible frequencies for 5G. The realization of the supervised internship was an official requirement to obtain the title of "Licensed Engineer of the Polytechnic Institute of Bordeaux, specialized in Electronic Engineering" by ENSEIRB-MATMECA and to obtain the title of "Network Communications Engineer" by the University of Brasília.

Keywords: Wireless channel, fading, statistical analysis of the channel, mobile signal quality, LTE 700MHz systems, digital TV, protection ratio, IMT-2020

TABLE OF CONTENTS

LIST OF FIGURES

LIST OF TABLES

LIST OF SYMBOLS

Latin Symbols

d	*Distance*
f	Frequency
T	Temperature
$E(\cdot)$	*Expectation operator*
r	*Random variable that refers to the signal envelope*
$f_x(r)$	*PDF of x distribution*
$I_n(\cdot)$	*Modified Bessel function of first kind and nth order*
K	*Ratio of the power in the LOS component to the power in the other (non-LOS) multipath components*
m	*Nakagami fading parameter related to the number of multipath clusters*
$\hat{r}$	*RMS envelope value*
$G_{t,r}$	Transmission/Reception antenna gain
N_0	Sea-level surface refractivity
ΔN	Average radio-refractive

Greek Symbols

Ω	*Average power*
σ	*Standard deviation*
σ^2	*Variance*
ρ	*Random variable that refers to the normalized envelope of the signal*
λ	*Wave-length*
$\gamma(\cdot)$	*Path loss exponent*
$\Gamma(\cdot)$	*Gamma function*
α	*Related to the non-linearity of the environment*
μ	*Number of multipath clusters*
κ	*Ratio between the total power of the dominant components and the total power of the scattered waves*
ε	*Mean error deviation*

Acronyms

dB	*Decibel*
dBi	*Gain of an antenna system relative to an isotropic radiator*
dBm	*Gain in decibel in relation to 1 miliwatt*
LOS	*Line Of Sight*
NLOS	*Non Line Of Sight*
PDF	*Probability density function*
CDF	*Cumulative density function*
UHF	*Ultra High Frequency*
VHF	*Very High Frequency*
LNA	*Low Noise Amplifier*
ISDB-T	*Integrated Services Digital Broadcasting Terrestrial*
LTE	*Long term evolution*
WiMAX	*Worldwide Interoperability for Microwave Access*
MIMO	*Multiple input multiple output*
CDMA	*Code division multiple access*
FDD	*Frequency Division Duplex*
TDD	*Time Division Duplex*
OFDM	*Orthogonal Frequency Division Multiplexing*
SC-FDMA	*Single Carrier Frequency Division Multiple Acess*
VoLTE	*Voice over LTE*
ERB	*Radio Base Station*
eNodeB	*Envolved Node B*
UE	*User Equipment*
E-UTRAN	*Evolved UMTS Terrestrial Radio Access Network*
EPC	*The Evolved Packet Core*
MME	*Mobility Management Entity*
SGW	*Serving Gateway*
HSS	*Home Subscriber Server*
PCRF	*Policy Control and Charging Rules Function*
PCEF	*Policy Control Enforcement Function*
DTV	*Digital television*
CPE	*Customer Premises Equipment*
ACLR	*Adjacent Channel Leakage Ratio*
PR	*Protection Ratio*
SNR	*Signal to Noise Ratio*
RF	*Radio frequency*

2G	*Second generation cellular technology*
3G	*Third generation cellular technology*
4G	*Fourth generation cellular technology*
5G	*Fifth generation cellular technology*
ITU	*International Telecommunications Union*
IMT	*International Mobile Telecommunications*
ANATEL	*National Telecommunications Agency*
3GPP	*Third Generation Partnership Project*
ETSI	*European Telecommunications Standards Institute*
IEEE	*Institute of Electrical and Electronics Engineers*
AWGN	*Additive white Gaussian noise*
GSM	*Global system for mobile communications*
UMTS	*Universal Mobile Telecommunication System*
AMPS	*Advanced Mobile System*
EDGE	*Enhanced Data rates for GSM Evolution*
WRC	*World Radiocommunication Conference*

1 INTRODUCTION

Wireless communication is one of the fastest growing segments of the communications industry, capturing more and more the industry's attention for its variety of applications. As a consequence, wireless systems have experienced exponential growth over the last decade and become a critical business tool and part of everyday life in most of developed countries [1]. However, the numerous services offered by Telecom companies along with the wide variety of applications of these services require increasingly robust wireless networks with higher transmission rates, availability and reliability.

To meet this accelerated growth and supplies the needs of these new intelligent networks, several challenges must be faced. With the increase of the amount of wireless devices in the same environment, it is of great significance to develop tools that can characterize and model the wireless channel and the future wireless networks in realistic environments. In addition, despite the need for experimental tests, it is not always possible to get everything together in a test setup for practical experiments, which makes simulators a great tool to help characterize and model the wireless environment. Moreover, another major challenge today in wireless communications is the interference between different systems, which become more important with the increasing use of multiple services in the same frequency range. Ideally, even after developed, tested and validated, wireless systems need to be frequently analyzed for interference that they suffer or may cause in other systems.

Aiming to cooperate with the development of solutions for the challenges created by the rapid growth in the wireless segment, this end of course project presents some contributions for modeling wireless channel from different projects that covers design, modeling and simulation of wireless systems.

1.1 GOALS

Each of the projects presented in this work have different goals, although they all revolve around the same common theme.

The first project proposes the study and experimental investigation of the generalized $\alpha-\mu/\Gamma$ composite distribution that characterizes environments that suffers the joint presence of slow and fast fading. The proposed distribution, besides being obtained in a closed formula and being very flexible, characterizes real environments that experience composite fading, such as those characterized by the slow movement of pedestrians and cars.

The second project presents a crowdsourcing system developed to measure cellular networks parameters through user's smartphones, using an application based on Android Operating System and that acts as a tool for measurement and statistical analysis of measured data. Due to the difficulty and financial cost of mapping cellular networks, the proposed system aims to be an online and transparent tool for users and mobile carriers in order to help not only the customer to choose their service provider, but also to provide useful analyzes to mobile carriers that may contribute to the improvement of cellular coverage in the different regions of Brazil.

The third project proposes a practical and theoretical interference study between the 700MHz LTE system and digital TV in Brasilia, a recent topic of great importance given the disconnection of the analog TV in Brazil until 2018. In this project, practical tests were carried out at the University of Brasilia and simulations were performed using the software CelPlanner in order to verify the protection ratio values obtained and compare this results with the minimum values required for the proper functioning of the services.

Finally, still in the subject of system interference, the fourth project is a contribution in the development of an IMT network simulator for use in sharing and compatibility studies proposed to produce technical data to support the position of the Brazilian Administration regarding the identification of new frequency bands for the IMT-2020. This simulator has been developed by the National Telecommunications Agency (ANATEL) in partnership with the Department of Electrical Engineering of the University of Brasilia, UnB. The contribution of this work in this project is based on the implementation of path loss models and propagation mechanisms used in the analysis of interference between systems.

1.1.1 Specific goals

- To implement the theoretical model of the α-μ/Γ Generalized distribution in the software Wolfram Mathematica;
- Isolate the Fast Fading + Shadowing composite fading for each set of empirical data and to find the corresponding first order statistics;
- Perform the experimental investigation of the generalized α-μ/Γ Generalized model with the empirical data at 700 MHz, 1.8 GHz and 5 GHz;
- Perform measurement campaigns with the signal's measurement application in order to obtain the necessary samples;
- Perform a statistical analysis of fading and channel characterization in order to generate interesting information to users and services providers;
- Practical study of interference between the LTE 700 MHz and the ISDB-T system in the laboratory;

- Simulation of coverage prediction of LTE 700 MHz and Digital TV systems on the neighborhood of Asa Norte, Brasilia, using the software CelPlan;
- Analysis of the protection ratios found in the practical tests, simulations and on the ANATEL base report of the subject;
- To implement the path loss models and propagation mechanisms used in the interference analysis between systems in the SHARC simulator using Python;
- Use the SHARC simulator to conduct a sharing study between IMT-2020 and the fixed satellite operating in the 27-27.5 GHz frequency range.

1.2 WORK ORGANIZATION

From the next chapters, this report is divided into five main parts.

Chapters 2 to 5 discuss each of the projects performed, presenting for each of them a theoretical foundation of wireless communications concepts that are important for the understanding and realization of the project, the methodology, implementation, results and a conclusion. Since this end of course work presents more than one project, the division of the projects by chapter was a direct and effective way to separate the projects and present them in a more organized way.

Finally, Chapter 6 contains the general conclusion and future perspectives based on the subjects that are outside the scope of this work.

2 THE $\alpha - \mu/\Gamma$ GENERALIZED COMPOSITE DISTRIBUTION: THEORY AND EXPERIMENTAL INVESTIGATION

In the trajectory between transmitter and receiver, besides the loss of propagation, the signal can be blocked by physical obstructions - the shadowing - and suffer multiple reflections, scattering and diffractions - multipath. Consequently, the amplitude and phase of the signal arriving at the receiver exhibit random fluctuations, varying according to the propagation environment where users are immersed, characterizing the phenomena of fading. Such fluctuations deteriorate the performance of the communication and can be modeled by signal fading distributions.

Large scale fading of the wireless channel are caused by the phenomenon of shadowing, which is widely modeled by the Lognormal distribution. Besides, in small scale in which multipath situations occur, several distributions are widely accepted for modeling fading, such as Rayleigh, Rice, Nakagami-m, Weibull and others. Although the latest distributions consider constant signal power environments, there are environments, such as those who are characterized by slow movement of pedestrians and cars, where the signal strength may not be constant, but rather random. In these cases, the resulting fading is given by the combination of shadowing and multipath.

For such situations of composite fading, several distributions that well describes the statistics of the mobile radio signal has been suggested in the literature. One of the most popular distributions, the Rayleigh-Lognormal distribution, which is a composition between the Rayleigh fast fading model and the Lognormal shadowing, has a drawback that considerably complicates the application of this distribution: the Rayleigh-Lognormal distribution has no closed formula. Trying to resolve this issue, Abdi proposes the use of the Gamma function [2] in place of the Lognormal distributions in order of modeling shadowing.

In this context, this work proposes the use of the composite distribution α-μ/Γ Generalized, in which the distribution α-μ [3], which has two degrees of freedom and therefore is more general and flexible than the Rayleigh distribution, is suggested to provide a more realistic analysis of signal and multipath propagation, and the generalized Gamma distribution [4] , a generalization of the form suggested by Liouville's extension to Dirichlet's integral formula, is suggested to model the shadowing. Thus, this work introduces field trials studies in the frequencies of 700 MHz, 1800 MHz and 5000 MHz and the experimental investigation of the data collected in the field with the theoretical models obtained from the composite distribution suggested.

2.1 THE MOBILE RADIO CHANNEL

The wireless radio channel poses a severe challenge as a medium for reliable high-speed communication due to its stochastic nature that penalizes the signal during the path between the transmitter and receiver. As a result, the amplitude and phase of the signal arriving at the receiver exhibits random fluctuations, characterizing the phenomena of fading. Such fluctuations deteriorate communication performance and can be caused by dissipation of the power radiated by the transmitter, by the multipath phenomenon related to Doppler effect or by obstacles between the transmitter and receiver that attenuate signal power through absorption, reflection, scattering, and diffraction. Thus, due to its nature, radio channel modeling is not an easy task, requiring theoretical studies and statistical data for its characterization.

Regarding the architecture of a general communication system, it is primarily composed by a transmitter, a receiver and a communication channel which is figuratively coupled to a noise source that can be represented by the composition of an additive noise and a multiplicative noise as shown in the Figures 2.1 and 2.2.

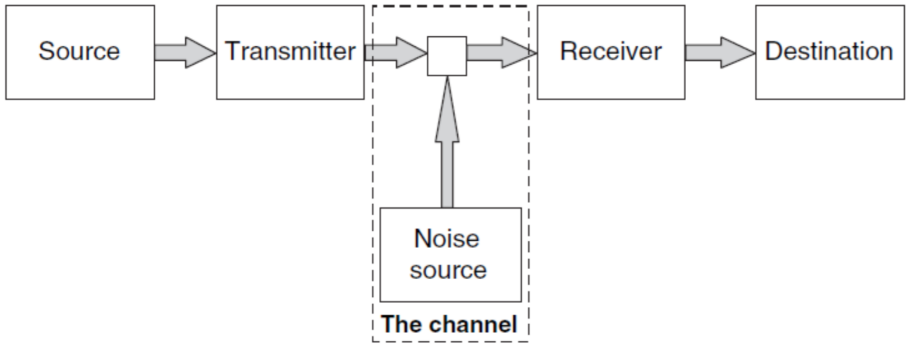

Figure 2.1: Generic communication system architecture [5].

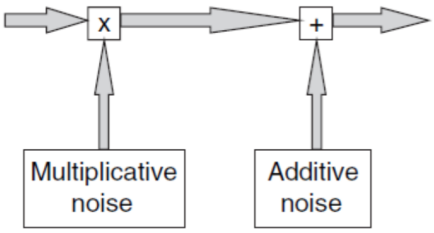

Figure 2.2: Types of noise in the communication channel [5].

The additive noise is generally represented by the Additive white Gaussian noise (AWGN) and the multiplicative, and more harmful noise, arises from various processes encountered by transmitted waves on their way between the transmitter and the receiver antenna. This processes, also known as propagation mechanisms, are listed below.

- Scattering: Objects are smaller than the wavelength of the propagation wave - e.g. foliage, street signs, lamp posts;
- Diffraction: The path between transmitter and receiver is obstructed by a surface (or object) with sharp irregular edges - e.g., edges like roofs and tops of hills;
- Refraction: A change in the direction of wave propagation due to a change in its transmission medium - e.g., atmospheric layers and some materials;
- Reflection: Propagation wave impinges on an object which is large when compared to a wavelength - e.g., the surface of the Earth, buildings, walls, etc;
- Absorption: The signal is absorbed by materials - e.g. walls, trees and the atmosphere.

Also, the multiplicative noise is conventional subdivided in the cannel into three types of fading: path loss, shadowing (or slow fading) and fast fading (or multipath fading) which appears as time-varying processes between the antennas [6], as shown in Figure 2.3.

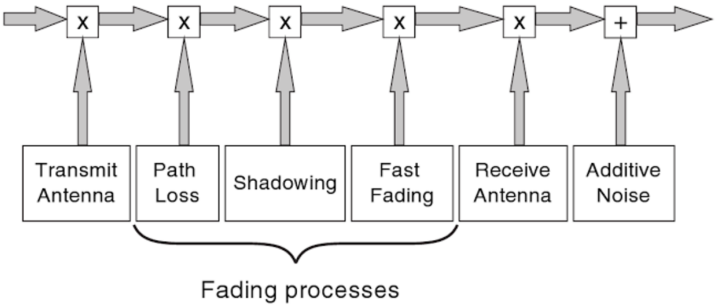

Figure 2.3: Multiplicative noise decomposition [5].

The path loss refers to the average signal intensity evaluated in terms of a large separation distance between the transmitter and the receiver. Basically, the average power of the signal decreases with the square of the distance between the transmitter and the receiver. A typical system may have variations of the order of 150 dB over its coverage area due to path loss.

Shadowing manifests itself through the fluctuation of the signal level with the distance due to the blockage caused by obstructions naturally imposed or created by man. In general, the variations of the signal due to the shadowing can reach up to 20 dB.

Fast fading, in its turns, refers to abrupt changes in signal amplitude and phase in small shifts between transmitter and receiver or at short intervals of time. The main characteristics of this fading are temporal scattering of the signal and the time-varying environment due to the relative mobility between the transmitter and the receiver. The effect of this mobility is the time-varying nature of the multipath. Variations of the signal due to fast fading phenomenal can reach up to 40 dB [6].

Figure 2.4 shows the three fading process separated from the total signal.

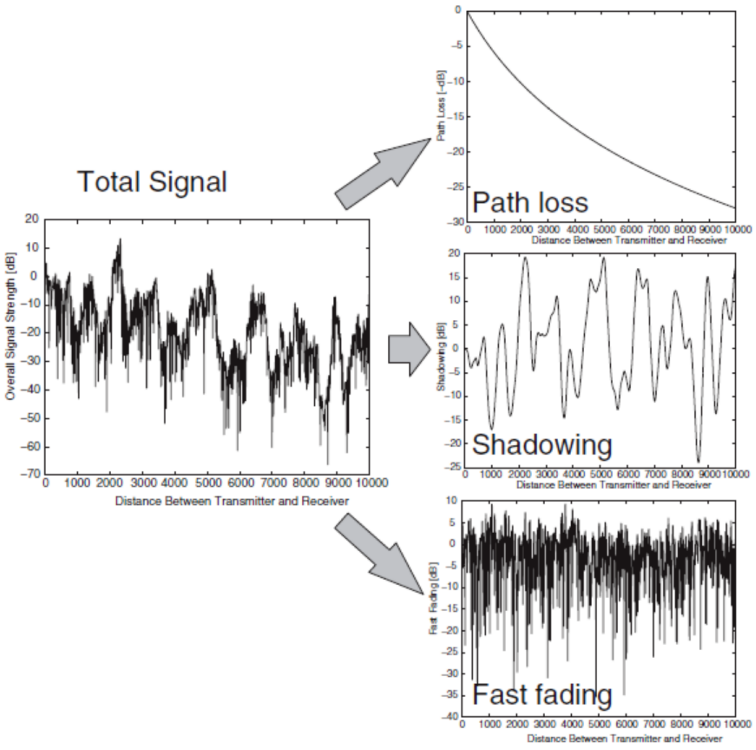

Figure 2.4: Wireless channel as a superposition of path loss, shadowing and fast fading [6].

Next sessions will treat each type of fading separately and illustrate the most used mathematical distributions for each type of fading.

2.2 LONG-TERM AND SHORT-TERM FADING DISTRIBUTIONS

As previously presented, fading processes are divided into three types: path loss, long-term fading (shadowing) and short-term fading (fast fading). In this section, a more detailed bibliographic review of each of these processes will be done.

2.2.1 Path Loss

Path loss is caused by dissipation of the power radiated by the transmitter as well as effects of the propagation channel. It is the only type of fading that is responsible for the signal power decay over distance and can be modeled by several models that describe the signal loss for point-to-point or point-to-multipoint links.

For the point-to-point case, the best known models study "ray tracing" between the transmitter and receiver and, although they need a more precise knowledge about the topological profile of the place, they offer a good signal prediction close to the real one.

For multipoint links, which is the case for cellular networks, these models, however, become rather laborious and are replaced by more generic models based on empirical measurements that provide the prediction of an average area power. This path loss models take into account specifications like geographic area, the specific frequency range and the antenna heights of the transmitting and receiving stations. Some examples of these models are, among others, the Okumura, Hata and COST 231 models and their results will be so much closer to the results obtained in the field, the more the characteristics of the environment resemble the sites used for the synthesis of the model itself.

Concerning indoor environments, it is widely known that indoor environments differs a lot from outdoor environments regarding their losses and fading. For indoor communication, the construction materials and obstacles that made up the building are high attenuators, having significant impact on path loss fading. Some studies have realized that for indoor environments attenuation per floor is greatest for the first floor that is passed through and decreases with each subsequent floor. Measurements [7] show a loss of 10-20 dB in the first floor with subsequent floor attenuation of 6-10 dB per floor for the next three floors, and then a few dB per floor for more than four floors. Another high attenuator in indoor environments are the partitions present in the environment. The partition loss (like cloth, window glass) is also relevant in indoors environments, although their values vary greatly from different researchers making it difficult to make generalizations about partition loss from a specific data set. Consequently, it is difficult to find generic models that can be accurately applied to determine empirical path loss in a specific indoor setting and approximations are made on the basis of preliminary studies.

2.2.2 Shadowing

In wireless communication, a signal transmitted will typically experience random variation due to blockage from objects in the signal path, giving rise to random variations of the mean signal level of the received power at a given distance. Such variations are caused by changes in the reflecting surfaces and objects that cause the signal to spread. The density of obstacles between the transmit and receive antennas depends very much on the physical environment. For example, outdoor environments have very little by way of obstacles while indoor environments pose many obstacles. Figure 2.5 shows a typical signal variation caused by shadowing effect.

Thus, as the location, size, dielectric properties of objects that block the signal, reflecting surfaces and scattering objects that causes the random attenuation phenomenon are generally unknown, a statistical model is necessary to characterize this attenuation and predict the received signal. Based on empirical measurements, there is a general consensus that shadowing can be modeled by a lognormal distribution for various outdoor and indoor environments [8].

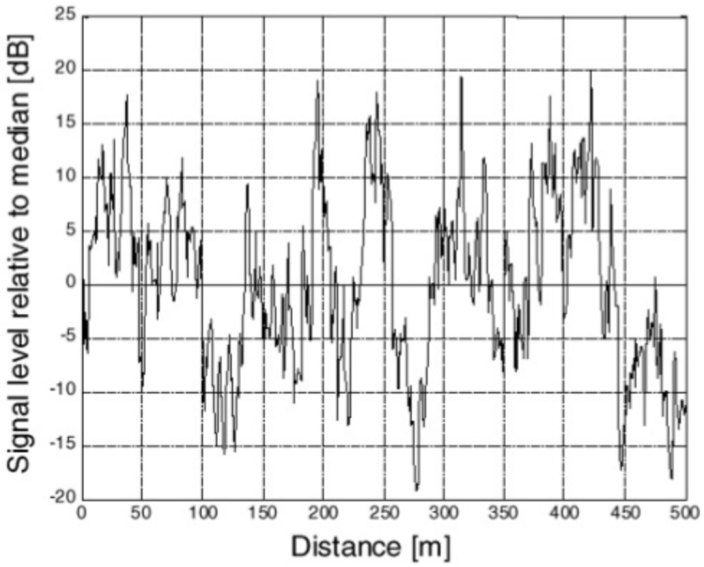

Figure 2.5: Typical shadowing variation.

In fact, while large-scale effects determine a mean power level over an area of tens to hundreds of meters, called average area power, shadowing introduces additional fluctuations of the local average power received. The term "local mean" is used to describe the mean level of signal over tens of wavelengths. An amount usually used to evaluate this local average is 40λ. The duration of a shadow fade lasts for multiple seconds or minutes, and hence occurs at a much slower time-scale compared to multipath fading [9].

2.2.2.1 Lognormal distribution

The Lognormal distribution is the most common model used for modelling the shadowing attenuation. This empirical model shows that the local average power Ω has the following probability density function (PDF) [10]

$$p_{\Omega}(r) = \frac{1}{\sqrt{2\pi\sigma^2}r} \exp[\frac{-ln^2(r/P_A)}{2\sigma^2}], \quad r > 0, \tag{2.1}$$

in which P_A is the average area power, σ is the standard deviation of shadowing and $2\sigma^2$ is the shadowing average power. In its normalized ($\rho = r/P_A$) version, the PDF equation is given by

$$p_L(\rho) = \frac{1}{\sqrt{2\pi\sigma^2}\rho} \exp[\frac{\ln^2 \rho}{2\sigma^2}], \quad \rho > 0. \tag{2.2}$$

Although the local average power is widely accepted to be lognormal, the mathematical form of the lognormal PDF is not convenient for some analytic calculations. In fact, with lognormal model of shadow fading, we cannot obtain closed-form and easy-to-use expressions for many performance measures of interest such as the average symbol error rate, diversity combining techniques, outage probability in the presence of multiple cochannel interferers, and so on.

Thus, studies of other models have been performed and the Gamma model has been highlighted by its practical results and mathematical ease of implementation.

2.2.2.2 Gamma distribution

Given the difficulties of implementing the Lognormal distribution in certain composite fading situations, the Gamma model [2] is proposed as an approximation and its PDF function of a random variable r is written as

$$f_G(r) = \frac{1}{b^a \Gamma(a)} r^{a-1} \exp(-r/b), \tag{2.3}$$

in which $\Gamma(\cdot)$ is the gamma function and the parameters a and b are estimated directly from r based on the following formulas

$$a = \frac{E[r]^2}{V[r]}, \qquad b = \frac{V[r]}{E[r]}. \tag{2.4}$$

Physically, the a parameter inversely describes the severity of the shadowing (same meaning of m-Nakagami parameter) and b/a represents the average power of the Gamma shadowing area.

2.2.2.3 Generalized Gamma distribution

The Generalized Γ distribution [4] is a 3 parameters function that has as spacial case the distributions exponential, Weibull, Lognormal and Gamma. For a signal in a long-term or shadowing fading, the probability density function (PDF) of r, $f_\Gamma(r)$, is written as

$$f_\Gamma(r) = \frac{\gamma \beta^{\lambda/\gamma} r^{\lambda-1}}{\Gamma(\lambda/\gamma)} \exp(-\beta r^\gamma), \tag{2.5}$$

in which for the limiting case, in which the gamma distribution is reduced to lognormal, the parameters are $\lambda = k^{1/2}/\sigma$, $\gamma = k^{-1/2}/\sigma$ and $\beta = k \exp(-\mu_L k^{-1/2})/\sigma$ with $k \to \infty$, in which σ is the scale parameter and μ_L is the location parameter.

The cumulative density function (CDF) of r, $F_\Gamma(r)$, is written in a closed formula as

$$F_\Gamma(r) = \frac{\gamma_l(\lambda/\gamma, \beta r^\alpha)}{\Gamma(\lambda/\gamma)}, \tag{2.6}$$

in which γ_l means the lower incomplete gamma function.

The k_{th} moment $E(R_k)$ of the Γ Generalized distribution is written as

$$E_\Gamma(R^k) = \beta^{-k/\gamma} \frac{\Gamma(\frac{\lambda+k}{\gamma})}{\Gamma(\frac{\lambda}{\gamma})}. \tag{2.7}$$

2.2.3 Fast fading

Short-term fading is characterized as fluctuations in the signal phase and amplitude caused primarily by local multipath effects, defined by rapid amplitude fluctuations of the received signal during a short period of time.

It exists two different multipath environments: the one where the path between the transmitter and the receptor is blocked causing a non line of sight (NLOS) situation where the received signal is a sum of the various multipaths components and those where the path between the transmitter and the receptor is not blocked and experiments a line of sight (LOS) situation, so that the receiver obtain a dominant signal and several other signals of lower intensity coming from multiple paths.

In a NLOS situation, the actual total power received over a much smaller distance varies considerably due to the destructive/constructive interference of multiple signals that follow multiple paths to arrive at the final destination after being reflected, diffracted or/and scattered. Figure 2.6 illustrates this process.

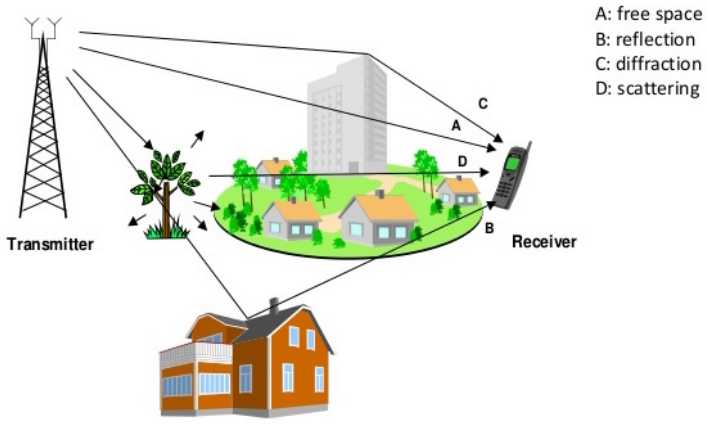

Figure 2.6: Multipath effects.

As like as in the shadowing fading, it is not possible to predict the exact value of the signal strength fluctuation caused by the multipath effect since it requires the knowledge of the position and electromagnetic characteristics of each received wave. Thus, a statistical analysis is again necessary, taking into account the different LOS and NLOS environments. As consequence, short-term fading in wireless channels has been described using several models. These include simple models such as Rayleight and Rice as well as complex models such as k-μ and $\alpha-\mu$. The main difference among these models is the quantity of parameters necessary to completely define them and consequently the flexibility in modeling statistical characteristics of channels [11].

2.2.3.1 Rayleigh distribution

The Rayleigh distribution, named after the English Lord Rayleigh, is the simplest mathematical model used for describing multipath situations. It's used for describing NLOS environments and has a good practical approximation to the empirical data. The probability density function of Rayleigh's models is written as

$$p_R(r) = \left(\frac{2r}{\Omega}\right) \exp\left[-\frac{r^2}{\Omega}\right], \tag{2.8}$$

in which r represents the signal envelope and $2\sigma^2$ the average signal power in the multipath components. In its normalized ($\rho = r/2\sigma^2$) version, the PDF equation is given by

$$p_R(\rho) = 2\rho \exp\left[-\rho\right]. \tag{2.9}$$

Generalizing the Rayleigh distribution, it can be developed the Rice and Nakagami-m distributions, which have one degree of freedom to better describe the environment where the prediction will be made.

2.2.3.2 Rice distribution

If the channel has a fixed LOS component then the signal envelope can be shown to have a Rician distribution. The probability density function of the r envelope is given by

$$p_{Ri}(r) = \frac{2\left(K+1\right)r}{\Omega} \exp\left[-K - \frac{(K+1)r^2}{\Omega}\right] I_0\left[2\sqrt{\frac{K(K+1)}{\Omega}}r\right], \quad r \geq 0, \;\; K \geqslant 0, \;\; \Omega \geq 0, \tag{2.10}$$

in which I_n is the modified Bessel function of first kind and nth order, Ω is the average received power and K is the ratio of the power in the LOS component to the power in the other (non-LOS) multipath components. For $K = 0$ the Rice distribution reduces to the Rayleigh distribution once there is no dominant component, and for $K = \infty$ we have no fading, i.e. a channel with no multipath and only a LOS component.

The normalized PDF version ($\rho = r/\sqrt{\Omega}$) is written as

$$p_{Ri}(\rho) = 2\,(K+1)\,\rho \exp\left[-K-(K+1)\rho^2\right] I_0\left[2\sqrt{K(K+1)}\right], \quad \rho \geq 0, \;\; K \geqslant 0. \quad (2.11)$$

Furthermore, the K parameter can be estimated [12] by using the follow expression

$$K = \frac{\sqrt{1-\xi}}{1-\sqrt{1-\xi}}, \quad (2.12)$$

in which $\xi = V[\rho^2]$.

2.2.3.3 Weibull distribution

Another generalization of Rayleight distribution is the Weibull [13] model, a well used distribution for describing indoor radio channel fading. When X and Y are i.i.d. zero-mean Gaussian variables, the envelope of $R = (X_2 + Y_2)^{\frac{1}{2}}$ is Rayleigh distributed. However, if the envelope is defined as $\mathrm{R} = (X_2 + Y_2)^{\frac{1}{2}}$, the corresponding PDF is Weibull distributed and written as

$$f_W(r) = \frac{k r^{k-1}}{\Omega} \exp(-\frac{r^k}{\Omega}), \quad (2.13)$$

in which $\Omega = E(r^2)$ and k is called the shape parameter.

Its normalized envelope PDF version ($\rho = r/\sqrt{\Omega}$) is written as

$$f_W(\rho) = k\rho^{k-2} \exp(-\rho^{k-1}). \quad (2.14)$$

For k=2, Weibull distribution reduces to Rayleight distribution.

2.2.3.4 Nakagami-m distribution

Thus, a more general NLOS fading distribution was developed to better fit a variety of empirical measurements. This distribution is called the Nakagami fading distribution, and it's PDF function is given by

$$p_N(r) = \frac{2}{\Gamma[m]} \left(\frac{m}{\Omega}\right)^m r^{2m-1} \exp\left[-\frac{m}{\Omega} r^2\right], \;\; r \geq 0, \quad (2.15)$$

in which Ω is the average received power, $\Gamma[.]$ is the Gamma function and the parameter m is called the "shape factor".

The Nakagami distribution is parameterized by Ω and the fading parameter m, that is related to the number of multipath clusters and is described in Eq. 2.16. For the extremes cases in which $m = 1$ the Nakagami distribution reduces to Rayleigh fading and for $m = \infty$ there is no fading: Ω is a constant. With $0.5 < m < 1$, the Nakagami model characterizes more severe fading conditions than the Rayleigh channels and its PDF has no longer a Gaussian shape.

$$m = \frac{E^2[r^2]}{V^2[r^2]}, \quad m \geq \frac{1}{2}. \tag{2.16}$$

After the normalization $\rho = r/\sqrt{\Omega}$, we have that the Nakagami-m PDF and its m parameter are also described as

$$p_N(\rho) = \frac{2m^m}{\Gamma[m]}\rho^{2m-1}\exp[-m\rho^2], \tag{2.17}$$

$$m = \frac{1}{V^2[\rho^2]}, \quad m \geq \frac{1}{2}. \tag{2.18}$$

2.2.3.5 κ - μ distribution

As shown in previous sections, there exist a great number of distributions that well describes the statistics of the mobile radio signal. In general, it is a consensus that fading statistics of the mobile radio channel may well be characterized by the Nakagami-m distribution, but frequently it is possible to found situations in which other distributions, such as Rice and Weibull, yield better results [14]. There are even situations where no distributions seems to adequately fit experimental data, though one or another may provide a moderate fit.

In order to obtain a more general distribution with more flexibility and that could be reduced to specific cases like Rayleigh, Rice and Nakagami-m, the κ - μ [15] distributions was developed. This general fading distribution is better suited for line-of-sight applications and is characterized in terms of measurable physical parameters, named κ and μ. It considers a signal composed of clusters of multipath waves propagating in a non-homogeneous environment. Within each cluster, the phases of these waves that arrive from the different paths are random, have identical powers and have similar delay time, but each cluster has a dominant component that presents an arbitrary power. Also, each cluster has a different delay-time spreads relatively high.

For a fading signal with envelope r, the κ - μ envelope probability density function, $f_{\kappa-\mu}(r)$, is written as

$$f_{\kappa-\mu}(r) = \frac{2\mu(1+\kappa)^{\frac{\mu+1}{2}}}{\kappa^{\frac{\mu-1}{2}}\exp[\mu\kappa]\hat{r}}\left(\frac{r}{\hat{r}}\right)^{\mu}\exp\left[\mu(1+\kappa)\left(\frac{r}{\hat{r}}\right)^{2}\right]I_{\mu-1}\left[2\mu\sqrt{\kappa(1+\kappa)}\frac{r}{\hat{r}}\right], \quad r,\kappa,\mu \geq 0. \tag{2.19}$$

Similar to Rice k-parameter, the parameter κ is the ratio between the total power of the dominant components and the total power of the scattered waves. The parameter μ resembles to the m-parameter of Nakagami-m distribution and relates to the number of clusters of multipath. The κ and μ parameters can be estimated as

$$\kappa^{-1} = \frac{\sqrt{2}\left(E[\rho^4]-1\right)}{\sqrt{2E^2[\rho^4]-E[\rho^4]-E[\rho^6]}} - 2, \tag{2.20}$$

$$\mu = \frac{E^2(r^2)}{V(r^2)}\frac{1+2\kappa}{(1+\kappa)^2}, \tag{2.21}$$

in which $\rho = \frac{r}{\hat{r}}$ with $\hat{r} = \sqrt{E(R^2)}$ is its normalized envelope. Also from its normalized envelope, its is possible to obtain the κ-μ normalized probability density function $f_{\kappa-\mu}(\rho)$ as

$$f_{\kappa-\mu}(\rho) = \frac{2\mu(1+\kappa)^{\frac{\mu+1}{2}}}{\kappa^{\frac{\mu-1}{2}}\exp[\mu\kappa]}\rho^{\mu}\exp\left[\mu(1+\kappa)\rho^2\right]I_{\mu-1}\left[2\mu\sqrt{\kappa(1+\kappa)}\rho\right], \quad r,\kappa,\mu \geq 0, \tag{2.22}$$

in which the μ parameter can be estimated as

$$\mu = \frac{1}{V(\rho^2)}\frac{1+2\kappa}{(1+\kappa)^2}. \tag{2.23}$$

In the case in which $\kappa = 0$ and $\mu = 0.5$, the $\kappa-\mu$ distribution is reduced to the Nakagami-m model with $m = 0.5$, in which m is the Nakagami-m parameter. When $\kappa = 1$ and $\mu = 1$, $\kappa-\mu$ distribution coincides with the Rice distribution with $k = 1$, in which k is the Rice parameter. From the Rice distribution, by setting $\kappa \to 0$ and $\mu = 1$, the Rayleigh distribution can be obtained in an exact manner.

2.2.3.6 α - μ distribution

Differently from the $\kappa - \mu$ distribution, the α-μ [3] model, a rewritten form of the Stacy (generalized Gamma) equation [4], can be used to better represent the small-scale variation of the fading signal in a non line-of- sight (NLOS) fading condition. As its name implies, it is written in terms of two physical parameters, namely α and μ. The power parameter $\alpha > 0$ is related to the non-linearity of the environment, in which the parameter $\mu > 0$ is associated to the number of multipath clusters. For a α-μ fading signal with envelope r and an arbitrary parameter $\alpha > 0$, with $\hat{r} = \sqrt[\alpha]{E(r)^{\alpha}}$, in which $E(\cdot)$ means the expectation operator, the α-μ envelope PDF, $f_{\alpha-\mu}(r)$, is written as

$$f_{\alpha-\mu}(r) = \frac{\alpha \mu^{\mu} r^{\alpha\mu-1}}{\hat{r}^{\alpha\mu}\Gamma(\mu)} \exp(-\mu \frac{r^{\alpha}}{\hat{r}^{\alpha}}), \tag{2.24}$$

in which μ can be estimated from its envelope from the equation

$$\mu = \frac{E^2[r^{\alpha}]}{V[r^{\alpha}]}, \quad \mu \geqslant \frac{1}{2}, \tag{2.25}$$

and the cumulative density function of r, $F_{\alpha-\mu}(r)$, is written as

$$F_{\alpha-\mu}(r) = \frac{\Gamma(\mu, \mu r^{\alpha}/\hat{r}^{\alpha})}{\Gamma(\mu)}, \tag{2.26}$$

in which $\Gamma(z, y) = \int_0^y t^{z-1} \exp(-t) dt$ is the incomplete Gamma function.

For the normalized version of the equations 2.24 - 2.26, the r envelope is substituted by $\rho = r/\hat{r}$ with $\hat{r} = \sqrt[\alpha]{E[r^{\alpha}]}$.

As well as the κ-μ model, the α-μ distribution includes other traditional distributions as special cases, such as the Nakagami-m ($\alpha = 2$), Weibull ($\mu = 1$) and Rayleigh ($\alpha = 2$, $\mu = 1$).

Although all the distributions presented so far consider environments with constant signal power, there are environments, such as those characterized by the slow movement of pedestrians and cars, where the power of the signal may not be constant but rather random. In these cases, the resulting fading is given by the combination of shading with multipath. Next section make a general overview about composite fading models.

2.2.4 Composite fading models

A composite probability distribution can be created from the superposition of two or more statistical distributions. The composition of a probability density function can be deduced by overlapping two or more statistical distributions. Mathematically, this method is expressed as follows

$$p_X(x) = \int_0^\infty p_{x|y}(x|y)p_y(y)dy, \tag{2.27}$$

in which for the composition made from the slow fading with fast fading, the first term $p_{x|y}(x|y)$ represents the slow fading and the second term $p_y(y)$ represents the fast fading.

Fading models that take into account simultaneously the multipath and shadowing effects are called composite fading models. For such composite fading situations, several distributions have been suggested in the literature. One of the most well-known distributions, Rayleigh-Lognormal, also known as the Suzuki model, which is a composition between Rayleigh's slow fading and Lognormal shadowing model, has a drawback that considerably complicates the application of the distribution: Rayleigh-Lognormal distribution has no closed formula. Trying to solve this problem, Abdi [2] proposes the use of the Gamma function in place of the Lognormal to model the shadowing. Later, the generalized Gamma function, first proposed by Stacy [4], is used to modelates Shadowing since it is very flexible, has a closed formula and reduces to the Lognormal model.

In this section it will be presented a composite model that uses the generalized Gamma distribution to characterize the shadowing and the generic α-μ distribution for the characterization of the short-term fading.

2.2.4.1 α-μ/ Γ generalized distribution

The α-μ/Γ generalized is a composite function made from the composition of the α-μ distribution combined with the generalized Γ model, having the following probability density function of r_c

$$f_{\alpha-\mu/\Gamma}(r) = \frac{\alpha\mu^\mu r_c^{\alpha\mu-1}\gamma\beta^{\lambda/\gamma}}{\Gamma(\mu)\Gamma(\lambda/\gamma)} \int_0^\infty x^{\lambda-\mu-1}\exp(-\mu\frac{r^\alpha}{x} - \beta x^\gamma)dx. \tag{2.28}$$

Using standard statistical procedures, the PDF of α-μ/Γ Generalized distribution is obtained in closed-form as

$$f_{\alpha-\mu/\Gamma}(r) = \frac{\alpha\mu^\mu r_c^{\alpha\mu-1}\beta^{\mu/\gamma}}{\Gamma(\mu)\Gamma(\lambda/\gamma)} H_{0,2}^{2,0}[r_c^\alpha\mu\beta^{1/\gamma}|_{(0,1);(\frac{\lambda-\mu}{\gamma},\frac{1}{\gamma})}^{-}], \tag{2.29}$$

in which H is the Fox H-Function.

The cumulative density function of r_c, $F_P(r_c)$, of the α-μ/Γ generalized distribution is written by

$$F_{\alpha-\mu/\Gamma}(r) = \frac{\alpha\mu^{\mu} r_c^{\alpha\mu} \beta^{\mu/\gamma}}{\Gamma(\mu)\Gamma(\lambda/\gamma)} H_{1,3}^{2,1}\left[r_c^{\alpha}\mu\beta^{1/\gamma}\middle|_{(0,1);(\frac{\lambda-\mu}{\gamma},\frac{1}{\gamma}),(-\alpha\mu,\alpha)}^{(1-\alpha\mu,\alpha)}\right]. \tag{2.30}$$

The α-μ/Γ model provides accurate characterisation of the simultaneous occurrence of multipath fading and shadowing effects. This is achieved thanks to the remarkable flexibility of their parameters which render them capable of providing good fittings to experimental data associated with realistic communication scenarios. Moreover, it is interesting to note that this model includes as special cases widely known composite fading models. The α-μ distribution can be reduced to Rayleigh, Nakagami-m and Weilbull while the generalized Gamma can be reduced to the Lognormal when $\lambda = k^{1/2}/\sigma$, $\gamma = k^{-1/2}/\sigma$ and $\beta = k\exp(-\mu_L k^{-1/2})/\sigma$ with $k \to \infty$.

Using the parameters $\alpha = 2$, $\mu = 1$ and $k \to \infty$, the distribution α-μ/Γ Generalized reduces to the composite Rayleigh/Lognormal distribution. Similarly, for $\alpha = 2$ and and $k \to \infty$ the composite Nakagami-m/Lognormal case is obtained and for $\mu = 1$ and $k \to \infty$ the composite Weibull/Lognormal is also obtained as a particular case.

After this brief discussion about the propagation channel and the main theoretical distributions that describes it, next sections will address the subjects of distribution implementation and model investigation.

2.2.5 Wolfram Mathematica

Mathematica is a well known system for modern technical computing based on the Wolfram Language and available since 1988. The system is widely admired for both its technical prowess and elegant ease of use. Mathematica provides a single integrated, continually expanding system that covers the breadth and depth of technical computing [16].

Its latest version, Mathematica 11, has approximately 5000 functions and as all its versions, is defined as a mathematical symbolic computation program used in many scientific, engineering, mathematical, and computing fields.

Wolfram Mathematica is divided into two parts, the kernel and the front end. The kernel interprets expressions and returns result expressions while the front end provides a GUI, which allows the creation and editing of Notebook documents. In addition, all content and formatting can be generated algorithmically or edited interactively. As it is based on symbolic computing, Mathematica was chosen as the computing program used in all fading distribution analyses performed in this work. Figure 2.7 illustrates the software.

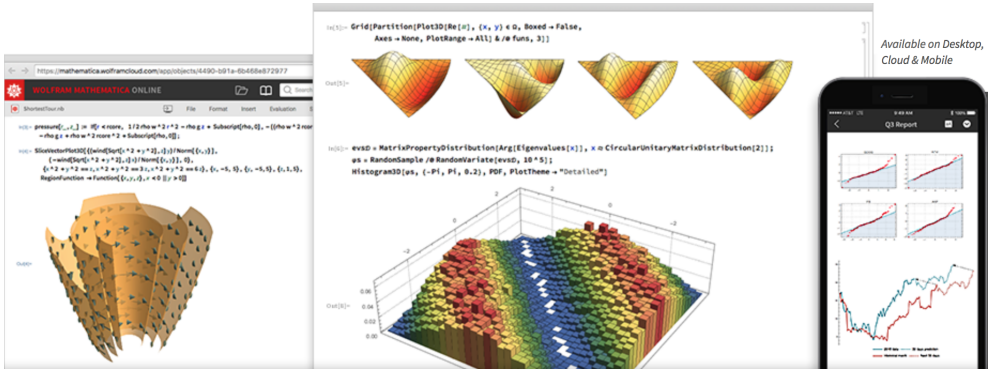

Figure 2.7: Wolfram Mathematica software [16].

2.3 THE α-μ/Γ GENERALIZED DISTRIBUTION IMPLEMENTATION

The first step of this project was to implement the theoretical model of the $\alpha - \mu/\Gamma$ generalized distribution in the software Wolfram Mathematica.

The family of curves for the PDF $f_{\alpha-\mu/\Gamma}(r)$, (Eq. 29), with $\mu = 2$, $k = 1$ and α as variable is presented in Figure 2.8.

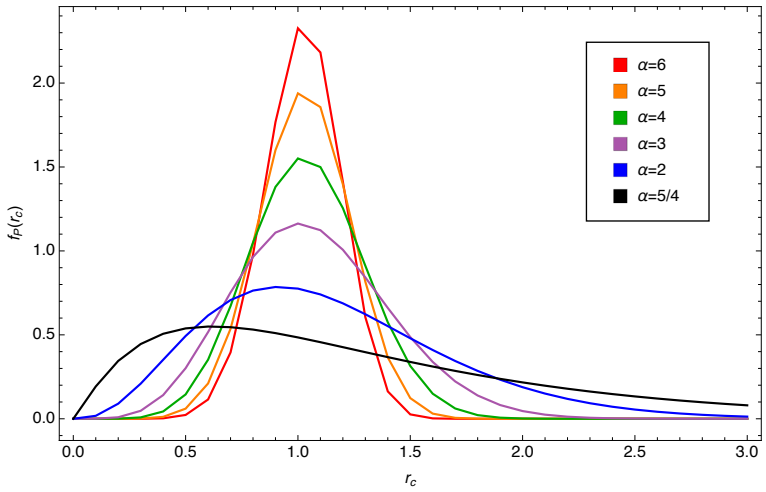

Figure 2.8: Family of curves of $\alpha - \mu/\Gamma$ Generalized distribution for $\mu = 2$ and $k = 1$.

As expected, while increasing the power parameter α, the PDF becomes more concentrated. The same behavior is observed when increasing the number of multipath cluster, μ. Note that for α less than 2 the fading is extremely severe, as expected.

Figure 2.9 presents the $f_P(r_c)$ PDF varying the μ parameter and keeping the others parameters fixed.

As expected, for $\alpha\mu/ < 1$ (i.e., $\mu < 1/\alpha$), $f_P(r_c)$ tends to infinity as r approaches zero and $f_P(r_c)$ decreases monotonically with the increase of r. For $\alpha\mu/ > 1$ (i.e., $\mu > 1/\alpha$), $f_P(r_c)$ is nil at the origin and it increases with the increase of r to reach a maximum and then decrease toward zero as r increases.

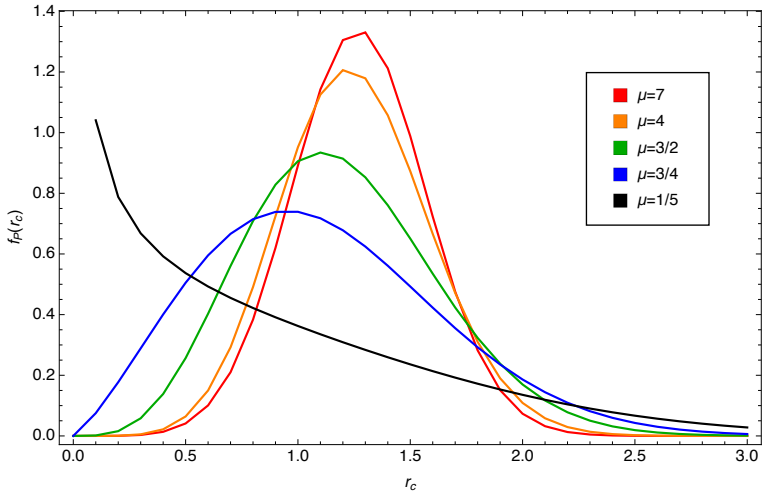

Figure 2.9: Family of curves of $\alpha - \mu/\Gamma$ Generalized distribution for $\alpha = 3$ and $k = 1$

The Figure 2.10 presents the the $f_P(r_c)$ PDF varying the k parameter and keeping the others parameters fixed.

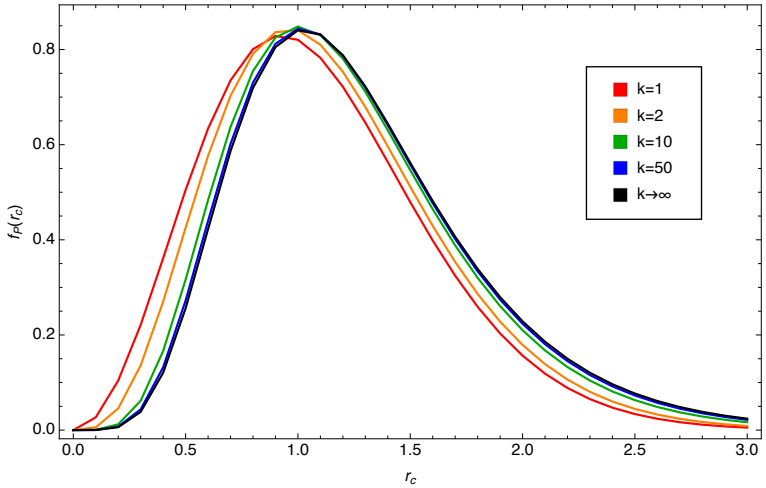

Figure 2.10: Family of curves of $\alpha - \mu/\Gamma$ Generalized distribution for $\alpha = 3$ and $\mu = 2$

It can be observed that increasing the k parameter, the simmetry and centrality of the PDF is changed. When $k \to \infty$, the composite distribution reduces to the $\alpha - \mu/Lognormal$.

2.4 FIELD TRIALS AND EXPERIMENTAL INVESTIGATION

A series of field trials was conducted at the University of Brasília (UnB) and the University of Campinas (Unicamp) in outdoor and indoor environments, in order to investigate and validate in practice the $\alpha - \mu/\Gamma$ Generalized distribution. To this end, the transmitter was placed on the rooftop of one of the buildings and the receiver travelled through each campus as well as within the buildings. In the acquisitions performed at UnB (700MHz), the receiver was installed in a car that was moving at a constant speed through the university, whereas in the measurement campaign carried out at the University of Campinas (1.8 GHz and 5 GHz), the receiver was installed in a stroller equipped with a remote transducer used to carry out the sampling of the signal.

The mobile reception equipment was especially assembled for this purpose and basically, the setup consisted of a vertically polarized omnidirectional receiving antenna, a low noise amplifier, a spectrum analyzer, and data acquisition apparatus like a notebook computer and a distance transducer in the measures carried out in Sao Paulo. The transmission consisted of individual continuous waves tones at 700 MHz, 1800 MHz and 5000 MHz. The following block diagram exemplifies the arrangement of the electronic blocks.

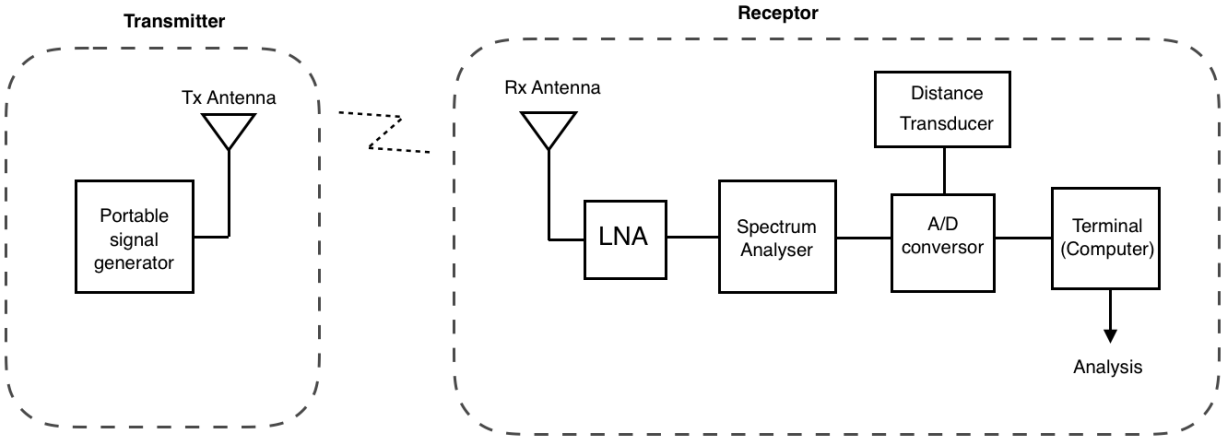

Figure 2.11: Transmission and reception block diagram

For each transmission frequency, it was used a different antenna specific to the used frequency band. For the measurement campaign in 700 MHz a pair of MU-35CI Omnidirectional antennas was used, operating in the range of 820 MHz to 860 MHz (very close to the working frequency range and then with acceptable use). For the 1800 MHz, a pair of K704784 Omnidirectional antenna was used, operating in the range of 1710 MHz to 1880 MHz and in 5 GHz, a SPA 5600/40/14/0/V planar antenna operating in the range 5150 MHz – 5875 MHz was used in transmission and a 80010249 multi-banda Omnidirectional antenna operating in the range 5150 MHz - 6000 MHz was used in the reception.

After obtaining the data, all the information was separated by frequency in time and power vectors. Each big set of data was divided into small sets of data to be analyzed by a code developed in the software Wolfram Mathematica version 11.

The code consists in a previous importation of the data, creation of the main vectors and analyzation of this vectors. For the suppression of path loss attenuation, a non-linear regression calculation was applied to the initial power vector. The final power vector including the composite fading (fast fading + shadowing) was obtained and a mean verification was realized to verify the path loss suppression.

In the end of the manipulation, the envelope r was obtained in Volts after the composite fading conversion for Watts. All empirical sets of data were confronted with the α -μ/Γ generalized distribution as well as with composite distributions already consecrated in the literature as Rayleigh/Lognormal, Nakagami/Lognormal and Weibull/Lognormal.

In order to obtain the best possible curve adjustments for each distribution, a non-linear estimator was created with the goal of indicate the best values for the distribution parameters for each set of data. This parameters can be evaluated by the nonlinear least squares method [17], which provides consistent estimates. In essence,

$$(\hat{x}, \hat{y}, \hat{z}) = \underset{\hat{x},\hat{y},\hat{z}}{argmin}\ MSE, \tag{2.31}$$

in which $MSE = \frac{1}{N}\sum_{l=1}^{N}[\hat{\rho} - \rho]^2$ with $\hat{\rho}$ as the composite distribution with estimated parameters and N as the total number of sample data.

For each set of frequency, the results of the adjustment curves are shown in the next sections. The mean error deviation, ϵ, between theoretical and experimental PDFs was calculated with the purpose of evaluating the numerical error between the trials and the observation of the composite model that best fits the practical data. The mean error deviation between the theoretical and experimental data is given by

$$\epsilon = \frac{1}{N}\sum_{i=1}^{N}\Big|y_i - x_i,\Big| \tag{2.32}$$

in which y_i is the theoretical data and x_i is the empirical data, for a given value of r_c.

2.4.1 Results in 700 MHz

The probability density function (PDF) and the cumulative distribution function (CDF) of the empirical data in 700MHz and of the main theoretical fading distributions are illustrated in the Figures 2.12 and 2.13. The non-linear estimator described in Eq. 2.31 was used in order to find the best parameter adjustment for each composite distribution in relation to empirical data.

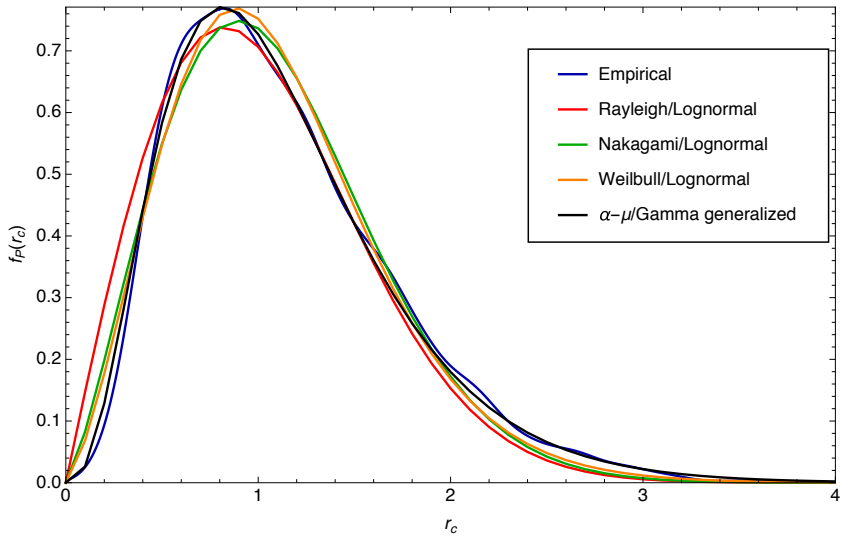

Figure 2.12: PDF for data in 700 MHz

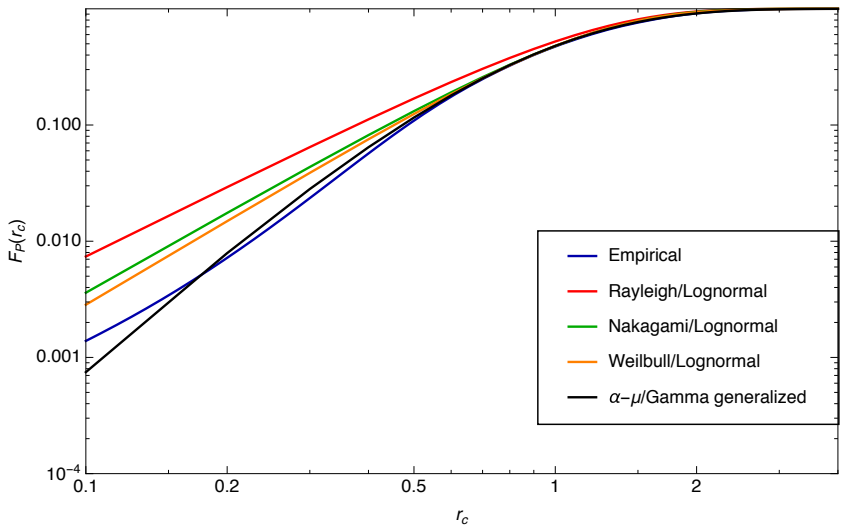

Figure 2.13: CDF for data in 700 MHz

It can be observed an excellent fit between the α -μ/Γ Generalized distribution curve and the empirical curve. The CDF graphic is presented in log-log scale to make the CDF tail more evident, which is the most important part of the CDF since along the x-axis all the curves tend to 1.

Table 2.1 presents the mean error deviation between the empirical data and each of the composite distributions studied. It is possible to verify that the α -μ/Γ Generalized distribution has the lowest mean error value.

Table 2.1: Mean error deviation for data in 700 MHz

Composite distribution	**PDF**	**CDF**
Rayleigh/Lognormal	2.952 %	2.611 %
Nakagami/Lognormal	2.461 %	1.184 %
Weibull/ Lognormal	2.114 %	0.939 %
α-μ/Γ generalized	1.155 %	0.671 %

2.4.2 Results in 1800 MHz

As in the previous session, the PDF and CDF functions graphs for a field measurement in 1800MHz are illustrated in the Figures 2.14 and 2.15.

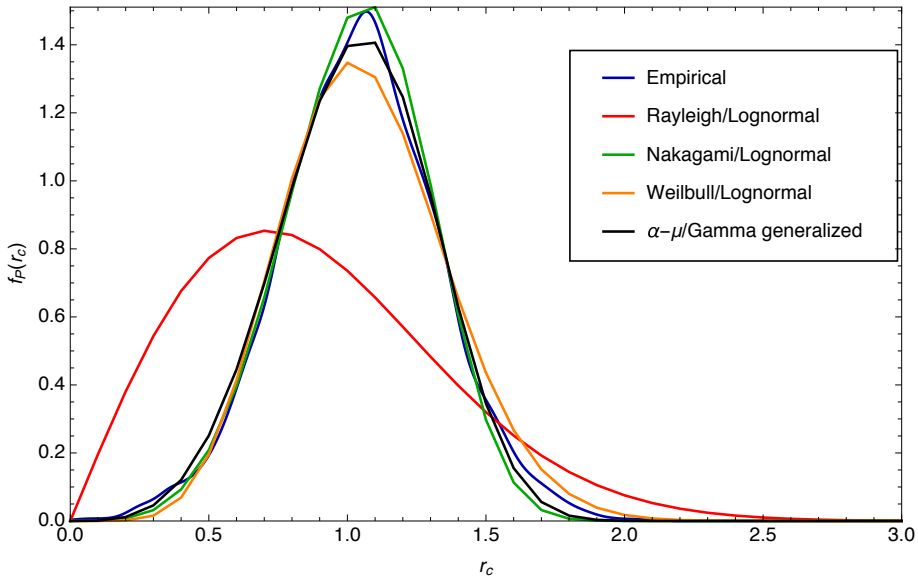

Figure 2.14: PDF for data in 1800 MHz

The PDF graphic and the mean error deviation presented below shows that the Rayleigh/ Lognormal distribution is far from an ideal fit, having more than 15% of error. The lowest PDF mean error was obtained with the Weibull/ Lognormal distribution while the α -μ/Γ Generalized distribution offered a lowest mean error deviation for the CDF function.

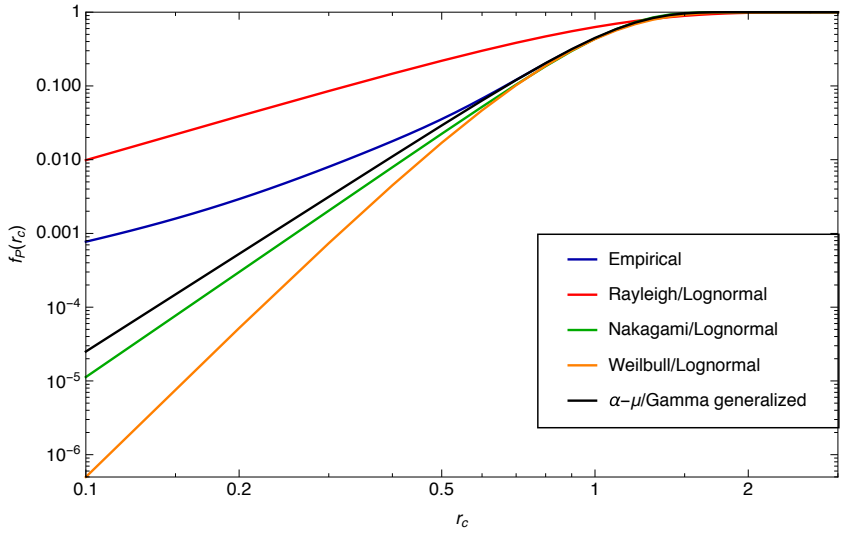

Figure 2.15: CDF for data in 1800 MHz

Table 2.2: Mean error deviation for data in 1800 MHz

Composite distribution	PDF	CDF
Rayleigh/Lognormal	15.416 %	5.077 %
Nakagami/Lognormal	4.004 %	0.965 %
Weibull/ Lognormal	1.491 %	0.504 %
α-μ/Γ generalized	1.674 %	0.474 %

2.4.3 Results in 5000 MHz

In 5000 MHz, the PDF and CDF are illustrated in the Figures 2.16 and 2.17 below.

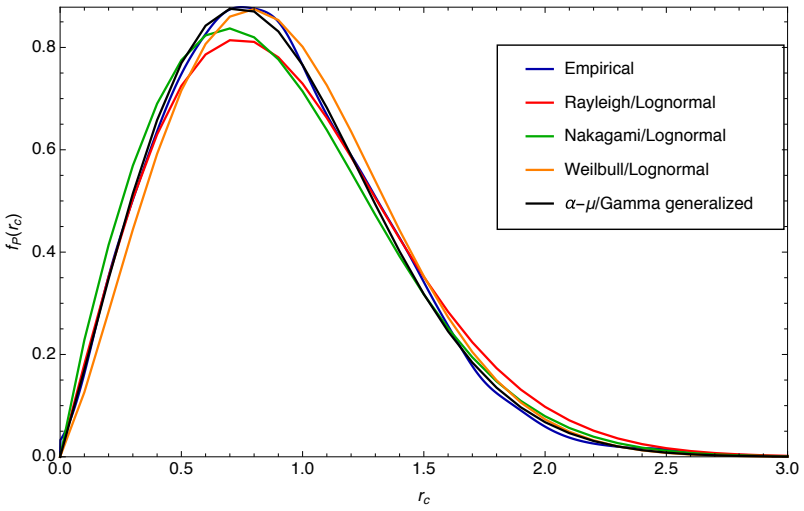

Figure 2.16: PDF for data in 5000 MHz

As expected, the α -μ/Γ Generalized distribution has the lowest mean error deviation of all the composite distributions. Theoretically, as the α -μ/Γ Generalized function has 3 degrees of freedom (α, μ and Γ), the function is more flexible and fits better the empirical curves, being able to reduce itself to other composite distributions when it is convenient.

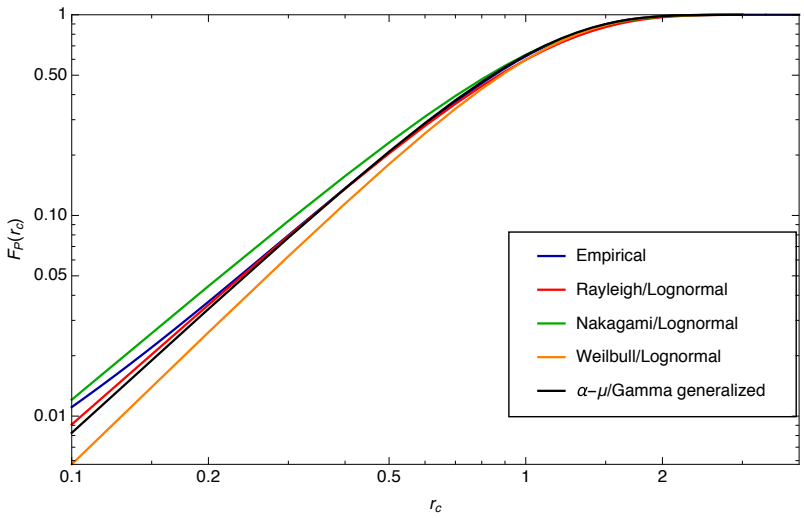

Figure 2.17: CDF for data in 5000 MHz

Table 2.3: Mean error deviation for data in 5000 MHz

Composite distribution	**PDF**	**CDF**
Rayleigh/Lognormal	1.226 %	0.342 %
Nakagami/Lognormal	1.837 %	0.571 %
Weibull/ Lognormal	1.399%	0.742 %
α-μ/Γ generalized	0.622 %	0.194 %

In summary, the Figures 2.18 and 2.19 show the best adjustments for each frequency. It is possible to observe an excellent fit between the curves of the empirical and theoretical PDFs for each one of the frequencies studied, being observed a mean error deviation, ϵ, of 1,155% for PDF of 700MHz, 1,674% for PDF of 1800MHz and 0,755% for the PDF of 5000MHz.

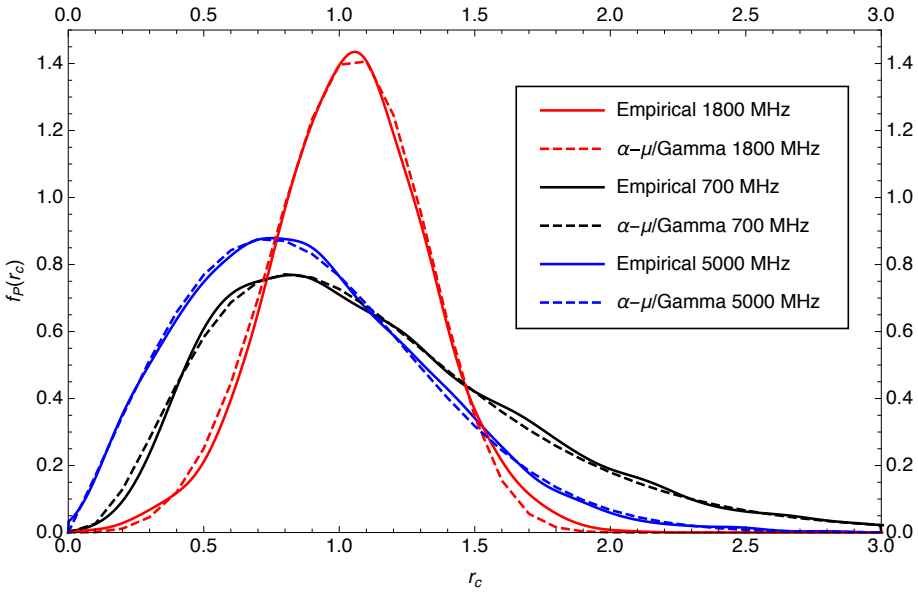

Figure 2.18: PDF of the three datasets

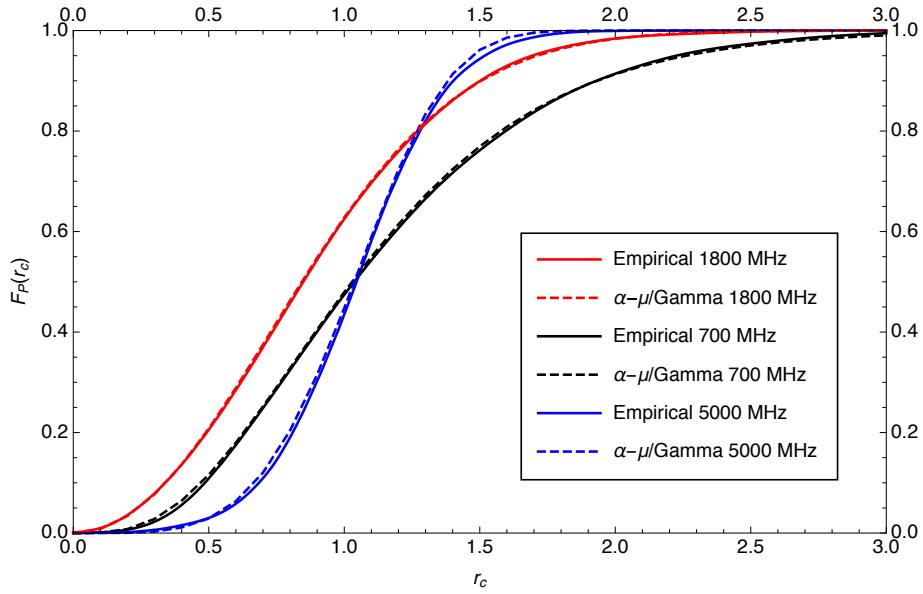

Figure 2.19: CDF of the three datasets

2.5 CONCLUSION

In this project, it was reported the results of field trials aimed to investigate the first-order statistics of the α -μ/Γ Generalized distribution. An excellent visual agreement and low mean error deviation between the experimental and the theoretical data was found.

The distribution suggested in this article, besides having closed formula and being easily applied, can be reduced to the traditional distribution Rayleigh-Lognormal using the right parameters values.

The measurements validates the PDF and CDF functions derived in closed-form for the composite α -μ/Γ Generalized fading signal. The probability density and cumulative distribution functions are considered mathematical tools of great utility in applications related to evaluation of the performance of wireless communications under composite channels.

Next chapter also presents a project based in statistical analyses of PDFs and CDFs in a wireless environment, sharing the same theoretical foundation of this project.

3 SYSTEM OF MEASUREMENT AND ANALYZE OF MOBILE NETWORKS' QUALITY

Mobile communications are experiencing significant growth in recent years, largely as consequence of accelerated usage growth and spread of smart devices. Linked to the growth of the number of devices is the increase in the number of complaints about the mobile telephony service provided in Brazil.

In recent years the telecommunications services has occupied the first places in the ranking of complaints of the consumer defense offices, what attracts the attention of the regulatory bodies to the measurement of the quality of services. Just in 2016, 288 thousand complaints were registered in the platform consumidor.gov.br [17], a complain platform created by the National Consumer Secretariat - SENACON / MJSP. This platform offers statistics and reports about the complaints and it is possible to verify, on Figure 3.1, the amount of complaints by segment in the year of 2016.

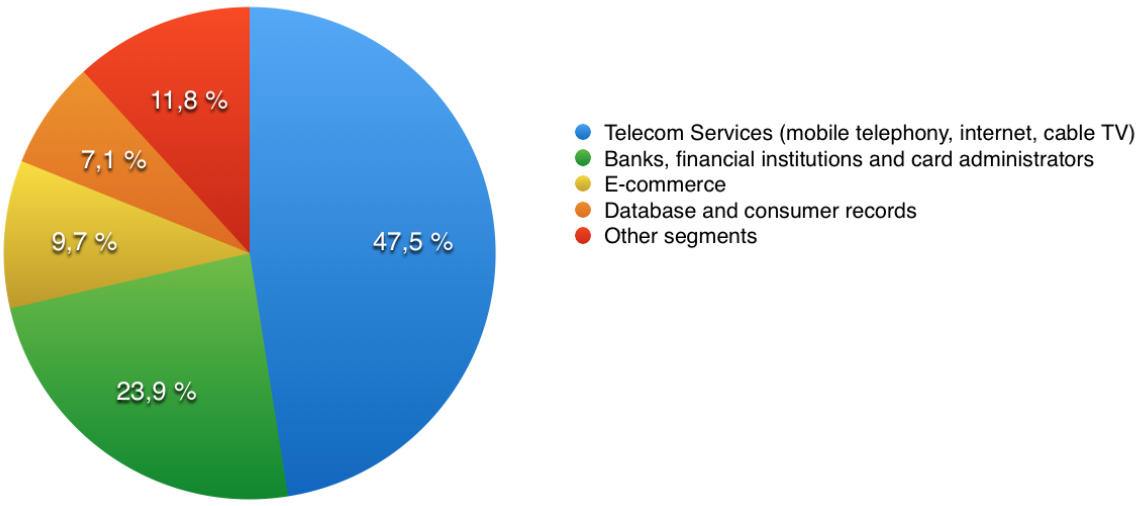

Figure 3.1: Complaints by segment [18].

As it is visible, the Telecommunication sector, especially mobile telephony, presents a very large portion of the complaints made on the platform, indicating a lack of contentment of the population with the services provided by the operators. Figure 3.2 indicates that about 20% of the complaints made in 2016 were about the mobile telephony service.

Despite the indicatives presented, most of the methods developed for qualify network and signal strength are kept in secret by the mobile carrier themselves and there is little information opened to the public, making it difficult to follow the information on the subject.

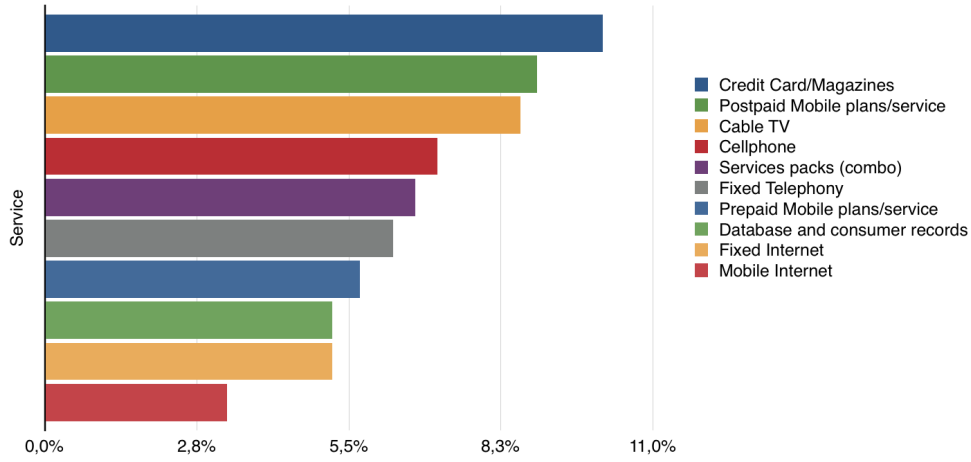

Figure 3.2: Most claimed topics [18].

Due to this lack of access to information about the quality of telecommunication networks, this project aimed to develop a network quality measurement system in the format of a mobile application. The proposed system consists on the collection and processing of data from cellular networks to measure the quality of communication services. The data is obtained through smartphones and the system is based on crowdsourcing, i.e, all the people who use the application contribute to the database and consequently to the measurement of the quality of the network, making the analysis of the application more complete. For example, customers from different neighborhoods help complement the quality map of an entire city. This strategy benefits both users and service providers. The information collected and presented in the system indicates the scenario of quality of the network closer to reality, since they were obtained by the users themselves.

This project presents a system that focus on general coverage visualization based on collected data and specialized inferences based on statistical information calculated with data measured by the system itself. Statistical data can have several applications for both end-users and mobile carriers. End-users will be interested in which carrier provides the best service and has the best coverage area in their region, while mobile carriers may be interested in knowing if the parameters of their network are appropriate. This end of course contribution on the project is based in the development of a code, in Python, that handles the data received by the App and presents preliminary statistical results obtained from controlled measurement campaigns in an outdoor environment.

The code was developed using Spyder development environment available in the Anaconda Navigator, a desktop graphical user interface included in Anaconda suite that allows to launch applications and easily manage conda packages, environments and channels without the need of using command line commands [19]. Spyder provides advanced editing, interactive testing, debugging and introspection features. Unlike Wolfram Mathematica, spyder is a numerical computing environment supported by IPython and popular Python libraries such as NumPy, SciPy and matplotlib [20]. This tool is very useful in the numerical implementation of formulas to develop systems in a high level language like Python. Figure 3.3 illustrates the Anaconda Navigator interface.

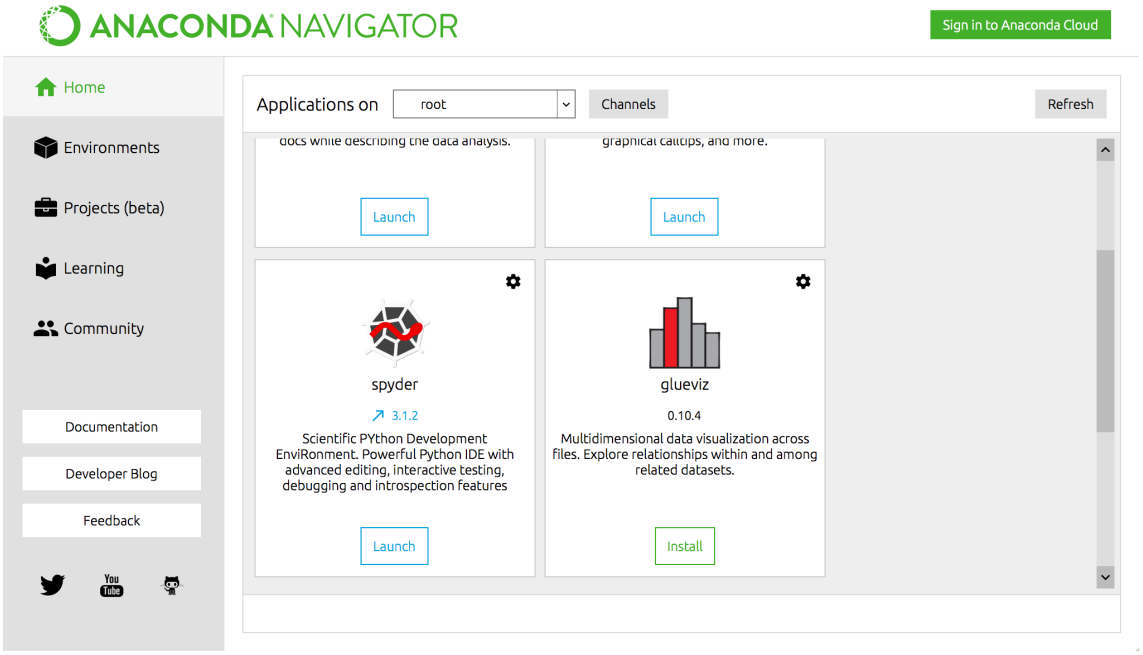

Figure 3.3: Anaconda Navigator with Spyder development environment [19].

3.1 SYSTEM ARCHITECTURE

The system is based on a client-server model in which the client-side is mainly composed by a mobile terminal that executes an Android application that interacts with an user while the application collects the data. The general operation is presented in Figure 3.4.

The data is collected at an approximate rate of 1 sample per second (1 Hz) and stored in memory waiting to be sent to the servers. A number of approximate 60 subsequent measurements are grouped and sent to the server as a single batch. The servers then process and save the data.

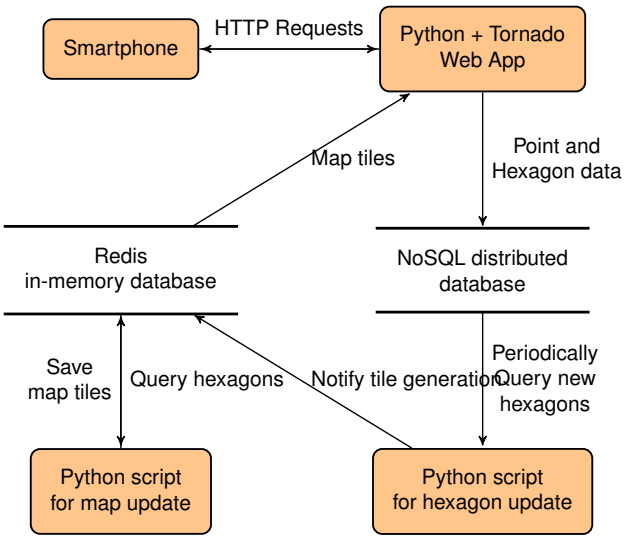

Figure 3.4: System architecture diagram

Each time a data is received by the server for processing, it must calculate the coordinates of the hexagon that circumscribes it. This hexagon is then marked for update in a database and the point is saved in a separated collection for future reference and calculations. From time to time, the server groups all the marked hexagons and calculates the average signal strength from all measurements points that are positioned within each polygon. When all hexagons are fully updated, it runs a script responsible for updating the map images that are displayed on the application.

Due to this mechanism, there is a small delay between the data being sent and the same data being reflected for visualization, hence the process cannot be considered fully real-time. Moreover, computing capacity grows with the number of points generated and is inversely proportional to the processing delay, thus deflagrating a Big Data challenge.

Each user can visualize the summarized information about each carrier and technology in any of the fixed size hexagons that are positioned over the map as shown in Figure 3.5. Regarding the meaning of the hexagon colors, the red color indicates signal strength average below -90 dBm, the yellow color indicates signal strength average between -90 and -80 dBm and the green color indicates signal strength average above -80 dBm. These hexagons are generated in the server by the aforementioned script responsible for map data generation. This data is mainly a great amount of PNG images organized to allow visualization using the EPSG:3857 projection coordinate system and stored in a key-value in-memory database for better performance.

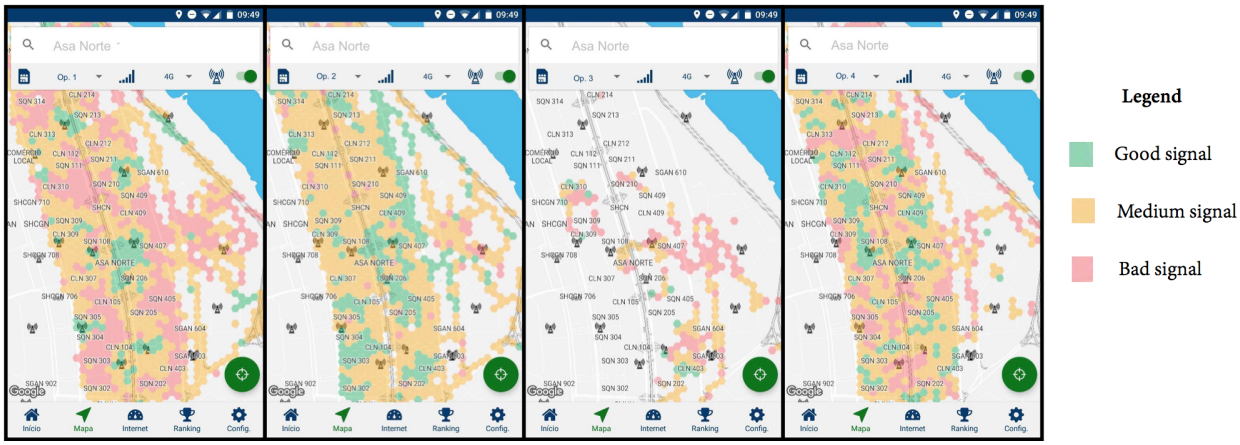

Figure 3.5: Screenshots from the Android application: Map visualization showing data collected from four different mobile carriers.

The mobile application can be used mainly with two different purposes: Firstly, as a generic *crowd-sourcing* tool which monitors signal from different devices at the same time generating the global generic visualization of signal quality shown in Figure 3.5, which can be useful for users that are seeking the best carrier in their region as well as regulatory bodies and mobile carries who will no longer need to hire drive tests to generate a coverage map of your mobile service saving considerable amounts of time and money and secondly, as a specific tool which allows a statistical analysis of data collected in a given time and space scope. This statistical analysis can be used for channel characterization and practical investigation of fading distributions, having diverse scientific applications in the investigation of experimental data and characterization of environments from the use of a simple and practical tool like a cell phone.

The main focus of the author on this project is the statistical analysis of the environment from the fading suffered by the signal between the transmission and reception. Next sub-section presents some results of these statistical analyzes.

3.2 STATISTICAL CHARACTERIZATION OF CELLS

The developed system can also be used for statistical analysis of different scenarios when more specific results are needed. In this case, the users may want to set up a controlled environment. This part of the system was developed with the objective of creating a tool of easy access and use for channel characterization of a given environment from its fading.

In this mode, the application is set up to mark the data sent to server in order to indicate whether they are part of a specific measurement. In this case, the user should indicate when the measurements starts and stop. Then, the data becomes available to export and to be analyzed with other tools, if desired by the system's user.

At the beginning of the data analysis, it is necessary to filter each of the three components of fading process present in the signal (fast fading, path loss and shadowing [6]) and separate the vector of interest, in this case the shadowing vector. The separation of fading permits us to develop and implement the proper technique to mitigate each type of fading in a separate way.

In order to filtrate the fast fading, a moving average filter was applied in the data to suppress the interference patterns caused due to multipath. Next, to filter path loss attenuation, a non-linear regression calculation was applied on the data. A function was developed to estimate the curve caused by the path loss and to correct the data to be zero mean, finally filtering the shadowing from the path loss. Figures 3.6 and 3.7 illustrate the results.

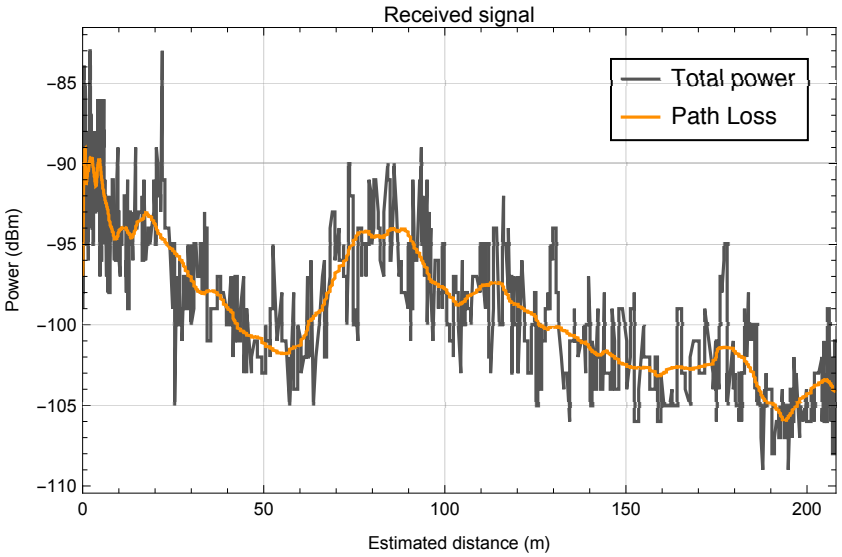

Figure 3.6: Received signal in a given radio-base station.

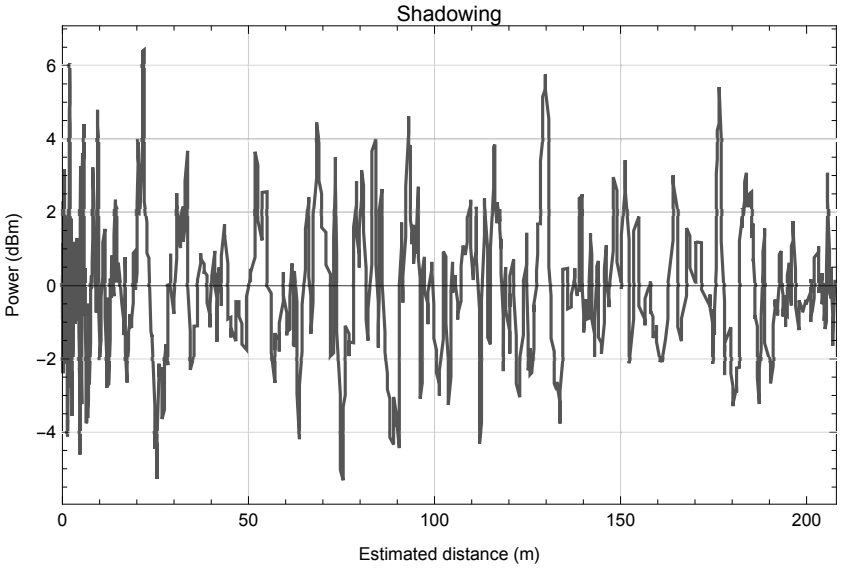

Figure 3.7: Filtered shadowing from original signal.

After the fading filtering, the envelope is found and its empirical first orders statistics (PDFs and CDFs) are obtained. The empirical data can now be confronted with fading distributions, can be used to generate comparisons between mobile carries or others applications.

3.2.0.1 Cell's measurements

In this measurement scope, the data was obtained in a walk test performed in a controlled outdoor environment with three different devices models at the same time using the same mobile carrier, receiving a 4G signal. Measures were taken along a sidewalk parallel to a main road with high movement of people and vehicles. In the walk test, the measurements were made with people using the cell phone under usual conditions, i.e, walking and carrying the cell phones in their hands. Figure 3.8 illustrates the environment where the tests were taken.

Figure 3.8: Tests environment.

Another interesting goal of this test is to verify the adjustment of the lognormal distribution, most common model used for modelling the shadowing, who has its normalized PDF written by Eq. 2.1.

Figures 3.9 and 3.10 section show probability density function (PDF) and cumulative density function (CDF) of 3 different cell phones models in order to compare the data reception of different devices in the same environment.

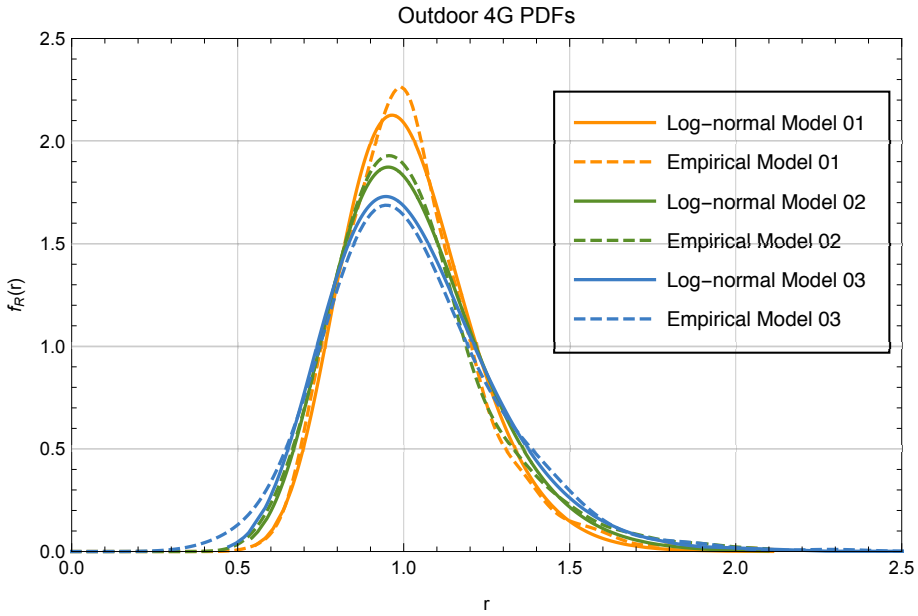

Figure 3.9: PDF for data of 3 different mobile models.

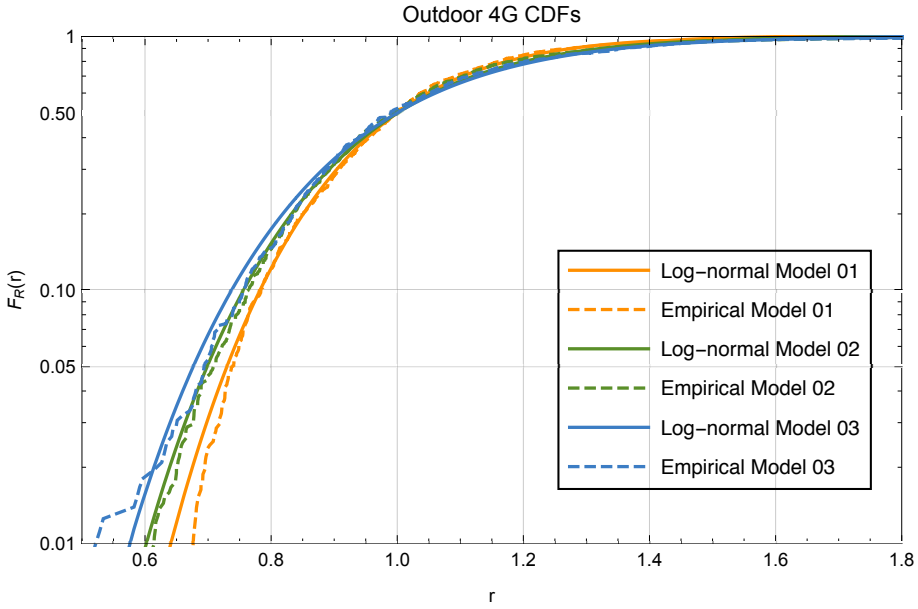

Figure 3.10: CDF for data of 3 different mobile models.

The results show an interesting difference in the signal reception for each of the mobile devices. Model 1 has a lot more deterministic reception while the model 3 has a well spread PDF function, indicating a reception with more signal fluctuations which can lead to communication problems for the user. In addition, this test was able to show optimal settings of the lognormal distribution for this test environment on all cell phone models.

Another interesting statistical test was the realization of a campaign of measurement in an outdoor environment with a unique cell phone and mobile carrier but changing the technology between 4G and 3G, the last one through a manual configuration in the device itself. Figures 3.11 and 3.12 show the PDF and CDF results. Is is possible to visualize a clear difference in the reception of 3G and 4G technologies in a single mobile device. 3G signal is clearly more deterministic and stronger than 4G signal, what is expected since 3G was measured in 2.147 GHz, 4G in 2.655 GHz and from the fact that the wavelength is inversely proportional to the frequency. It is also possible to check in both Figure 3.11 and Figure 3.12 an optimum adjustment of the lognormal distribution for the environment in 3G and 4G.

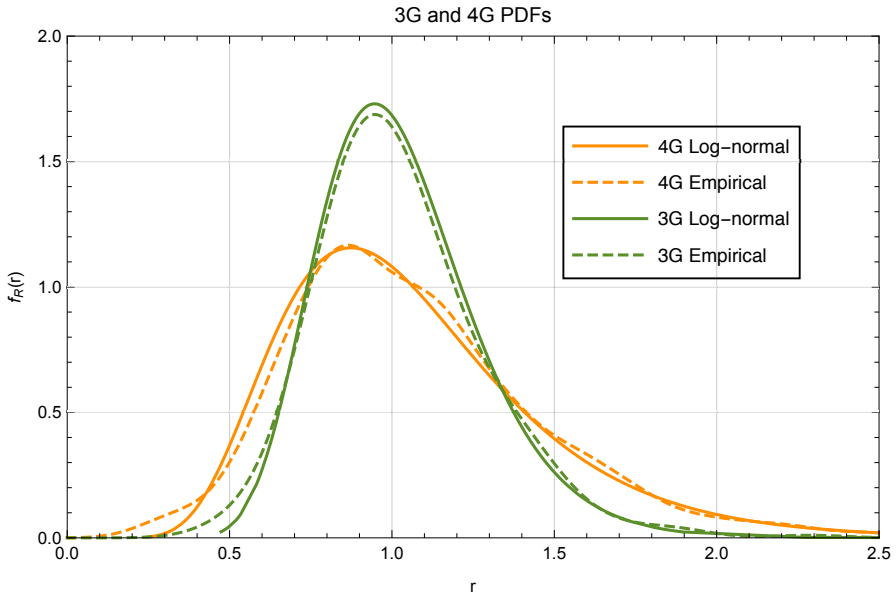

Figure 3.11: PDF of different technologies.

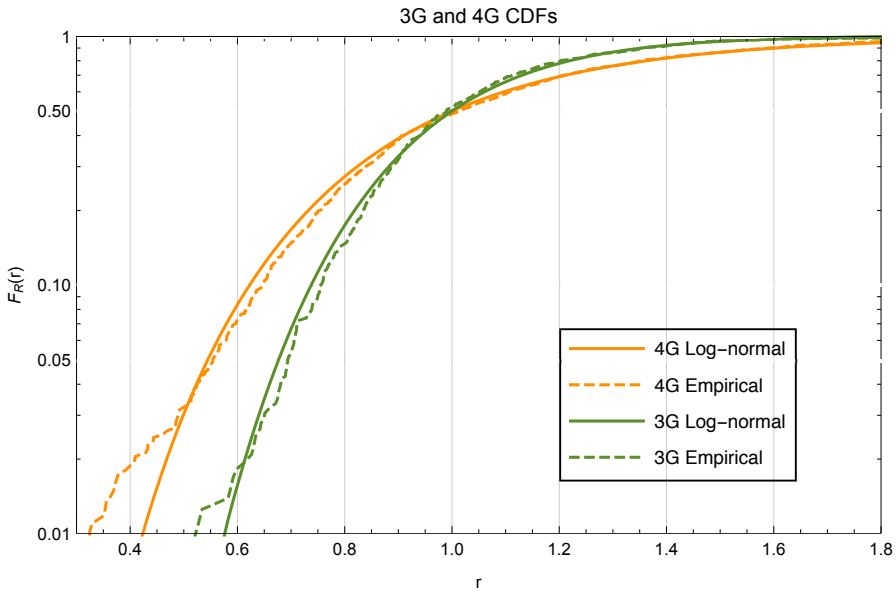

Figure 3.12: CDF of different technologies.

3.2.0.2 Model's investigation

Although the local average power is widely accepted to be lognormal, the mathematical form of the lognormal PDF is not convenient for some analytic calculations and does not always perform a perfect fit to the empirical curve. In such a way, it is interesting to know which distribution best fits the actual environment data. The next test performs a practical analysis of the adjustments between empirical data measured with the mobile application and two distributions: The lognormal model and the α-μ distribution [3], which is a rewritten form of the Stacy (generalized Gamma) distribution [4] defined in Eq. 2.24.

Figure 3.13 shows the adjustment results for both lognormal and α-μ distributions. Note that the green curve obtains a better result in the adjustment with the empirical curve, which tells us that lognormal model is not always the best option and shows another useful application of the system.

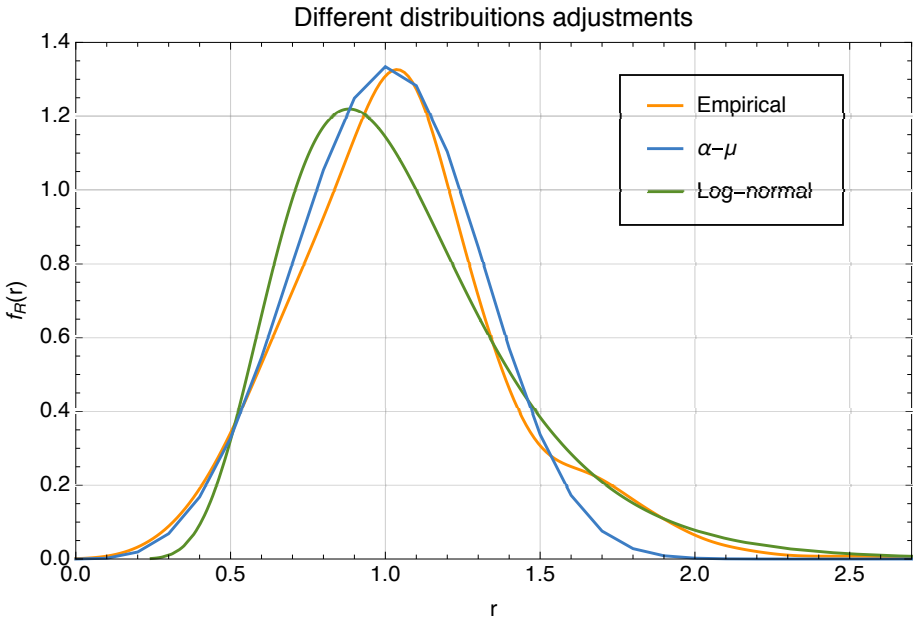

Figure 3.13: Different distribution adjustments for a empirical data.

3.3 CONCLUSION

This chapter presents a crowdsourcing based system whose main purpose is to inform users and mobile carries the coverage map of a given region based on actual data measured by the users themselves. It is also a quality analysis tool which can be used for various other purposes. In parallel with the objective of visualizing the coverage map, this system also aims to be a measurement system that returns statistics analysis about the channel characterization and practical investigation of fading distributions. The results presented in this report give the idea of the amount of information that can be implied from the analysis of the signal power graphs, helping both users and mobile operators

The statistical module can be used by students or people from the scientific community who are interested in doing practical and statistical analyzes using a low cost and high access tool like a cellphone.

4 STUDY OF COEXISTENCE BETWEEN LTE CELLULAR NETWORKS AND ISDB-T SYSTEMS IN 700MHZ

This project aims to perform realistic analyzes between the LTE standard and the ISDB-T system motivated by the current analogue TV disconnection occurring in Brazil and the incessant search for available spectrum for wireless communication.

Fourth-generation (4G) cellular systems use the Long Term Evolution (LTE) standard to refers to the evolution of third generation technology and aims to improve end-user data traffic by increasing the width of Bandwidth, decreasing latency and through optimizing access radio technology with packets that travel at up to 100Mbps. This technology, based on the OFDM modulation technique, was first implemented in Brazil in 2012 after the allocation of the frequency band of 2.500MHz - 2.690MHz [21] previously destined to MMDS by the National telecommunications agency (Anatel).

Despite the good operation of the LTE at 2500 MHz, the signal coverage at this frequency is relatively small since the wavelength is inversely proportional to the frequency and the cost of implementing and maintaining the technology is expensive, given the amount of antennas and infrastructure required for its proper functioning. In this context, the 700MHz spectrum band, already used by LTE in the USA and in Europe, began to be targeted by the national telecommunication companies. In this sense, on April 2014, Anatel published an important LTE coexistence report between LTE and the ISDB-T [22] systems in the 700 MHz band, which became a technical reference document for the analysis of coexistence between such systems. Also in 2014, Anatel coordinated the bidding of the 700 MHz frequency band for the expansion of the 4G networks in Brazil, which is being made gradually according to the analogue TV disconnection in each city until 2018.

In this context, this work aims to perform a realistic coexistence analysis between the LTE standart and ISDB-T systems as well as between the LTE and IEEE 802.11a/n systems, in order to determine the protection ratio between such systems in order to guarantee the operation with acceptable levels of interference and performance.

4.1 SHARING AND COEXISTENCE STUDIES

Society's increasing use of radio-based technologies highlight the importance of the radio spectrum, a huge but not infinite range of frequencies of electromagnetic radiation. The electromagnetic spectrum is used for all forms of wireless communication including cellular telephone, radio and television broadcasting, GPS position locating, satellite command and control[23].

Technological progress has continually opened doors to a variety of new radio applications that have spurred interest in and demand for spectrum, but like most natural resources, the electromagnetic spectrum is a scarce resource. The frequencies that compose the spectrum have different physics and different interactions with the environment, becoming more or less attractive for a specific service. In fact, wavelength's size is inversely proportional to the frequency, causing low frequencies to have waves with high power of penetration and reach. In this way, the vast majority of radio-based services like TV broadcast and mobile telephony are interested in operating in VHF or UHF frequencies, congesting the spectrum below 5GHz. Figure 4.1 illustrates the most used radio frequencies ranges.

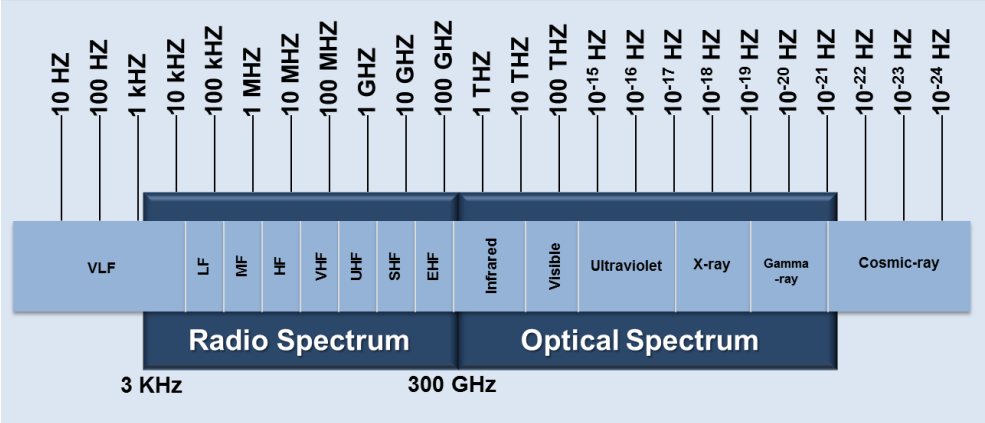

Figure 4.1: Radio frequencies bands [23].

This electromagnetic spectrum dispute has incited new debates and encouraging research into new technologies that operate on frequencies of millimetric waves, such as 5G, but since to operate nowadays at high frequencies poses too many challenges, the major mobile communications services (TV broadcast, cellular networks, Wi-Fi) operate in very close bands, which can generate major interference problems.

To ensure the correct and efficient use of available spectrum, each country appoints a national regulatory body responsible to divide and supervise their use. In Brazil, the allocation of spectrum for the various telecommunication services is regulated by the National Telecommunications Agency (ANATEL), that is also responsible for specifying the terms of usage for every spectrum chunk as well as specifies the types of services that could be provided over any spectrum segment. The national regulatory body of each country cooperate with each other through the international organizations which make sure that national spectrum regulations provide the means for interoperability and that harmful interference between different countries is avoided. Currently, the national organization responsible for this task is the international telecommunications union (ITU).

In this context, sharing and coexistence studies between services are important to investigate and mitigate interference that one service can cause to the other in order to fullfil the coexistence requirements and enable the proper functioning of all services at the same time. In addition, with the advancement on 5G researchers, coexistence studies are required to identify possible future frequency bands for IMT-2020.

4.1.1 LTE 700 MHz and DTV challenges

Faced with the scenario described, Brazil is going through another innovation in the telecommunication sector. Currently, the majority of the Brazilian territory operates the TV broadcast service with the two analogue and digital systems in parallel. At the same time, there is a need to expand 4G LTE coverage mainly in urban and suburban areas, what is occurring at the 700 MHz frequency range - previously dedicated to analog TV transmission - called digital dividend. As in many places this expansion is still underway, there is a need to study the two systems in the same frequency range and analyze the interference that one system can cause in the other. In 2014, ANATEL has conducted a preliminary study of interference between LTE 700 MHz and the digital TV service that would operate in a frequency range close to the LTE. The results were promising and in 2016 the analogue TV shutdown process was started in Brazil, being expected to be finished until 2018.

As digital compression systems now available for digital television systems allow the transmission of several standard digital television channels of acceptable quality in the radio-frequency spectrum previously used by a single analogue channel, an important frequency band will be available for others services after the total transition from analog to digital TV.

This frequency band, defined by the European Commission as "the spectrum beyond the frequencies needed to serve the broadcasting services in a fully digitized environment" is called "Digital dividend" (DD) and represents a very disputed frequency band by television operators and mobile carrier because it presents better signal coverage, reduced infrastructure and maintenance expense and because it presents a much higher degree of immunity to signal degradation compared to other frequencies above the UHF band. The Figure 4.2 presents in rouge the frequency band of the Digital dividend.

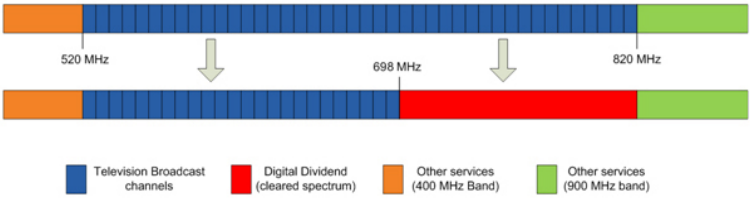

Figure 4.2: Digital dividend spectrum.

Still in 2014, after ANATEL's study and official decision to auction off the digital dividend band to the mobile telephony service, the main Brazilian mobile carrier participated in the auction and guaranteed their services at 700 MHz after the gradual shutdown of analog TV. On the other hand, the new distribution of the TV and LTE channels in close frequency bands generated several discussions about possible interference problems between the systems, which would cause enormous financial losses.

In this context, coexistence studies between the described services and coverage prediction analyzes are important to verify possible situations of undesired interference.

4.1.1.1 LTE characteristics and architecture

Long Term Evolution (LTE) is a registered trademark owned by the European Telecommunications Standards Institute (ETSI) for the wireless data communications technology and a development of the GSM/UMTS standards. It's main goal is to increase the capacity and speed of wireless data networks using new digital signal processing techniques and digital higher order modulations. This new data communication technology was redesign to be IP-based in order to reduce transfer latency compared to the 3G architecture. As its wireless interface is incompatible with 2G and 3G networks, it must be operated on a separate radio spectrum. Figure 4.3 show the LTE most known symbol and characteristics.

Figure 4.3: LTE slogan.

Initially, the 4G future was divided between WiMAX and LTE, two technologies with different specifications for the same purpose of becoming the new technology of wireless communication. In this way, some CDMA operators planned to upgrade its networks to WiMAX, but all the major CDMA operators (such as Verizon, Sprint, MetroPCS, Bell, Telus, SK Telecom, China Telecom and China Unicom) have announced that they intend to migrate to LTE after all. In order to carry out only one standard, LTE was chosen and gained worldwide visibility.

One of the important features of LTE is the ability to implement time division duplex (TDD) or frequency division duplex (FDD). Besides that, LTE supports mixed data, voice (VoLTE), video and messaging traffic. LTE uses OFDM (Orthogonal Frequency Division Multiplexing) in direct link and SC-FDMA (Single Carrier Frequency Division Multiple Acess) in the reverse links, helping to reduce interference and increase network capacity. Figure 4.4 illustrates LTE multiple access technique.

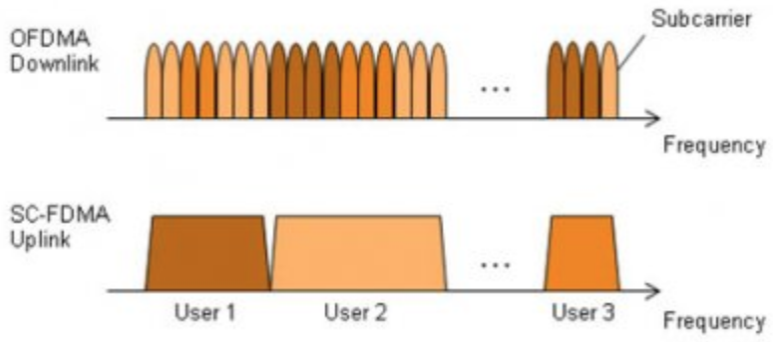

Figure 4.4: LTE multiple access technique [24].

In later releases of LTE, it is used MIMO (Multiple Input Multiple Output) antenna technology, increasing the signal to noise ratio (SNR) at the receiver. In general, the combination of MIMO technique along with OFDM, provides improved coverage and throughput, especially in dense urban areas. In theory, LTE has the potential for peak data rates of 380 Mbps downstream and 80 Mbps upstream, reduced latency, scalable bandwidth capacity, and backwards compatibility with existing GSM and UMTS technology. In November 2016, OpenSignal's "The State of LTE" [25] report indicates than while LTE continues to expand and see strength, globally, download speeds average 17.4 Mbps but speeds approach 50 Mbps in the most advanced 4G countries. It's evolution, called LTE Advanced seeks to offer peak rates up to 1 Gbit/s fixed speeds and 100 Mb/s to mobile users using carrier aggregation technique in parallel with MIMO and higher order form of modulation.

Regarding its high-level network architecture, there are three main components in LTE's system architecture evolution. Theses components are described bellow and illustrated in Figure 4.5.

- The User Equipment (UE)

Comprised of two distinct elements; the USIM (universal subscriber identity module) and theME (mobile equipment).

- The Evolved UMTS Terrestrial Radio Access Network (E-UTRAN)

Handles the radio communications between the mobile and the evolved packet core (EPC) and has just one component, the evolved base stations, called eNodeB or eNB.

- The Evolved Packet Core (EPC)

It's the core network and is responsible for the overall control of the UE and establishment of the bearers. The main logical nodes of the EPC are:

- Mobility Management Entity (MME)

It is responsible for all the control plane operations. Process the signals between the User equipment and the central network.[26]

-Serving Gateway (SGW)

SGW acts as a local mobility entity for inter eNB handovers. It also acts a mobility anchor for inter 3GPP mobility.[26]

-PDN Gateway (PGW)

Responsible for all the IP packet based operations such as deep packet inspection, UE IP address allocation, Transport level packet marking in uplink and downlink, accounting. [26]

-Home Subscriber Server (HSS)

Central database that contains user-related and subscription-related information.[26]

-Policy Control and Charging Rules Function (PCRF)

Responsible for policy control decision-making as well as for controlling the flow-based charging functionalities in the Policy Control Enforcement Function (PCEF), which resides in the P-GW.[26]

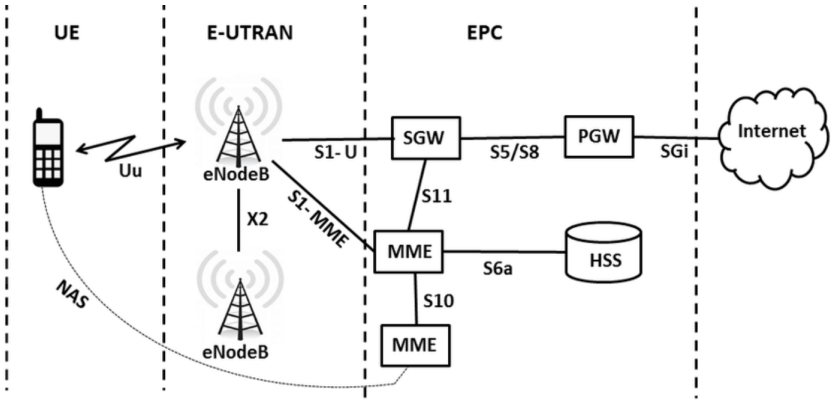

Figure 4.5: LTE architecture [27].

4.1.1.2 LTE in Brazil

Consecrated as the main 4G pattern adopted in the world, LTE was first implemented in Brazil in 2013 after ANATEL's decision to reserve to LTE the frequency band of 2.500 MHz to 2.690MHz, previously reserved to MMDS services. The implementation of the new technology was part of initiatives aimed at improving the country's infrastructure ahead of the World Cup and the Olympic Games. As consequence of this motivation, mobile carriers received a series of requirements by Anatel for the implementation of LTE networks, such as covering all cities which hosted the 2014 Fifa World Cup matches by the end of 2013 and covering all Brazilian cities with over 200,000 inhabitants by the end of 2015 [28].

In december 2012, a Northeastern city called Recife was the first city to receive 4G coverage in Brazil and the implementation of the technology continued throughout the year on 2013 all over the country. In 2014, in order to improve some coverage problems encountered and to complement the LTE in 2600MHz, some mobile carriers started working in the 1800MHz range. At the same time, in September 2014, Anatel decides to auction a slice of the spectrum in 700 MHz band known as the digital dividend resulted from the transition between analog and digital TV until 2018. Currently we are living this transition period of analog to digital TV and implementation of LTE technology at 700MHz.

Although it still presents serious problems of coverage and availability, 4G technology has seen significant growth in the last 12 months, according to numbers from the Brazilian Telecommunications Association (Telebrasil). In May 2017, 80.6% of the Brazilian population was supplied with 4G, what represents more than 2200 cities [29]. Similarly, the number of cell phones with the 4G technology increased considerably in the period from 2015 to 2017, as seen in the Figure 4.6.

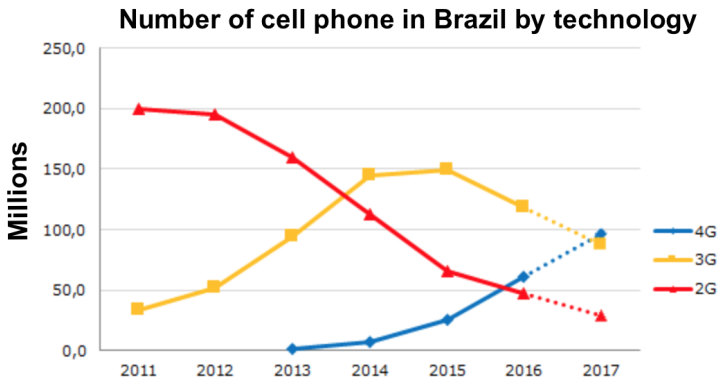

Figure 4.6: Numbers of cell phones in Brazil [29].

Regarding the network speed, Brazil's overall 4G speed averages 19.7 Mbps, putting it more than 2 Mbps ahead of the global average, according to Open's signal recent "State of LTE" report [25] but still far from the expected for the technology. In terms of 4G availability, Brazil still ranks near the bottom among both its global and South American peers. On average, 4G users were able to connect to an LTE signal 59.2% of the time.

With the deployment of LTE at 700MHz, the number of necessary towers will be reduced and the LTE cost of coverage (including equipment, infrastructure and all the bureaucracies related to the rent of the physical space) would be lower inciting the interest to cover more cities in the countryside, increasing the signal coverage and potentially improving signal quality.

4.1.1.3 Digital TV characteristics and architecture

Television has a special social rule in Brazil, being a great tool for information transferring, culture and leisure of citizens. The first TV broadcast occurred in 1950 specially for the World cup hosted in Brazil. Since then, TV service has always being in development and since 2016 we are living an important transition time from analogical to digital transmission.

The Brazilian Digital TV format is a variation of the original ISDB-T system as it has implemented various additions like new video compression, interaction middleware and improved frame rate for transmission to portable devices. This format uses MPEG-2 as multiplexing standard for broadcast and BST-OFDM for modulation.

BST-OFDM (Band-segmented Transmission Orthogonal Frequency Division Multiplexing) is an evolution of the COFDM modulation, works with band segmentation, dividing the 6 MHz width into 13 segments, and, depending on the transmission chosen, uses one or more segments for each layer, transmitting up to three simultaneous data beams with different modulations.

On Digital TV, audio and video transmission change to digital signals which, codified, allows an efficient use of electromagnetic specter, according to the increase of tax data transmission in the band of available frequency. [30]. Digital transitions have several advantages: more channels (until 4) in the same frequency used by an analogical channel, High Definition images, access to additional informations like programation menu and user's interaction with the TV using interaction Middlewares as Ginga [31].

4.1.2 LTE 700 MHz and DTV ANATEL's coexistence studies

The main study on the subject of LTE 700 MHz and digital TV coexistence was carried out by ANATEL in 2014 in the city of Pirenópolis- GO. The field test in the city of Pirenópolis evaluated the mutual coexistence between LTE systems operating in the 700 MHz band and DTV in suburban propagation environment, including the study of mitigation techniques.

The DTV transmission system consisted of a transmitter with possibility of channel change, including the use of a critical mask filter. The maximum power of emission was 100 W. The reception was evaluated with commercial receivers with technology silicon tuner and can tuner, that present a dispersion of performance. The tests were performed at four different points with internal and external antennas, with and without amplifier.

The LTE system was composed of a base station and CPE, both provided by Huawei and by a mobile terminal (UE) provided by Qualcomm. The maximum power was 46 dBm/layer MIMO for the eNodeB and 23 dBm for the CPE/UE.

To this end-of-course work, the most important part of this study was the "Downlink LTE" part in which the influence of a LTE signal was verified in the TV reception on channel 51, the closest TV channel of the LTE band. In theses tests, it was found that the value of ACLR (adjacent channel leakage ratio) on channel 51 presented by the eNodeB used in the test was on average 17 dB higher than those calculated from the spurious emission thresholds established by Resolution 625/2013. It is emphasized that the greater the value of ACLR, the better the coexistence between the systems, reducing the possibility of interference [22].

A summary table containing the minimum protection ratio (PR') values required for the coexistence of services is described in Table 4.1.

Table 4.1: PR' summary table [22].

	Bandwidth	Channel	Antenna	Turner	PR	Oth	PR0	ACS	ACLR'	PR'
DOWNLINK IDLE	10 MHz (Bloco 2-3)	51	active internal	si-tuner	-42	-17	3	45	64,2	-42
				can-tuner	-20	NO	5	25	64,2	-20
			passive external	si-tuner	-67	NO	3	70	64,2	-61
				can-tuner	-69	6	5	74	64,2	-59
			external with booster	si-tuner	-63	-1	3	66	64,2	-59
				can-tuner	-66	-2	5	71	64,2	-59
	20 MHz (Bloco 2-5)	51	passive external	si-tuner	-62	4	0	66	64,2	-62
				can-tuner	ND	ND	ND	ND	ND	ND
			external with booster	si-tuner	-46	NO	0	46	64,2	-46
				can-tuner	ND	ND	ND	ND	ND	ND
DOWNLINK 100%	5 MHz	51	active internal	si-tuner	-39	-18	18	58	64,2	-39
				can-tuner	-43	-18	18	61	64,2	-41
			passive external	si-tuner	-59	-1	18	99	64,2	-46
				can-tuner	-69	0	18	ND	64,2	ND
			external with booster	si-tuner	-57	-5	18	79	64,2	-46
				can-tuner	-64	-5	18	ND	64,2	ND
	10 MHz (Bloco 2-3)	51	active internal	si-turner	-33	NO	14	47	64,2	-33
				can-turner	-33	NO	14	47	64,2	-33
			passive external	si-tuner	-61	0	14	77	64,2	-50
				can-tuner	ND	ND	ND	ND	ND	ND
			external with booster	si-tuner	-59	-7	14	75	64,2	-49
				can-tuner	ND	ND	ND	ND	ND	ND
		48	passive external	si-tuner	NA	NA	NA	NA	NA	NA
				can-tuner	-59	-8	14	75	64,2	-35
			external with booster	si-tuner	NA	NA	NA	NA	NA	NA
				can-tuner	-39	-28	14	54	64,2	-33
	20 MHz (Bloco 2-5)	51	passive external	si-tuner	-53	NO	11	78	64,2	-53
				can-tuner	ND	ND	ND	ND	ND	ND
			external with booster	si-tuner	-51	NO	11	73	64,2	-53
				can-tuner	ND	ND	ND	ND	ND	ND

in which ND means "Not disponible", NA means "Not applicable", PR is the protection ration, Oth is the receiver front-end overload threshold, PR0 is the co-channel protection ratio, ACL' is the adjacent channel selectivity and PR' is the corrected protection ratio in accordance with Resolution No. 625 used for the final calculation of the protection ratio.

Besides the analysis in table 4.1, it is necessary to consider the regulatory limits for the undesirable emissions evaluating PR 'with and without filter for verifying the filter applicability, as presented in Table 4.2.

Table 4.2: PR' with and without low pass filter considering normative ACLR [22].

	Bandwidth	Channel	Antenna	Turner	Measurement without filter	Without filter	With filter
DOWNLINK IDLE	10 MHz (Bloco 2-3)	51	active internal	si-tuner	-42	-42	-61
				can-tuner	-20	-20	-59
			passive external	si-tuner	-67	-61	-61
				can-tuner	-69	-59	-59
			external with booster	si-tuner	-63	-59	-61
				can-tuner	-66	-59	-59
	20 MHz (Bloco 2-5)	51	passive external	si-tuner	-62	-62	-62
				can-tuner	ND	ND	ND
			external with booster	si-tuner	-46	-46	-62
				can-tuner	ND	ND	ND
DOWNLINK 100%	5 MHz	51	active internal	si-tuner	-39	-39	-46
				can-tuner	-43	-41	-46
			passive external	si-tuner	-59	-46	-46
				can-tuner	-69	ND	ND
			external with booster	si-tuner	-57	-46	-46
				can-tuner	-64	ND	ND
	10 MHz (Bloco 2-3)	51	active internal	si-turner	-33	-33	-50
				can-turner	-33	-33	-50
			passive external	si-tuner	-61	-50	-50
				can-tuner	ND	-50	-50
			external with booster	si-tuner	-59	-49	-50
				can-tuner	ND	-50	-50
		48	passive external	si-tuner	NA	NA	NA
				can-tuner	-59	35	-50
			external with booster	si-tuner	NA	NA	NA
				can-tuner	-39	-33	-50
	20 MHz (Bloco 2-5)		passive external	si-tuner	-53	-53	-53
				can-tuner	ND	ND	ND
			external with booster	si-tuner	-51	-53	-53
				can-tuner	ND	-53	-53

The tests conclude that respecting the frequency range established for each service, the interference that the LTE can cause in the TV signal is not enough to break the protection ratio. In addition, in order to protect the system from possible adverse situations, the use of a low-pass filter in the RF input or just after the antenna is the most recommended solution.

4.2 ASSEMBLING OF TESTS

Analysis of coexistence of technologies are extremely important tasks for the implementation of new technologies while ensuring the good performance of those that already exist. The TV service is consecrated and it is a very important technology for society, having a notable social role in the dissemination of information, in the entertainment and leisure of citizens.

With the need of new frequency bands to expand coverage of more recent technologies such as LTE, Anatel decided to work with the digital dividend generated by the end of analogue TV until 2018 and allocate a portion of the 700 MHz band to personal mobile services. However, the allocation of mobile services such as LTE, in the digital dividend range, could lead to a "technological conflict" due to the interference that might arise between these same services and digital television.

4.2.1 LTE and ISDB-T tests architecture

Channel 22 (currently empty) was used to receive a LTE signal and to analyze adjacent channel interference on channels 21 (512 MHz - 518 MHz, "Rede Globo") and 23 (524 MHz - 530 MHz, "Rede Record"). Each channel has 6 MHz, the LTE signal transmitting antenna and the TV's reception antenna were spaced apart by 4 meters and the channels are arranged in frequency according to Figure 4.7.

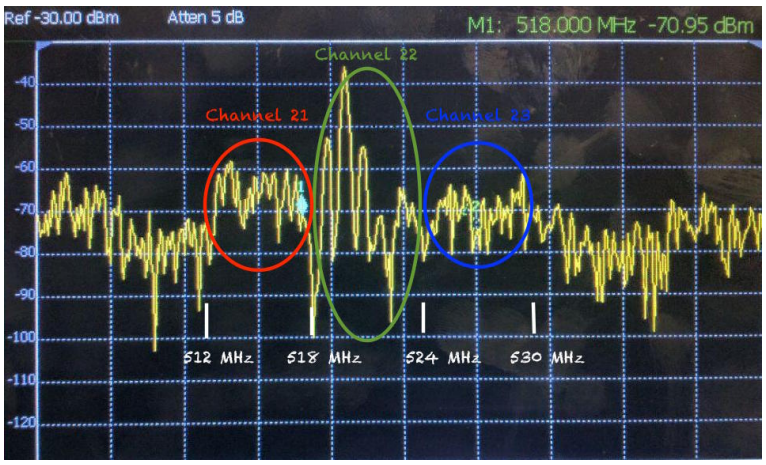

Figure 4.7: TV channels 21 to 23.

The experiment scenario consists of two transmission chains - the Brasília digital TV tower and a signal generator coupled to a directional antenna (Wilson Electronics Model 204411) - and a reception chain composed of a TV antenna (Philips SDV2210 / 55), a splitter, a N9914A FieldFox spectrum analyzer and a digital TV with integrated LNA, as shown in Figure 4.8. A second part of the experiment is composed by the same transmission and reception chain but at that time analyzing channel 51 (last DTV channel, 692 MHz - 698 MHz) and the first LTE channel at 708 MHz.

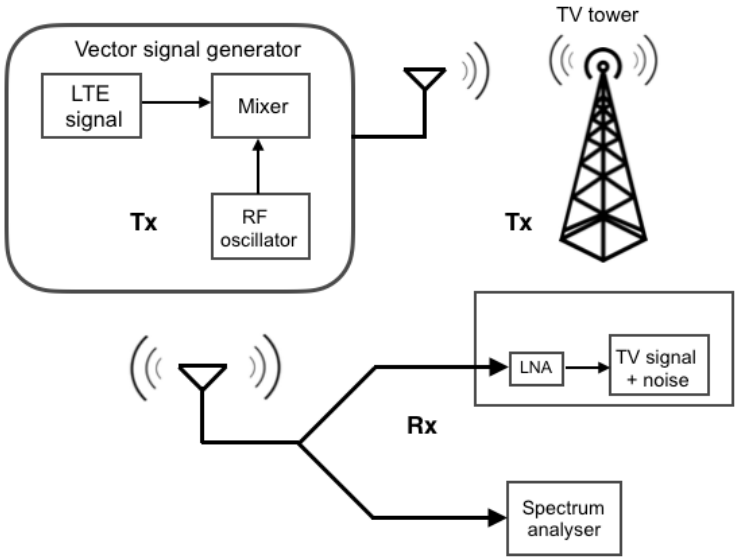

Figure 4.8: Transmission and Reception Diagrams of the LTE - ISDB-T scenario.

The Figures 4.9 and 4.10 illustrate the scenario created for the accomplishment of the test.

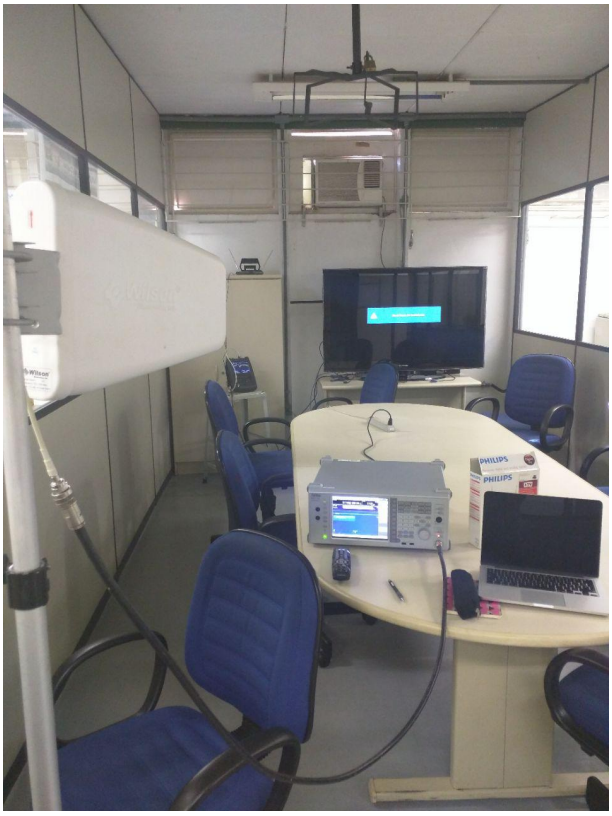

Figure 4.9: LTE and ISDB-T Systems scenario for coexistence analysis tests.

Figure 4.10: Digital TV Tower in Brasília.

4.3 PRACTICAL TESTS RESULTS

It is noted, as expected, that there was no change in signal quality on channel 21 or channel 23 with the insertion of the LTE signal on channel 22 using the maximum amplification of the signal generator (17 dBm). In order to find the values of the protection ratio for the channel 21 and 23, the LTE signal was translated in frequency until a signal drop in channels 21 and 23 be observed. The minimum values of the protection ratios (dB), obtained by means of Eq. (1), is presented at the end of Table 4.3.

$$P_R(dB) = Power_{Interfered}(dBm) - Power_{Interfering}(dBm), \tag{4.1}$$

in which $Pot_{Interfered}$ is the ISDB-T's power signal in the TV's reception antenna (already deducted the losses of cables and splitter) and $Power_{Interfering}$ is the LTE's power signal in the LTE's transmission antenna (already deducted the cable's losses).

Table 4.3: Channel 21 and 23 results with LNA turned ON.

	Channel 21	**Channel 23**
Signal level on LTE antenna	12,7 dBm	12,7 dBm
Signal level on TV antenna	-24,8 dBm	-27,2 dBm
LTE frequency that disrupts signals	517,960 MHz	524,410 MHz
Protection ratio (PR)	-37,5 dB	-39,9 dB

At this point, we will do the same experiment by turning of the TV's LNA.

Table 4.4: Channel 21 and 23 results with LNA turned OFF.

	Channel 21	**Channel 23**
Signal level on LTE antenna	12,7 dBm	12,7 dBm
Signal level on TV antenna	-31,8 dBm	-29,7 dBm
LTE frequency that disrupts signals	517,000 MHz	524,300 MHz
Protection ratio (PR)	- 44,5 dB	- 42,4 dB dB

It's easy to verify the importance of the integrated low noise amplifier. With the LNA turned on, the noise that arrives in the TV is softened and the necessary value of interference to make impossible the transmission in the TV is greater.

For the last digital channel located in the physical channel number 51 (692 MHz - 698 MHz) and the first LTE channel located at 708 MHz, practical experiments show that, in the conditions of this experiment, LTE signal do not interfere in the ISDB-T signal, since there is a 10 MHz guard between them. In this experiment, a 10 MHz LTE channel was created on the first available LTE channel (708 MHz - 718 MHz) and channel 51 did not presented any visible quality changes. To verify the protection ratio, the LTE signal was again translated in frequency and the Table 4.5 presents the results of this experiment. It is observed that for the LTE signal to interfere with the TV signal in order to make it impossible to see the TV programming it is necessary the protection ratio to be broken and in this experiment, the protection ratio was only broken when the channel 51 band was invaded by at least more than half by the LTE signal.

Table 4.5: Channel 51 results.

	LNA turned ON	**LNA turned OFF**
Signal level on LTE antenna	12,7 dBm	12,7 dBm
Signal level on TV antenna	-26,8 dBm	-27,8 dBm
LTE frequency that disrupts signals	698,460 MHz	698,650 MHz
Protection ratio (PR)	-39,5 dB	-40,5 dB

4.4 PREDICTION OF COVERAGE USING CELLPLANNER

In order to perform a coverage analysis of a system, it's necessary to determine and analyze several intrinsic aspects of the communication system such as location of base stations, characteristics of antennas and radio, parameters of transmission and reception (losses and gains), among others. For this coverage simulation, it will be used a software named CelPlanner whose settings and main characteristics are described in the following section.

4.4.1 CelPlanner Suite

CelPlanner™ is a advanced radio network design solution developed in close relationship with Ericsson used for planning and optimize wireless communication systems. It allows engineers to simulates results quickly and accurately. CelPlanner ™ works with many different existing wireless communications technologies, including AMPS (Advanced Mobile System), GSM, CDMA, GPRS, EDGE (Enhanced Data rates for GSM Evolution), WiMAX (Worldwide Interoperability for Microwave Access), among others. This tool was designed by the company CelPlan and some licenses were ceded to the University of Brasília for educational purposes.

It's main features includes

- Accurate Propagation Models
- Simultaneous multi-resolution 3D models for topography and morphology
- Multi-Technology Support
- Multiple image layers
- Propagation Analysis
- Multi-layered traffic information

CelPlanner software eliminates the exhaustive and empirical work of generating propagation parameters for a particular area of interest, since it is the only software that automatically determines the prediction parameters directly from the field measurements, offering degrees of precision and resolution never seen before.

The main use of the software in this work is the realization of RF coverage prediction studies (individual, composite) performed through classical algorithms.

To perform the RF coverage prediction, the software loads topology and site morphology information. Through the information of topography and morphology, each point in the propagation path between the ERB and the mobile station is analyzed in order to verify the existence of obstructions in the passage of signal, to determine the type of coverage on the ground (trees, buildings, water, avenues or squares) and the point of reflection in the soil and to obtain the effective height of the ERB's antenna. Figure 4.11 illustrate a screen shot of the CelPlanner software.

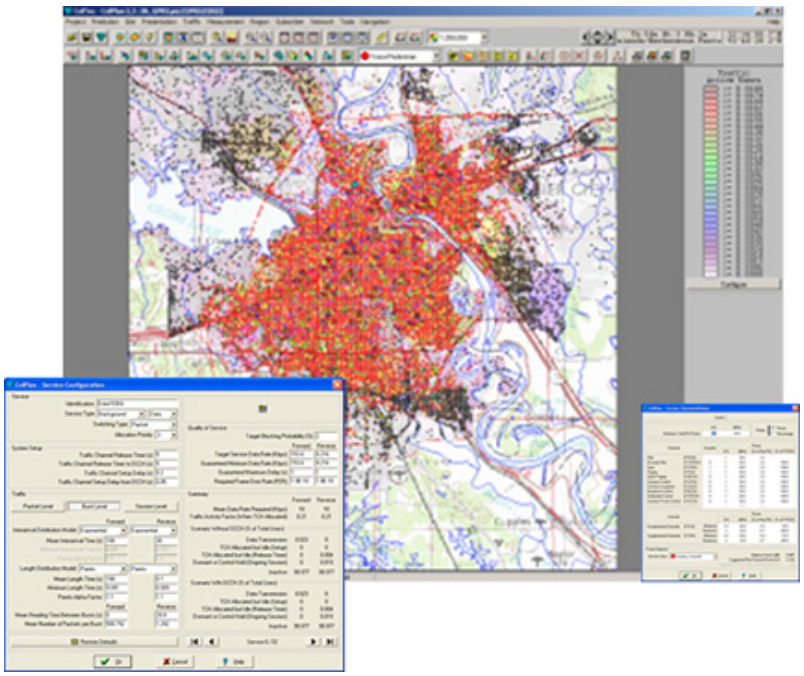

Figure 4.11: CelPlanner interface [32].

In this project, CelPlanner software is used to perform a combined coverage prediction of a 700 MHz LTE signal and TV signal on the neighborhood of Asa Norte, Brasília. The goal is to analyze the signal coverage offered to each subscriber and to compare the protection ratio (PR) obtained in the simulation with the values found in the practicals tests made by me in the university's lab and by the ANATEL in the city of Pirenópolis in order to verify whether the protection ratio will be broken or not.

For the same conditions of the tests made in laboratory (downlink, channel 51, subscribe with a intern antenna), the ANATEL's report shows a protection ratio (PR) between -39 dB and -41 dB, very close to the values found in the pratical tests of the previous section. For a scenario with a external antenna, the ANATEL's report shows a protection ratio (PR) of -46 dB. In this context, we will simulate the protection ratio of several subscribers in a specific part of Brasília and compare to the minimum PR values found in these practical tests.

4.4.2 Parametrization of CelPlan software

The CelPlan software has packages with morphological and topographic data of the Federal District, however it is necessary to parameterize and set the scenario of interest.

In this way, it was necessary to set some variables like the location of 700 MHz base radio stations (e-NodeB) in Brasília, characteristics of LTE and TV antennas (gain, tilt, type), information about the TV radio station and so on. In this simulation, it was considered 4 LTE radio base stations, a TV tower (Brasília's digital tower) and 107 subscribers evenly distributed in the neighborhood of Asa Norte.

The most important information of the simulation parametrization will be described below and in Tables 4.6 to 4.8.

- Earth curvature factor in the value of 1.333;
- Required service availability of 99.99%;
- Gausian distribution for human body attenuation with mean of 3dB and standard deviation of 2dB;
- Gausian distribution for penetration attenuation with mean of 0dB and standard deviation of 1dB;
- Punctual precipitation rate of 79.44 mm/h.

Table 4.6: Fading parameters

Fading	
Area attenuation factor	35 (dB/Dec)
Coverage probability	90 %
Probability Universe	Edge
Intra cell correlation factor	0.9
Inter cell correlation factor	0.3
Shadow Fading	
Distribution	Lognormal
Standard deviation	1 dB
Multipath Fading	
Distribution	Rician
K Factor	Prediction (Morphology)
Results	
Fading severity	Moderate
Prediction margin	4.282 dB

4.4.2.0.1 TV parametrization Regarding the TV link, with the aim of getting as close as possible to the real features of the scenario it was used an omnidirectional antenna with gain of 10dB with link information chosen in order to obtain an output power value of 3kW with a effective radiated power of 4730W, real values practiced in the city of Brasília. Figure 4.12 illustrates the radiation pattern.

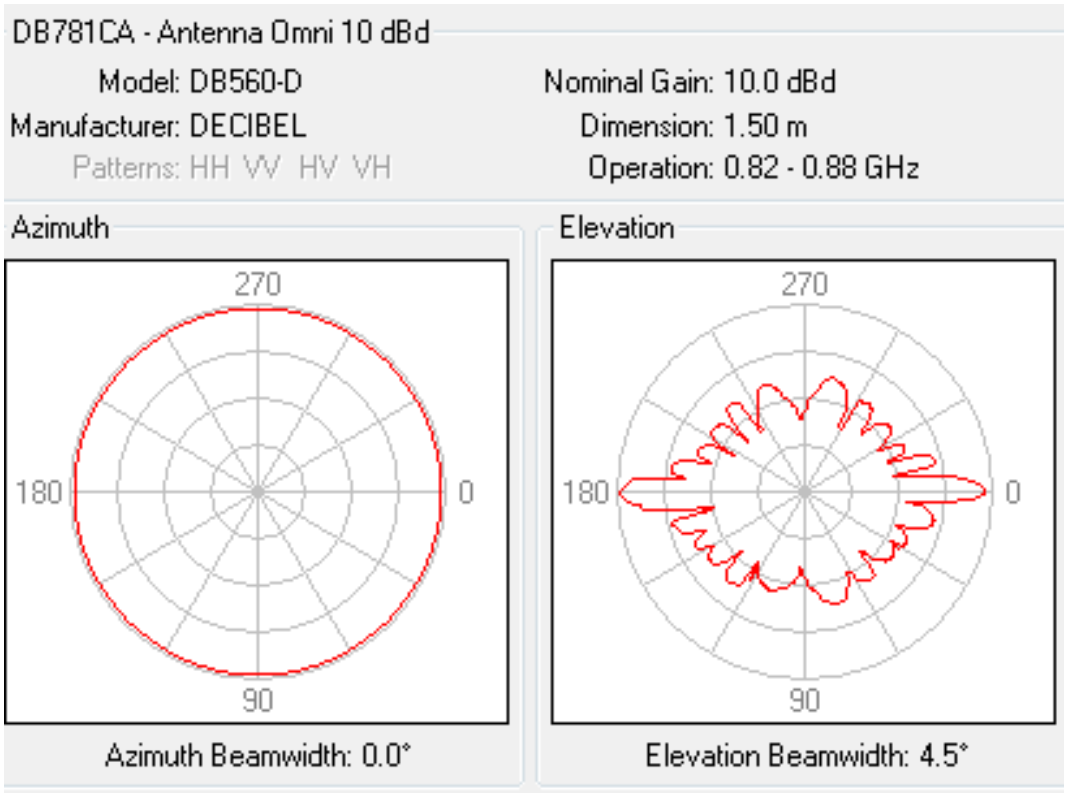

Figure 4.12: TV Antenna radiation pattern.

Regarding the link budget information, Table 4.7 illustrates its information.

Table 4.7: TV cell link budget

Tx Parameters	
Amplifier Output Power	2999 W
Reference Signal Power	18.24 dBm
Cable Losses	4 dB/100 m
Cable Lenght	28 m
Connection Loss	0.5 dB
Number of Connections	4
MIMO	
Number Tx Antennas	1
Radiated Power	
Effective Radiated Power	4731 W (66.7 dBm)

It is also important to say that the TV antenna is 170m from the ground, has horizontal polarization, no tilt and 50 m of cell radius, covering the entire city of Brasília. ITU-R P.1546-4 is the prediction model used in the cell.

4.4.2.0.2 LTE parametrization Then, regarding the LTE parameterization, it was used a 120 sectorial antenna of 14.4 dBd gain in order to obtain an output power value of 10W for the LTE base station. Figure 4.13 shows the radiation pattern of the LTE antenna used in the simulation.

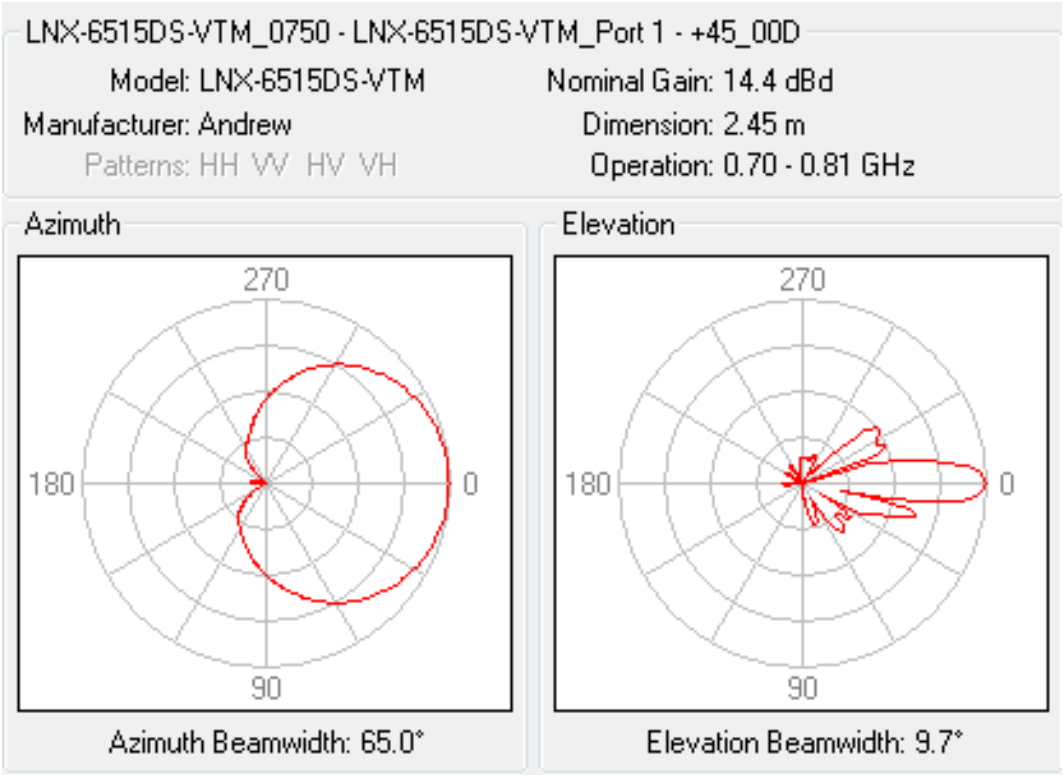

Figure 4.13: LTE Antenna radiation pattern.

The LTE link budget with all LTE link information is illustrated in Table 4.8. It is important to highlight the Tx power of 10 W, the losses in cables and connectors and the antenna gain already specified before.

Table 4.8: LTE cell link budget

Tx Parameters		**Rx Parameters**	
Amplifier Output Power	10 W	Subscriber Output Power	0.199
Reference Signal Power	18.24 dBm	Base Antenna Rx Gain	14.4 dBd
Transmission Gains	0 dB	Reception Gains	3 dB
Transmissions Losses	0 dB	Reception Losses	0 dB
Cable Loss	4 dB/100 m	Cable Loss	4 dB/100 m
Cable Lenght	10 m	Cable Lenght	10
Connection Loss	0.5 dB	Connection Loss	0.5 dB
Number of Connections	4	Number of Connections	4
Base Antenna Tx Gain	14.4 dBd		
Radiated Power			
Effective Radiated Power		158.5 W (52.0 dBm)	
MIMO			
Number Tx Antennas		1	

Besides all the parameters previously presented, each LTE cell was configured as shown below

- Use of the ITU-R P.1812-1 prediction model;
- Vertical polarization for Transmission and Reception;
- No antenna vertical inclination (0 tilt);
- 10 km radius reach;
- Antenna height of 30 m.

4.4.2.0.3 Subscribers parametrization For the subscribers, the coverage simulation was divided into 2 parts: the subscriber on the first floor of a residential building (5 meters from the ground) using an internal dipole antenna with gain 0 dBm and the subscriber on the third floor of a residential building (15 meters from the ground) using an external Yagi antenna of gain 10 dBm. This parameters aims to verify the signal coverage in two different but common situations for residential users in Brasília. Figure 4.14 illustrates the radiation pattern for the dipole and for the Yagi antenna, respectively.

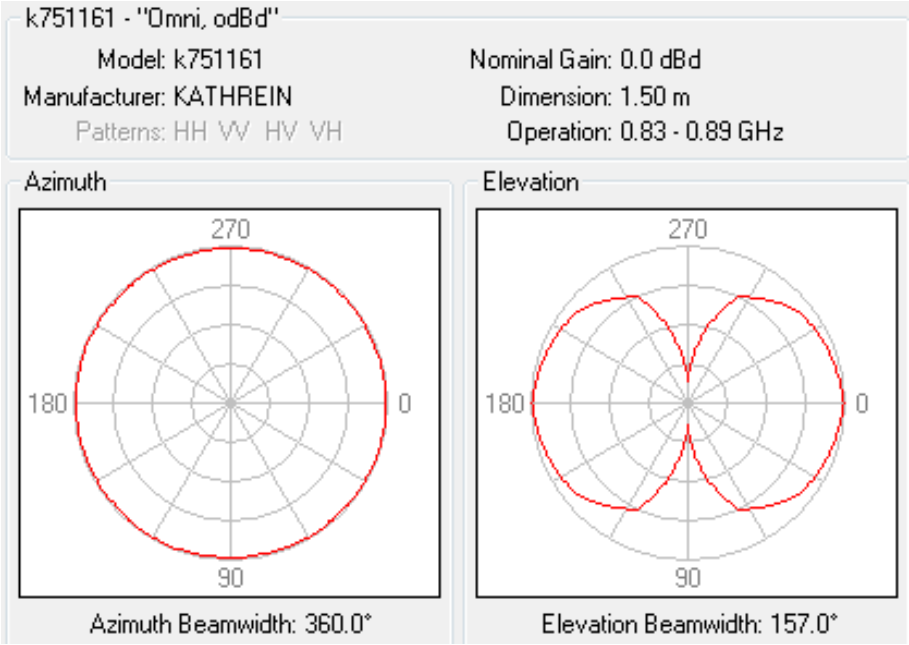

Figure 4.14: Subscriber antenna radiation pattern for the case of a user in the first floor.

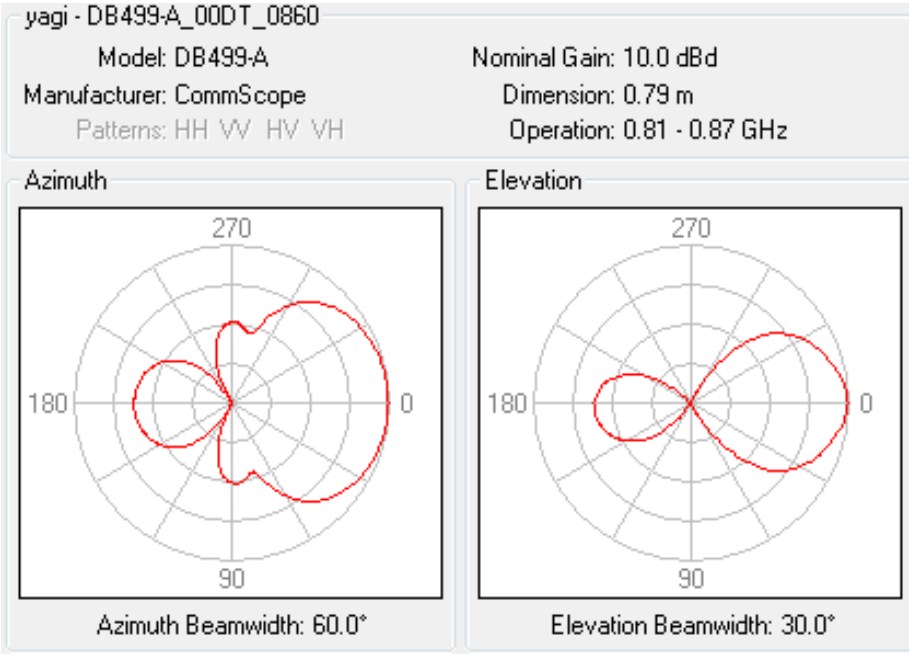

Figure 4.15: Subscriber antenna radiation pattern for the case of a user in the third floor.

4.4.3 Predictions and results

After finalizing the parameterization of the scenario and subscribers around the area of interest, the predictions were made and the power values (in dBm) of each LTE base station and TV cell were captured for each subscriber. For this work, a C code was developed in order to speed up the data processing.

The software CelPlanner, taking into account all the parameters defined by the the environment and morphology of the city of Brasília, presents the coverage area of each cell of the simulation. In this project, we are interested in knowing the coverage area of the TV cell and of the set of LTE base stations, as presented in the Figures 4.16 and 4.19.

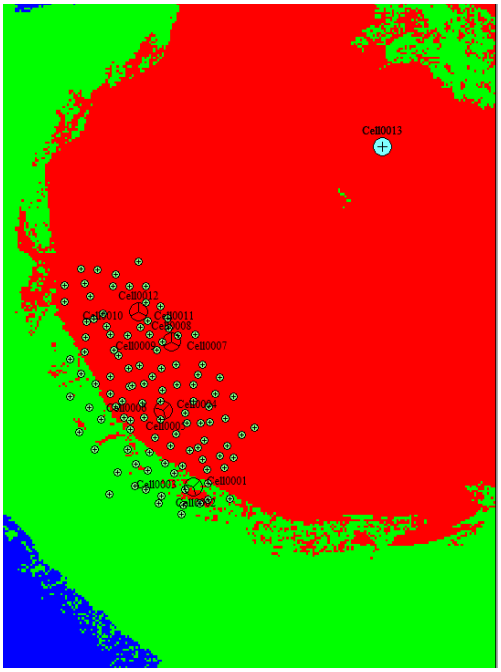

Figure 4.16: Tv coverage area.

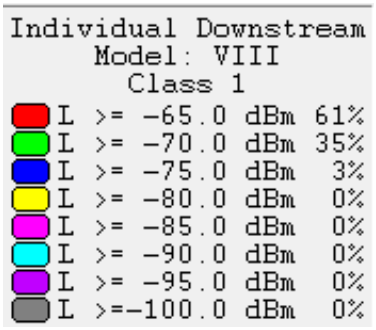

Figure 4.17: Tv coverage area label.

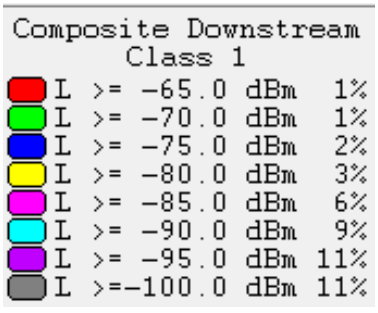

Figure 4.18: LTE coverage area label.

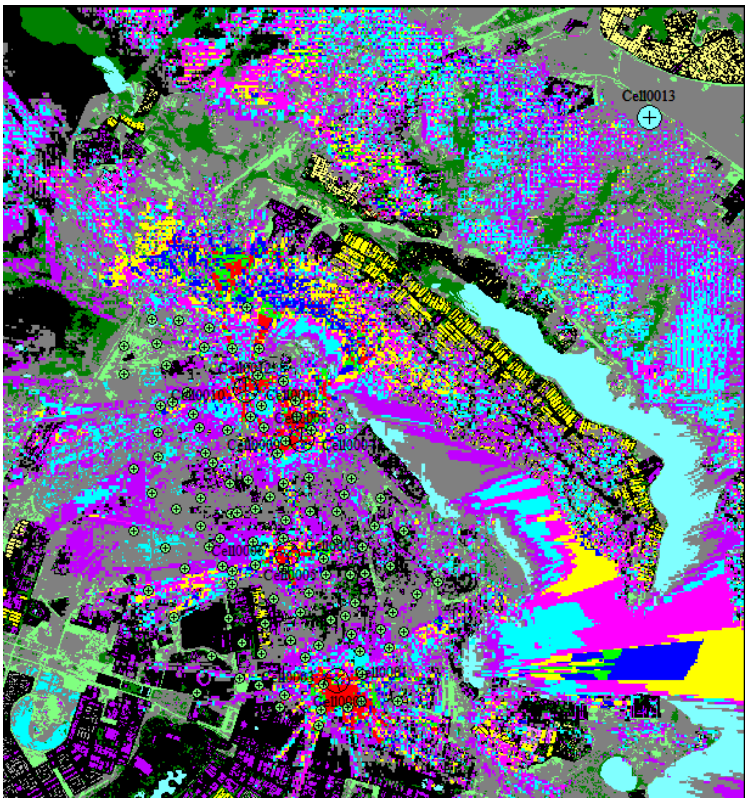

Figure 4.19: LTE coverage area.

Regarding the two subscribers cases, two simulations were performed. In the first simulation the subscriber was on the first floor of a residential building and in the second simulation the subscriber was on the third floor of a residential building. Like in Brasília most of residential properties have 3 floors, for a subscriber on the top floor it is more likely that he will be using an external antenna that is placed on the slab of the building.

For the first simulation, the protection ratio for each LTE cell was calculated using the formula in Eq 4.1. After, for each LTE cell, the highest and lowest protection ratio is illustrated in the Figure 4.20.

```
Subscriber antennas at 5 meters from the ground

Cell 1 : MAX: 89.00 (usu: SbCr0000054), MIN: -4.00 (usu: SbCr0000088)
Cell 2 : MAX: 121.00 (usu: SbCr0000054), MIN: -24.00 (usu: SbCr0000020)
Cell 3 : MAX: 81.00 (usu: SbCr0000033), MIN: -26.00 (usu: SbCr0000095)
Cell 4 : MAX: 90.00 (usu: SbCr0000034), MIN: -16.00 (usu: SbCr0000068)
Cell 5 : MAX: 106.00 (usu: SbCr0000037), MIN: -1.00 (usu: SbCr0000070)
Cell 6 : MAX: 98.00 (usu: SbCr0000016), MIN: -17.00 (usu: SbCr0000068)
Cell 7 : MAX: 102.00 (usu: SbCr0000035), MIN: 7.00 (usu: SbCr0000067)
Cell 8 : MAX: 110.00 (usu: SbCr0000105), MIN: -18.00 (usu: SbCr0000002)
Cell 9 : MAX: 80.00 (usu: SbCr0000101), MIN: -21.00 (usu: SbCr0000026)
Cell 10 : MAX: 77.00 (usu: SbCr0000086), MIN: 12.00 (usu: SbCr0000062)
Cell 11 : MAX: 88.00 (usu: SbCr0000033), MIN: -5.00 (usu: SbCr0000055)
Cell 12 : MAX: 106.00 (usu: SbCr0000019), MIN: -17.00 (usu: SbCr0000055)
Cell 13 : MAX: 0.00 (usu: Sb0000001), MIN: 0.00 (usu: Sb0000001)


MAX TOT : 121.00 , MIN TOT: -26.00
```

Figure 4.20: Result of highest and lowest protection ratio calculated in each cell in dBm for internal antenna at 5m from the ground.

For the second simulation, changing the antenna height and type, the same kind of results are presented in the Figure 4.21.

```
Subscriber antennas at 15 meters from the ground

Cell 1 : MAX: 85.00 (usu: SbCr0000048), MIN: -19.00 (usu: SbCr0000085)
Cell 2 : MAX: 118.00 (usu: SbCr0000054), MIN: -21.00 (usu: SbCr0000020)
Cell 3 : MAX: 78.00 (usu: SbCr0000051), MIN: -22.00 (usu: SbCr0000095)
Cell 4 : MAX: 82.00 (usu: SbCr0000034), MIN: -13.00 (usu: SbCr0000068)
Cell 5 : MAX: 99.00 (usu: SbCr0000053), MIN: -1.00 (usu: SbCr0000070)
Cell 6 : MAX: 90.00 (usu: SbCr0000086), MIN: -17.00 (usu: SbCr0000070)
Cell 7 : MAX: 99.00 (usu: SbCr0000054), MIN: 7.00 (usu: SbCr0000060)
Cell 8 : MAX: 106.00 (usu: SbCr0000105), MIN: -19.00 (usu: SbCr0000073)
Cell 9 : MAX: 73.00 (usu: SbCr0000077), MIN: -21.00 (usu: SbCr0000026)
Cell 10 : MAX: 69.00 (usu: SbCr0000019), MIN: 5.00 (usu: SbCr0000072)
Cell 11 : MAX: 85.00 (usu: SbCr0000033), MIN: -12.00 (usu: SbCr0000072)
Cell 12 : MAX: 99.00 (usu: SbCr0000020), MIN: -18.00 (usu: SbCr0000055)
Cell 13 : MAX: 0.00 (usu: Sb0000001), MIN: 0.00 (usu: Sb0000001)


MAX TOT : 118.00 , MIN TOT: -22.00
```

Figure 4.21: Result of highest and lowest protection ratio calculated in each cell in dBm for external antenna at 15m from the ground.

Like to a scenario with a intern antenna the ANATEL's report show a PR value between -39 dBm and -41 dBm and the Figure 4.20 shows that the minimum PR value found was -26 dBm, the subscribes of this scenario will not be affected by interferences between the LTE signal and the digital TV.

For the second scenario we find the same conclusion. The ANATEL's report says it is necessary at least -41 dB of PR to the TV signal be effectively affected by LTE's signal and the lowest PR value found in the scenario was -22 dBm.

As seen in the above results, for the both simulated scenario the protection ratio will not be broken. In this way, to broke the protection ratio some changes must be made, like

- Change antenna characteristics such as pointing and height;
- Decrease the DTV effective transmission power;
- Increase the LTE effective transmission power.

Like decreasing the DTV effective transmission power is not feasible in a real scenario, for breaking the the protection ratio it is necessary to increase the LTE effective transmission power in lots of Watts.

4.5 CONCLUSION

Through the coexistence analysis between the LTE an ISDB-T systems, we obtain the protection ratio values for each scenario with and without the intern LNA. The realistic tests shows that it is difficult to interfere with the TV signal, modulated in OFDM, if the frequency ranges of each channel are respected. Regarding the tests in laboratory, the values found for the protection ratio were very similar to the values found by ANATEL in 2014 at Pirinopolis.

For the CelPlan simulations, as the characteristics of the antennas as gain and height were equivalent to the real data and given the low probability of decreasing the effective transmission power of the antenna of the TV station, it is verified that in this real scenario of the neighborhood of Asa Norte, taking into account the urban morphology and the RF characteristics, the users will not have problems with the TV signal due to interference from the 700MHz LTE signal.

5 SHARC SIMULATOR FOR USE IN SHARING AND COMPATIBILITY STUDIES

The increasing use of mobile broadband services and the increasing user's expectations for better mobile internet experiences are motivating industry, academia, and governments to explore ways to address these demands. With the objective of enabling the technical aspects to meet the demand for more services and capacity for mobile broadband, the identification of new frequency bands for "International Mobile Telecommunications (IMT)" is under discussion.

In order to prepare a research and development scenario for the IMT-2020, the International Telecommunication Union - ITU created the program "International Mobile Telecommunications (IMT) for 2020 and beyond", which motivated the inclusion of the item 1.13 in the Agenda of the World Conference Radiocommunication Conference to be held in 2019 (WRC-19).

"Item 1.13: to consider identification of frequency bands for the future development of International Mobile Telecommunications (IMT), including possible additional allocations to the mobile service on a primary basis, in accordance with Resolution 238 (WRC-15);"

Given this scenario, it is important to the Brazilian Administration to highlight the relevance of searching technical basis to satisfy this agenda item based on the development of studies in the identification of possibles new frequency bands for IMT-2020, with a focus on sharing with other services. In this sense, it is observed the need to develop modeling and simulations systems for IMT through an open source simulator that allows the elaboration of constructive contributions for the study.

The initial scope of the simulator is presented on the New Recommendation Draft ITU-R M. [IMT.MODEL] (Modeling and simulation of IMT networks and systems for use in sharing and compatibility studies), document which will be used as a base document to the implementation of the models.

The recommendation ITU-R P.452 "Prediction procedure for the evaluation of interference between stations on the surface of the Earth at frequencies above about 0.1 GHz", specifies the most important propagation interference mechanisms to the scenario of two stations on the surface of the Earth. The Figure 5.1 illustrates some of this mechanisms and the next sections will discuss the mathematics implementation of these mechanisms.

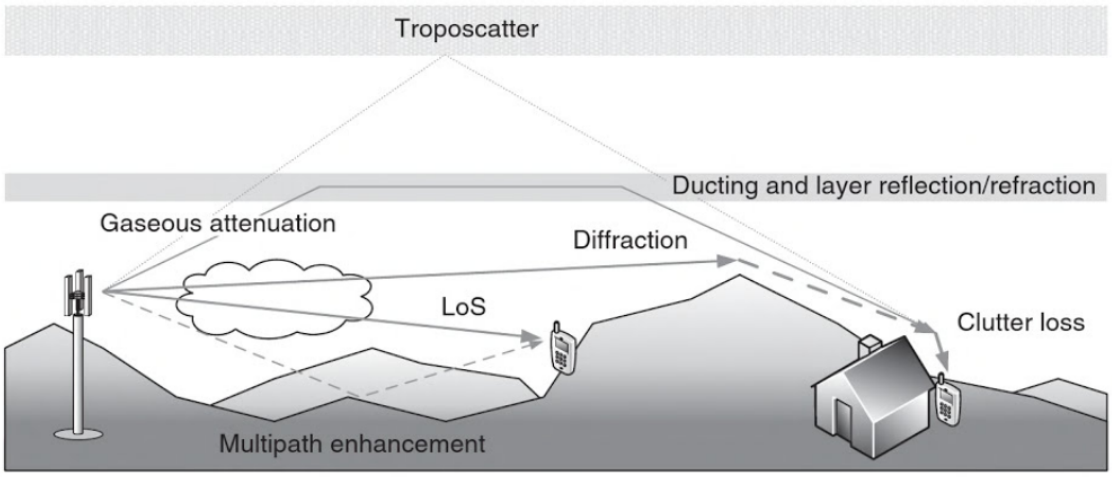

Figure 5.1: Elements in Recommendation ITU P.452: propagation models [33].

In the end of 2016, the sector of Spectrum, Orbit and Broadcast Management (ORER) of the Brazilian national telecommunications agency (ANATEL) and the department of Electrical engineering of the University of Brasília made some arrangements to start working on the SHARC projet. To develop the simulator, each participant of the project was responsible for one module of development and after the conclusion of all the modules necessary for the studies of spectrum sharing, all participantes were free to carry out the studies they wanted since the tool would be freely accessible.

The contribution of this final course work on this project is based in the development of the module that implements the propagation interference mechanisms for stations on the surface of the Earth using the ITU recommendation ITU-R P.452 and the implementation of some important pathloss models previously defined in accordance with the interests of the group. After the development of all the modules, the final goal was to perform a study of coexistence between the IMT-2020 (5G) and the services that already exist today in the frequency band of 24.25 - 27.5 GHz, one of the most rated bands for 5G. The basic input data required for the procedure is given in Table 5.1. All other information required is derived from these basic data during the execution of the procedure.

The entire simulator code was developed in Python using Spyder development environment. The results of each implementation will be present in graphical form since it better illustrates each mechanism implementation behavior along frequency variation.

Table 5.1: Main variables and their values

Variable	Definition	Value
d	Distance (Km)	0 Km to 40 Km
f	Frequency (GHz)	5GHz to 40GHz
T	Temperature (K)	288 K
ρ	Water vapour density	$3g/m^3$
H_0, H_n	Ground height of interfering and interfered-with station (m)	15 m, 17 m
H_{te}, H_{re}	Effective height of interfering and interfered-with antenna (m)	50 m, 50 m
p	Dry air pressure (hPa)	1013 hPa
p_t	Percentages of time (%)	40%
P	Probability that loss is not exceeded	0.9
Ω	Fraction of the total path over water	0
θ_t, θ_r	Transmit and receive horizon elevation angles	20 mrad, 20 mrad
G_t, G_r	Antenna gain (dBi)	10 dB, 10 dB
d_{lt}, d_{lr}	Distance from the transmit and receive antennas to their respective horizons (km)	30 km, 10 km
d_{ct}, d_{cr}	Distance over land from the transmit and receive antennas to the coast (km)	10 km, 10 km
N_0	Sea-level surface refractivity	355
ΔN	Average radio-refractive	60
H_{ts}, H_{rs}	Transmit and receive antenna centre height above mean sea level (m)	280 m, 244 m
H_{st}, H_{sr}	Transmit and receive height of the smooth-Earth surface (amsl)	48 amsl, 45 amsl
A_{ht}, A_{hr}	Additional losses to account for clutter shielding the transmitter and receiver (dB)	0 dB, 0 dB

5.1 PROPAGATION MECHANISMS OF ITU P.452

This section presents the implementation results of ITU P.452 mechanisms illustrated in section 2.3.2.1 to 2.3.2.4 of this document.

5.1.1 Line-of-sight (including short-terms effects)

The first propagation model discuted in the ITU P.452 recommendation is the Line-of-sight model, which is a basic transmission loss due to free-space propagation and attenuation by atmospheric gases. This loss is written as

$$L_{bfsg} = 92.5 + 20\log(f) + 20\log(d) + A_g, \tag{5.1}$$

in which A_g is the total gaseous absorption (dB) described in the recommendation ITU-R P.619 as

$$A_g = [\gamma_o + \gamma_w(\rho)]d, \tag{5.2}$$

in which

- γ_o, γ_w are the specific attenuation due to dry air and water vapour;

- ρ is water vapour density : $\rho = 7.5 + 2.5\omega\ g/m^3$;

- ω is the fraction of the total path over water.

The specific attenuation equations are described as

$$\gamma_o + \gamma_w = 0.1820f(N"_{oxygen}(f) + N"_{WaterVapour}(f)) \quad (dB/Km), \tag{5.3}$$

in which

$$\begin{array}{l} N''_{oxygen}(f) = \sum_{i(oxygen)} S_i F_i + N''_D(f), \\ N''_{waterVapour}(f) = \sum_{i(waterVapour)} S_i F_i, \end{array} \tag{5.4}$$

and

$$\begin{array}{ll} S_i = a_1 \times 10^{-7} p\theta^3 \exp[a_2(1-\theta)] & for \quad oxigen, \\ S_i = b_1 \times 10^{-1} e\theta^{3.5} \exp[b_2(1-\theta)] & for \quad water \quad vapour, \end{array} \tag{5.5}$$

The parameters in equation 2.35 are defined in Recommendation ITU-R P.676 [34] as

- p: the dry air pressure (hPa);

-e: water vapour partial pressure (hPa), $e = \frac{\rho T}{216.7}$;

-θ: represented as 300/T.

The line-shape factor is given by

$$F_i = \frac{f}{f_i}[\frac{\Delta f - \delta(f_i - f)}{(f_i - f)^2 + \Delta f^2} + \frac{\Delta f - \delta(f_i + f)}{(f_i + f)^2 + \Delta f^2}], \tag{5.6}$$

in which f_i is the oxygen or water vapour line frequency and Δf is the width of the line written as

$$\begin{array}{ll} \Delta f = a_3 \times 10^{-4}(p\theta^{(0.8-a_4)} + 1.1e\theta) & for \quad oxigen, \\ \Delta f = b_3 \times 10^{-4}(p\theta^{b_4} + b_5 e\theta^{b_6}) & for \quad water \quad vapour, \end{array} \tag{5.7}$$

δ is a correction factor that arises due to interference effects in oxygen lines given by

$$\begin{array}{cc} \delta = (a_5 + a_6\theta) \times 10^{-4}(p+e)\theta^{0.8} & for \quad oxigen, \\ \delta = 0 & for \quad water \quad vapour, \end{array} \tag{5.8}$$

and $N''_D(f)$ is the dry continuum due to pressure-induced nitrogen absorption and the Debye spectrum given by

$$N''_D(f) = fp\theta^2[\frac{6.14 \times 10^{-5}}{dist[1+(\frac{f}{dist})^2]} + \frac{1.4 \times 10^{-12} p\theta^{1.5}}{1 + 1.9 \times 10^{-5} f^{1.5}}], \tag{5.9}$$

in which $dist$ is the width parameter for the Debye spectrum written as

$$dist = 5.6 \times 10^{-4}(p+e)\theta^{0.8}. \tag{5.10}$$

The variables a_1 to a_6 and b_1 to a_5 in Eq.5.7 are illustrated in Recommendation ITU-R P.676 [34].

This propagation model was implemented in Python using the ITU-R P.676 as basis and the ITU-R P.836 [35](Water vapour: surface density and total columnar content) to find the values of water vapour. The Figure 5.2 shows the values of water vapour for each latitude and longitude.

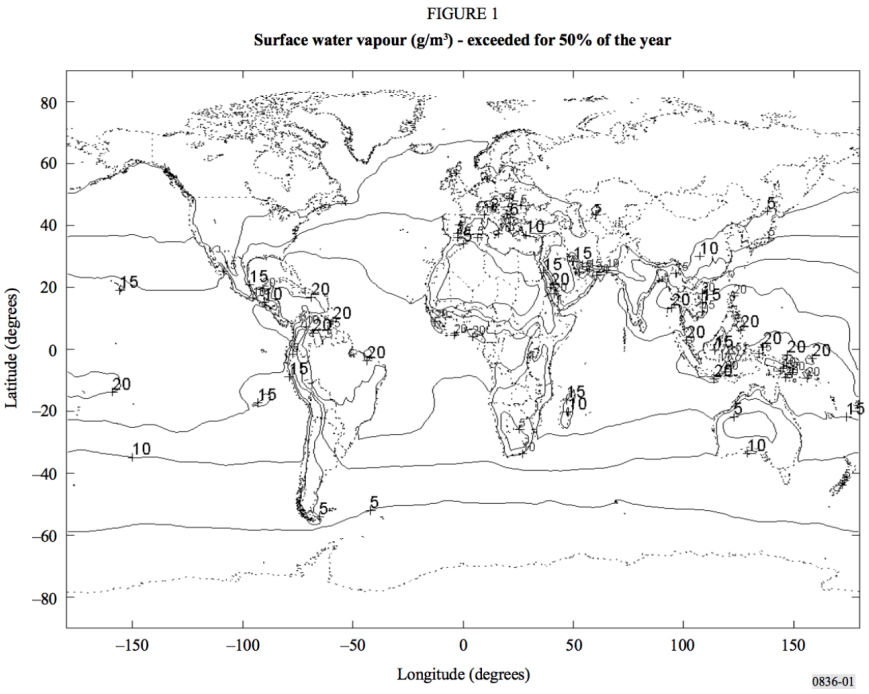

Figure 5.2: Water vapour values for each latitude and longitude [35].

Some corrections for multipath and focusing effects at p and β_0 percentage times are written as

$$E_{sp} = 2.6[1 - \exp(-0.1(d_{lt} + d_{lr}))]log(p/50), \tag{5.11}$$

$$E_{s\beta} = 2.6[1 - \exp(-0.1(d_{lt} + d_{lr}))]log(\beta_0/50), \tag{5.12}$$

and the final losses after corrections are written as

$$L_{b0p} = L_{bfsg} + Esp, \tag{5.13}$$

$$L_{b0\beta} = L_{bfsg} + Es\beta. \tag{5.14}$$

5.1.1.1 Line-of-sight implementation results

Line of sight basic transmission loss due to free-space propagation and attenuation by atmospheric gases (A_g) is described in Eq. 5.1. Using the parameters of Table 5.1, the specific attenuation due to atmospheric gases is illustrated in the Figure 5.3.

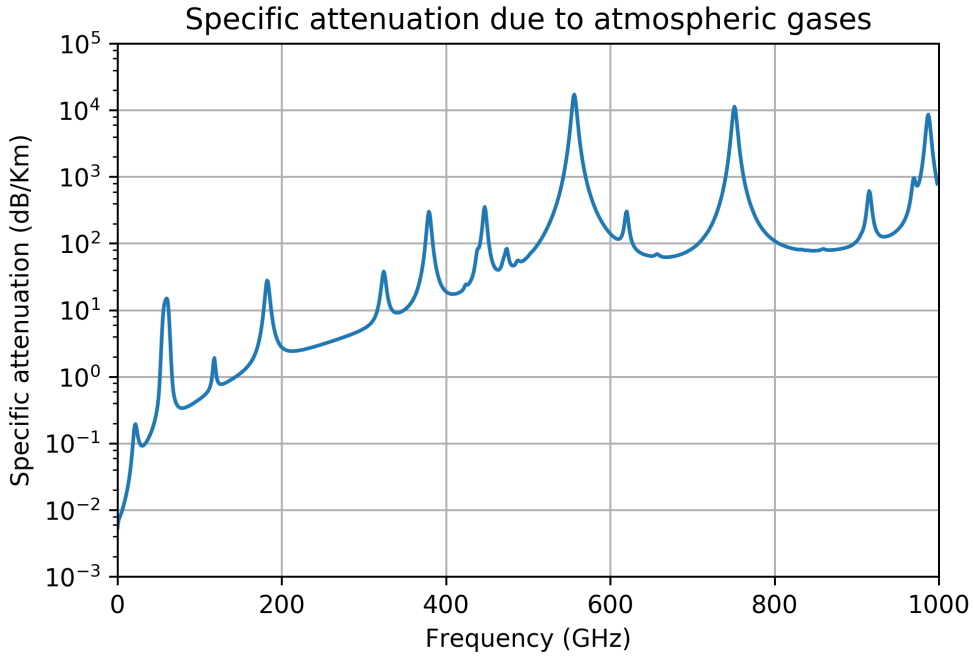

Figure 5.3: Specific attenuation due to atmospheric gases.

This figure shows how the attenuation increases with frequency increasing. For frequencies until 15GHz, the attenuation factor in less than 0.1 dB/Km, what makes this frequency range very disputed. Shortly thereafter it is possible to verify another point of low attenuation values between 26GHz and approximately 42 GHz. It is from the interpretation of this kind of information that possible frequency bands for the 5G are raised. Currently, first deployments of higher 5G bands in the US are 27.5 – 28.35 GHz and 37 – 40 GHz, exactly the first ranges of lower atmospheric gas attenuation after 15GHz.

After the implementation of the attenuation due to atmospheric gases, the Line-of-sight propagation model was implemented using the Eq. 5.2 and the results for its losses varying the frequency from 5GHz to 40GHz and the distance from 0 Km to 40 Km are illustrated in the Figure 5.4.

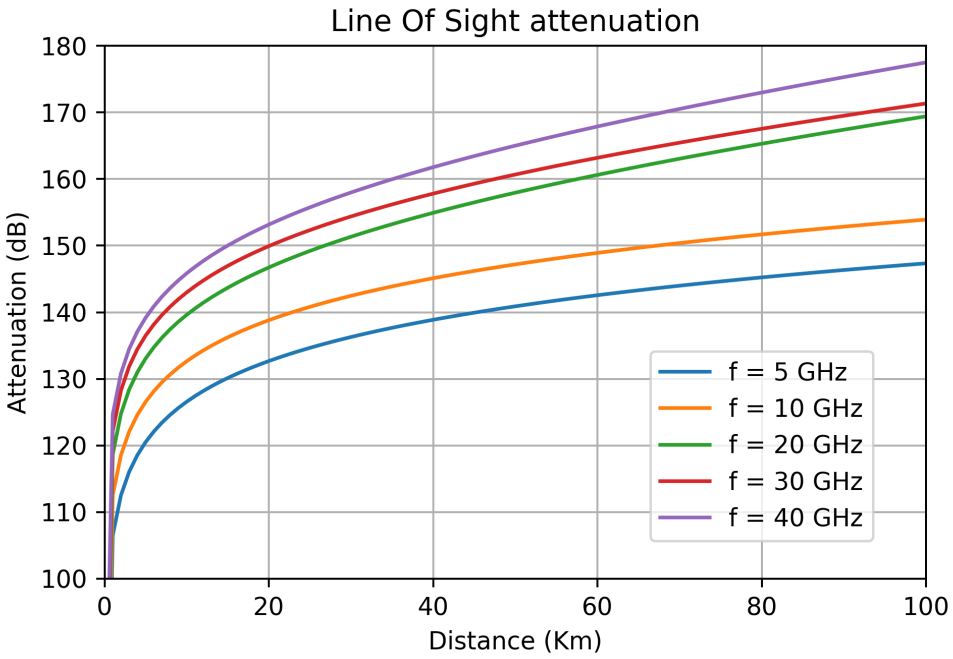

Figure 5.4: Line-of-sight attenuation.

As expected, the line-of-sight attenuation varies its values in function of the distance, the frequency and the atmospheric parameters used to calculate the total gaseous absorption. Figure 5.4 shows also that the attenuation difference between the frequencies of 5GHz and 40GHz under the same conditions can reach 30 dB/Km, a considerable value that should be taken into account.

5.1.2 Tropospheric scatter

Troposcatter communications systems emerged during the 1950s, during the period of intensive strategic competition between the NATO nations and the Warsaw Pact, prior to the advent of satellite communications.

Differently from conventional microwave relay communications networks, the beam is bounced off the upper troposphere, providing a true BLOS point to point communications capability. These systems rely on the irregularity of the refractivity gradient at such altitudes, resulting in impinging microwave power being scattered forward in an irregular fashion.

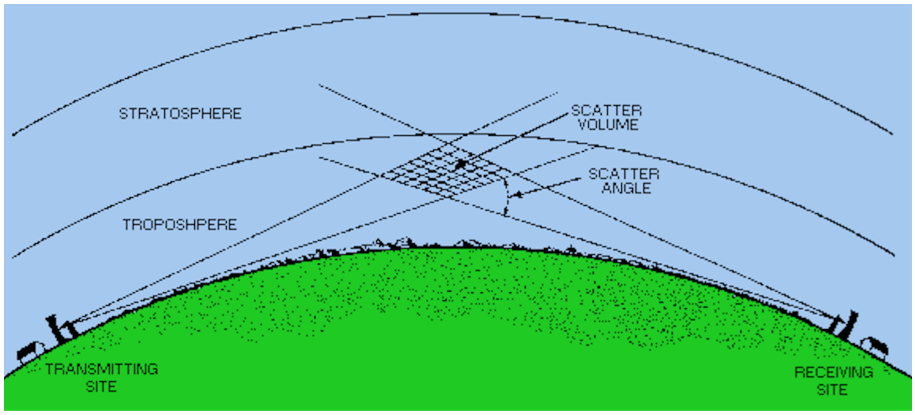

Figure 5.5: Troposphere scattering propagation.

Although the achievable channel capacity and thus data rates for troposcatter systems are quite poor in comparison with direct line of sight (LOS) and although the required high power transmitters, sensitive receivers and high gain antennas, troposcatter systems provides a very convenient data transmission system for many radio communications applications an it is cheaper than using satellites for many medium distance applications. In this section it will be discussed the basic transmission loss due to troposcatter not exceeded for any percentage, p, below 50%.

The basic transmission loss formula is given by

$$L_{bs} = 190 + L_f + 20\ log(d) + 0.573\theta - 0.15N_0 + L_c + A_g - 10.1[-\ log(p_t/50)]^{0.7}, \quad (5.15)$$

in which

- L_f is the frequency dependent loss

$$L_f = 25\log(f) - 2.5[\log(f/2)]^2, \quad (5.16)$$

- L_c is the aperture to medium coupling loss (dB)

$$L_c = 0.051e^{0.055(G_t+G_r)}, \quad (5.17)$$

-N_0 is the path centre sea-level surface refractivity derived from ITU-R P.453-6 [36],

-A_g is the gaseous absorption derived from Eq. 5.1 of this document using $\rho = 3\ g/m^3$.

The path angular distance θ (mrad) is calculated using the medium value of effective Earth radius a_e using the equations 5.18 to 5.20

$$\theta = \frac{10^3 d}{a_e} + \theta_t + \theta_r, \tag{5.18}$$

$$a_e = 6371.k_{50}, \tag{5.19}$$

$$k_{50} = \frac{157}{157 - \Delta N}. \tag{5.20}$$

The values of N_0 and ΔN (radio refractivity index) are derived from ITU-R P.453-6 and showed in the Figures 5.6 and 5.7 for longitude and latitude values.

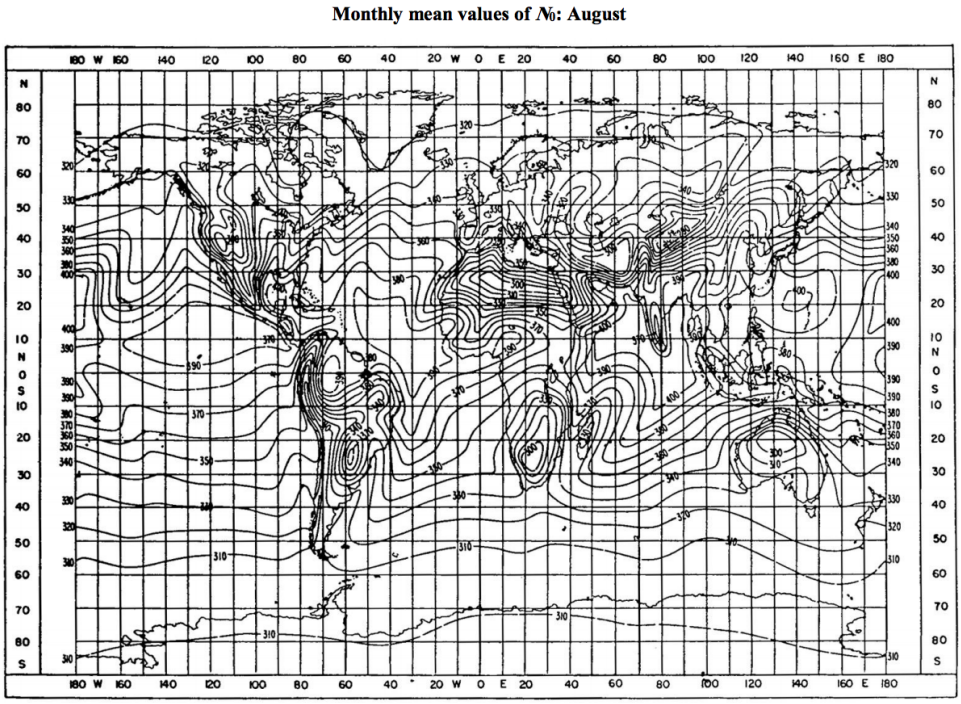

Figure 5.6: Sea-level surface refractivity for August [36].

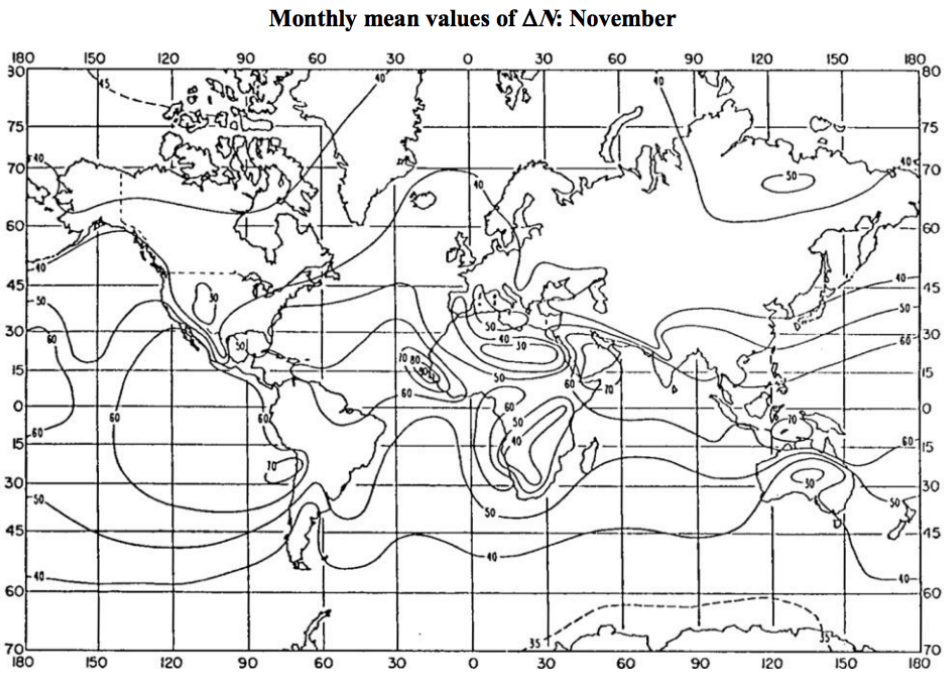

Figure 5.7: Radio refractivity index for November [36].

5.1.2.1 Tropospheric implementation results

After the implementation of the equations that modelates the tropospheric scatter mechanism and using parameters of Table 5.1, the attenuation values for the tropospheric scatter propagation varying the frequency from 5GHz to 40GHz and the distance from 0 Km to 40 Km is illustrated in the Figure 5.8.

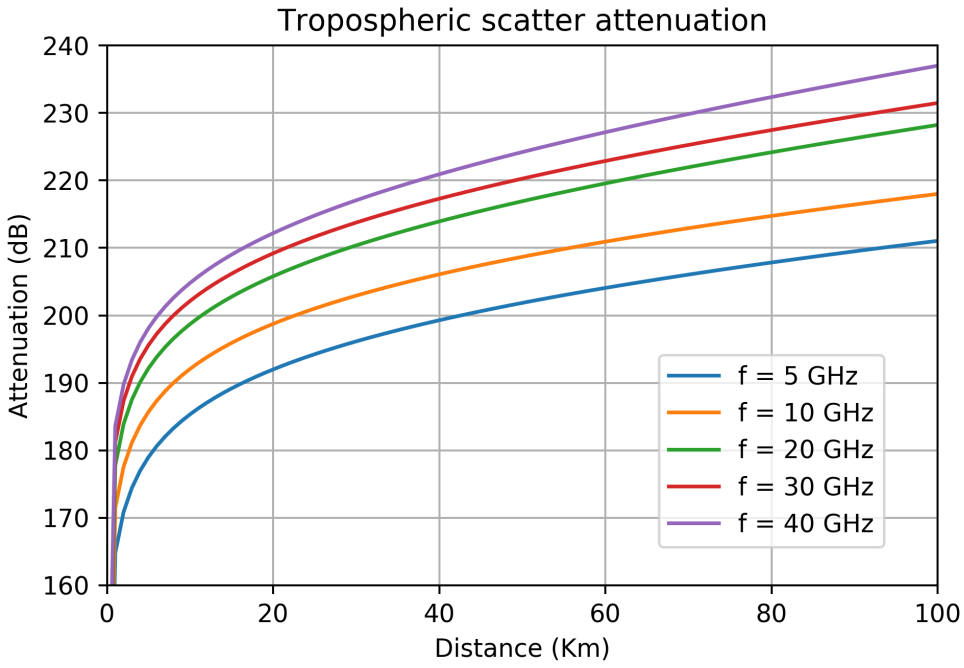

Figure 5.8: Tropospheric scatter attenuation.

Analyzing the graph, the same behavior of the previous session is found. The attenuation increases as a function of distance and frequency, with differences of up to 30 dB between the lowest and highest frequencies. It is also notable that the tropospheric scatter attenuation is much higher when compared to the line-of-sight attenuation, what is expected.

5.1.3 Ducting an layer reflection/refraction

Anomalous propagation includes different forms of radio propagation due to an unusual distribution of temperature and humidity with height in the atmosphere. One of the main causes of anomalous propagation is the ducting and layer reflection, that can guide part of the radiated and target-reflection energy of a system over distances far greater than the normal range.

The prediction of the basic transmission loss occurring during periods of ducting and layer reflection is based on the equation

$$L_{ba} = A_f + A_d(p) + A_g, \tag{5.21}$$

in which

- A_f is the total of fixed coupling losses between the antennas and the anomalous propagation structure

$$A_f = 102.45 + 20\log(f) + 20\log(d_{lt} + d_{lr}) + A_{lf} + A_{st} + A_{sr} + A_{ct} + A_{cr}, \tag{5.22}$$

- A_{lf} is the correction to account for the increasing attenuation with wavelength inducted propagation (dB)

$$A_{lf}(f) = \begin{cases} 45.375 - 137f + 92.5f^2 & if < 0.5GHz \\ 0 & otherwise, \end{cases} \tag{5.23}$$

- $A_{st,sr}$, A_{sr} are the site-shielding diffraction losses for the interfering and interfered-with stations

$$A_{st,sr} = \begin{cases} 20\log[1 + 0.361{\theta_{t,r}}''(f d_{lt,lr})^{1/2}] + 0.264{\theta_{t,r}}'' f^{1/3} & for {\theta_{t,r}}'' > 0 \quad mrad \\ 0 & for {\theta_{t,r}}'' \leqslant 0, \end{cases} \tag{5.24}$$

in which

$${\theta_{t,r}}'' = \theta_{t,r} - 0.1 d_{lt,lr} \quad mrad, \tag{5.25}$$

-A_{ct}, A_{cr} are the over-sea surface duct coupling corrections for the interfering and interfered-with stations

$$A_{ct,cr} = \begin{cases} 3e^{-0.25d_{ct,cr}^2}[1 + tanh(0.07(50 - h_{ts,rs}))] & for \quad \omega \geqslant 0.75, \quad d_{ct,cr} \leqslant d_{lt,lr}, \quad d_{ct,cr} \leq 5km \\ 0 & otherwise, \end{cases} \tag{5.26}$$

and $A_d(p)$ is the time percentage and angular-distance dependent losses in dB

$$A_d(p) = \gamma_d \theta' + A(p), \tag{5.27}$$

.

In the Eq. 5.27, it's main parameters are defined as

- γ_d: specific attenuation in dB/mrad

$$\gamma_d : 5 \times 10^{-5} a_e f^{1/3}, \tag{5.28}$$

- θ': angular distance to allow for the application of the site shielding model

$$\theta' = \frac{10^3 d}{a_e} + \theta'_t + \theta'_r, \tag{5.29}$$

$$\theta'_{t,r} = \begin{cases} \theta_{t,r} & for \quad \theta_{t,r} \leq 0.1 d_{lt,lr} \quad mrad \\ 0.1 d_{lt,lr} & for \quad \theta_{t,r} > 0.1 d_{lt,lr} \quad mrad, \end{cases} \tag{5.30}$$

- A_p: time percentage variability (cumulative distribution) in dB

$$A_p = -12 + (1.2 + 3.7 \times 10^{-3} d) \log(\frac{p_t}{\beta}) + 12(\frac{p_t}{\beta})^{\Gamma}, \tag{5.31}$$

in which

$$\Gamma = \frac{1.076}{(2.0058 - log\beta)^{1.012}} \times e^{-(9.51 - 4.8 log\beta + 0.198(log\beta)^2) \times 10^{-6} d^{1.13}}, \tag{5.32}$$

$$\beta = \beta_0 \mu_2 \mu_3 \quad \%, \tag{5.33}$$

- μ_2: correction for path geometry

$$\mu_2 = [\frac{500}{a_e} \frac{d^2}{(\sqrt{h_{te}} + \sqrt{h_{re}})^2}]^{\alpha}, \tag{5.34}$$

- μ_3: correction for terrain roughness

$$\mu_3 = \begin{cases} 1 & for \quad h_m \leq 10m \\ exp[-4.6 \times 10^{-5}(h_m - 10)(43 + 6d_I)] & for \quad h_m > 10m, \end{cases} \tag{5.35}$$

in which the value of α should not exceed 1

$$\alpha = -0.6 - \varepsilon \times 10^{-9} d^{3.1} \tau, \tag{5.36}$$

and $\varepsilon = 3.5$, τ shall not be allowed to reduce below –3.4

$$\tau = [1 - e^{-(4.12 \times 10^{-4} d_{lm}^{2.41})}]. \tag{5.37}$$

5.1.3.1 Ducting/layer reflection implementation results

Using parameters of Table 5.1, the attenuation values for the ducting/layer reflection propagation varying the frequency from 5GHz to 40GHz and the distance from 0 Km to 100 Km is illustrated in the Figure 5.9.

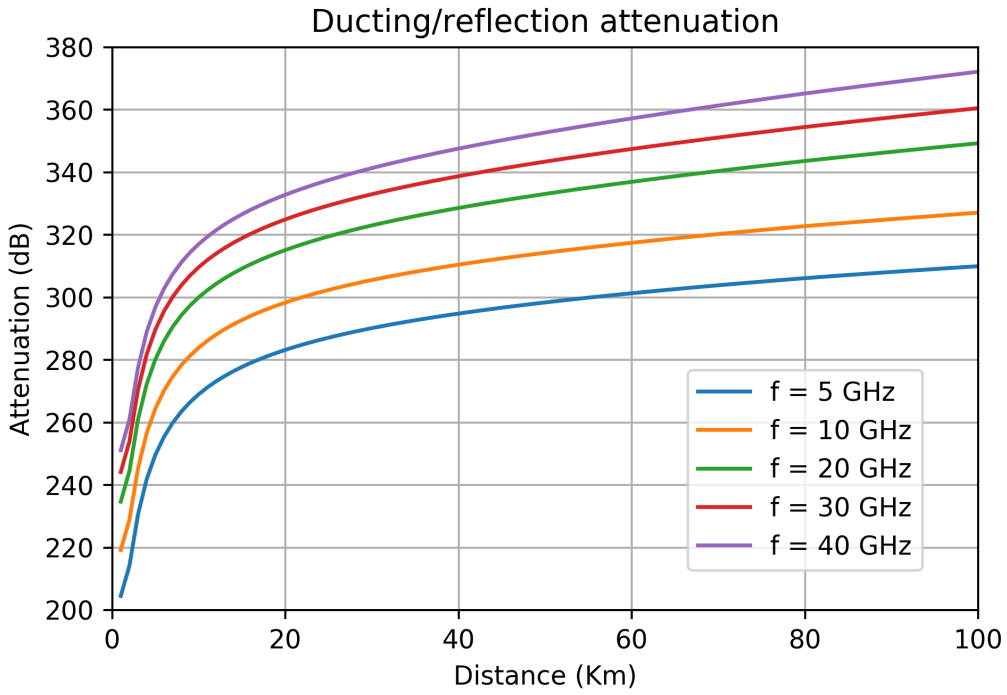

Figure 5.9: Ducting/layer reflection attenuation.

Although the attenuation rate should theoretically become smaller at higher frequencies for a uniform duct, Figure 5.9 shows the opposite. In fact, horizontal inhomogeneities and small scale scatter begin to be important at microwave frequencies. [37]

5.1.4 Diffraction

The diffraction loss is calculated by the combination of a method based on the Bullington construction and spherical-Earth diffraction.

The basic transmission loss associated with diffraction not exceeded for $p_t\%$ time is given by

$$L_{bd} = L_{b0p} + L_{dp}, \tag{5.38}$$

in which L_{b0p} is given by Eq. 5.13 and the diffraction loss, L_{dp} in dB is given by $L_d = L_{d50}$ if p = 50% or is given by

$$L_{dp} = L_{d50} + F_i(L_{d\beta} - L_{d50}). \tag{5.39}$$

The definitions of F_i, L_{d50} and L_d are complex and fully available in session 4.2 of the Recommendation ITU-R P.452.

5.1.4.1 Diffraction attenuation results

Diffraction attenuation has its results presented in this section. It's final implementation varying the frequency from 5GHz to 50GHz and the distance from 0 Km to 100 Km is presented in the Figure 5.10.

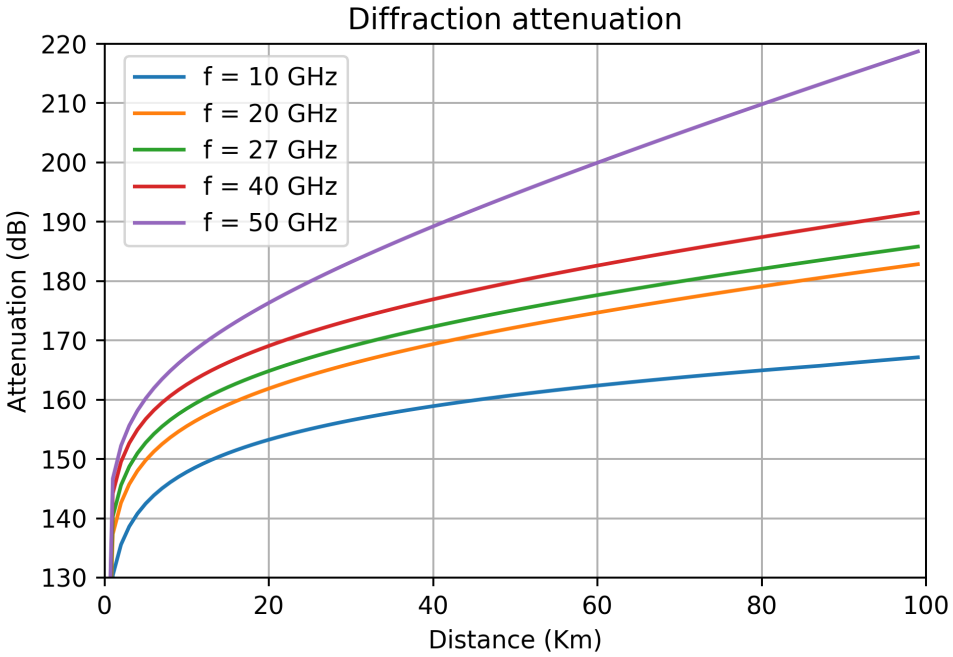

Figure 5.10: Diffraction attenuation.

As it is expected, the attenuation by diffraction increases with the increase of frequency and distance. It is interesting to observe the comportment of the 50GHz curve since its curve is very steep for great distances, showing until 30 dB of difference from its closest curve (40 GHz) .

5.1.5 Additional Clutter loss

The clutter correction in section 4.5 of Recommendation ITU-R P.452 should not be used for the TG 5/1 interference analyses, as it assumes specific knowledge of the location of the transmitter, receiver and nearby obstacles. Instead, the method of the draft new Recommendation ITU-R P.[CLUTTER] [38] should be used to calculate additional loss due to clutter. Additional loss due to building entry loss should also be calculated, using the draft new recommendation ITU-R P.[BEL] - Prediction of Building Entry Loss.

The draft new recommendation ITU-R P.[CLUTTER] describes two scenarios that are possible to be used by the TG 5/1 interference analyses. The itens 3.2 and 3.3 describes statistical models from 2 -100 GHz for different scenarios.

Table 5.2: Summary of possible scenarios

Terminal environment	**Ref.**	**Frequency range (GHz)**	**Description**
Terrestrial terminal within the clutter	§ 3.2	2 – 67	A statistical model which can be applied for modelling the clutter loss distribution for urban and suburban environments. This correction may be applied to both ends of the path.
One terminal is within the clutter and the other is a satellite, aeroplane or other platform above the surface of the Earth.	§ 3.3	10 – 100	A statistical distribution of clutter loss not exceeded for percentage locations for angles of elevation between 0 and 90 degrees.

Ref 3.2 - Statistical clutter loss model for terrestrial paths:

The clutter loss not exceeded for p% of locations for the terrestrial to terrestrial path, L_{ctt}, in dB is given by

$$L_{ctt} = -5log(10^{-0.2l_t} + 10^{-0.2l_s}) - 6Q^{-1}(p/100), \tag{5.40}$$

in which $Q^{-1}(x)$ is the inverse complementary normal distribution function, L_t is defined as

$$L_t = 23.5 + 9.6log(f), \tag{5.41}$$

and L_t is written as

$$L_s = 32.98 + 23.9log(d) + 3log(f). \tag{5.42}$$

After the scenario implementation, the median clutter loss at each frequency with respect to the distance between the transmitter and receiver varying the frequency from 2Hz to 67GHz and the distance from 0.2 Km to 100 Km is illustrated in the Figure 5.11.

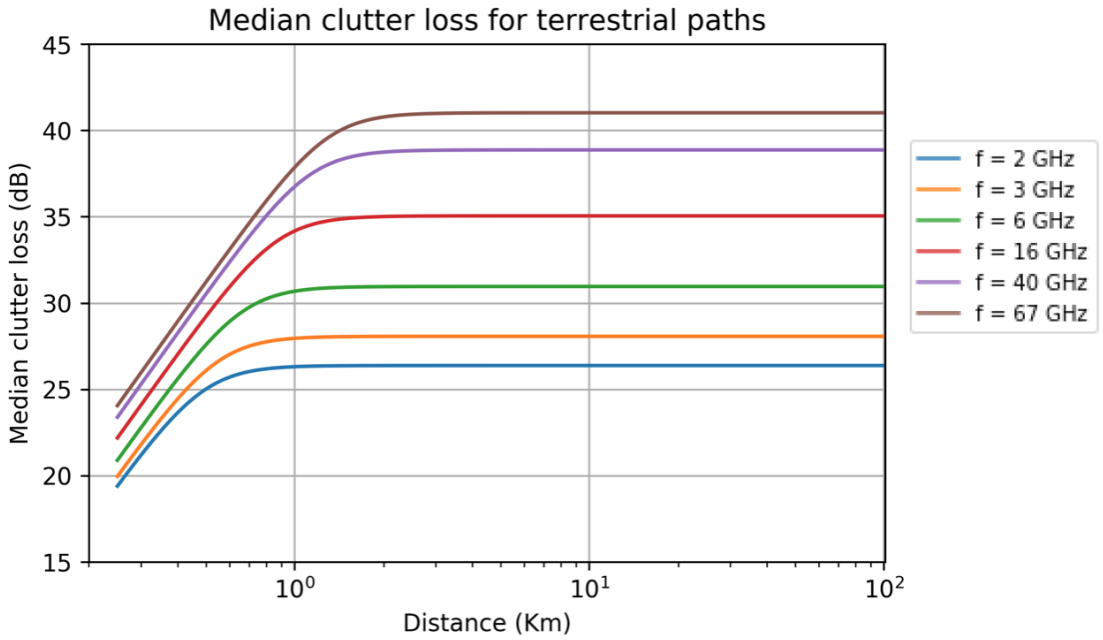

Figure 5.11: Median clutter loss for terrestrial paths.

The calculation example is assumed for clutter loss between terrestrial stations. It is clear that in a short distance, the clutter losses decrease because the incident angle for the obstructing buildings becomes small. As the distance becomes longer, the incident angle can be considered constant, so the clutter losses are also a fixed value.

Ref 3.3 - Earth-space and Aeronautical statistical clutter loss model:

The equations bellow are used to calculate the statistical distribution of clutter loss where one end of the interference path is within man-made clutter, and the other is a satellite, aeroplane, or other platform above the surface of the Earth.

The clutter loss not exceeded for p% of locations L_{ces} for the terrestrial to airborne or satellite path is given in dB by

$$L_{ces} = [-K_1[ln(1 - \frac{p}{100})]cot[A_1(1 - \frac{\theta}{90}) + \frac{\pi\theta}{180}]]^{[0.5(90-\theta)/90]} - 1 - 0.6Q^{-1}(p/100), \quad (5.43)$$

in which

$$K_1 = 93(f^{0.175}), A_1 = 0.05. \quad (5.44)$$

After implementation, the cumulative distribution of clutter loss curves for percentage locations at varying elevation angles for 30 GHz illustrated in the Figure 5.12.

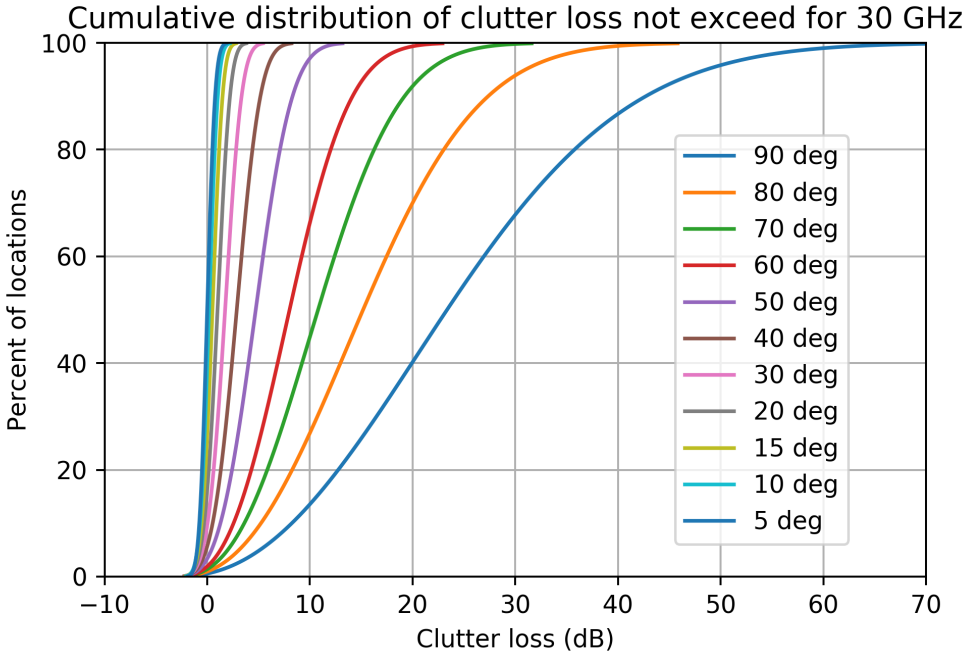

Figure 5.12: Cumulative distribution of clutter loss.

Building entry loss:

Building entry loss will vary depending on building type, location within the building and movement in the building.The building entry loss not exceeded for the probability, P, is given by

$$L_{BEL}(P) = 10log(10^{0.1A(P)} + 10^{0.1B(P)} + 10^{0.1C}), \quad (5.45)$$

in which

$$A(P) = F^{-1}(P)\sigma_1 + \mu_1, \quad (5.46)$$

$$A(P) = F^{-1}(P)\sigma_2 + \mu_2, \tag{5.47}$$

and $C = -3.0$, $\mu_1 = L_h + L_e$, $\mu_2 = w + xlog(f)$, $\sigma_1 = u + vlog(f)$, $\sigma_2 = y + zlog(f)$.

The values of the variables L_h and L_e are given by

$$L_h = r + slog(f) + tlog(f)^2. \tag{5.48}$$

The coefficients r to z are well known for each building type and are described in the recommendation "DRAFT NEW RECOMMENDATION ITU-R P.[BEL]" [39].

The Figure 5.13 shows the Median building entry loss for two different building classes.

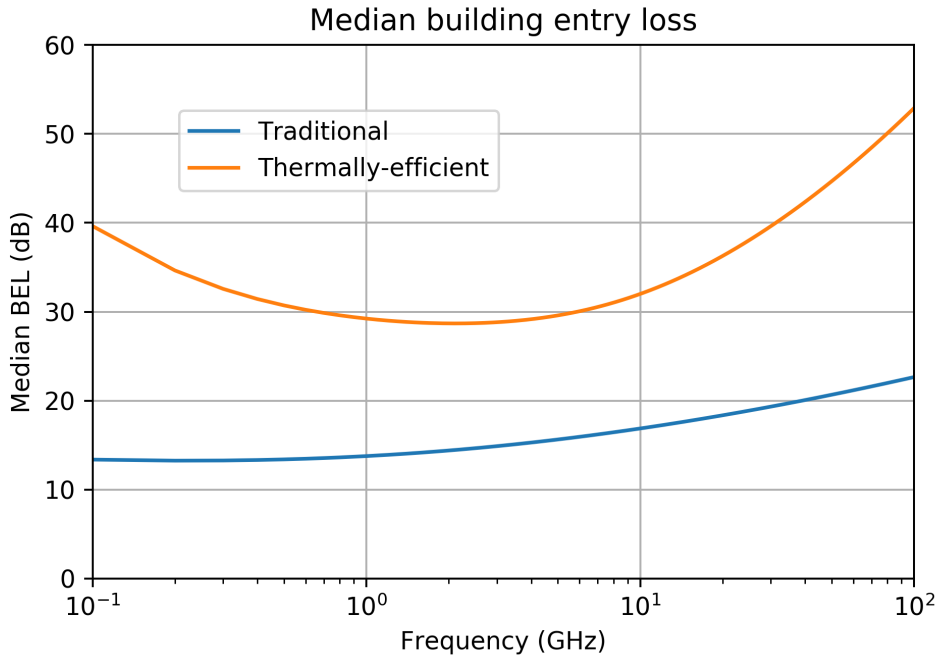

Figure 5.13: Median building entry loss.

5.1.6 Overall prediction

The method described in 5.2.1 to 5.2.5 provides the basic transmission loss between the two stations. In order to calculate the overall prediction due to the combination of the losses, we have to calculate the final basic transmission loss not exceed for $p_t\%$ time, named L_b (dB) and given by

$$L_b = -5log(10^{-0.2L_{bs}} + 10^{-0.2L_{bam}}) + A_{ht} + A_{hr}, \tag{5.49}$$

in which

- L_{bam} is a modified basic transmission loss which takes in account diffraction and LoS or ducting/layer-reflection enhancements, given by

$$L_{bam} = L_{bda} + (L_{minb0p} - L_{bda})F_j, \tag{5.50}$$

- L_{bda} is a notional basic transmission loss, associated with diffraction and LoS or ducting/layer-reflection enhancements, given by

$$L_{bda} = \begin{cases} L_{bd} & for \quad L_{minbap} > L_{bd} \\ L_{minbap} + (L_{bd} - L_{minbap})F_k & for \quad L_{minbap}L \leq_{bd}, \end{cases} \tag{5.51}$$

- L_{minbap} is a notional minimum basic transmission loss associated with LoS and transhorizon signal enhancements given by

$$L_{minbap} = \eta \ln(\exp(\frac{L_{ba}}{\eta}) + \exp(\frac{L_{b0p}}{\eta})), \tag{5.52}$$

- L_{minb0p} is a notional minimum basic transmission loss associated with LoS propagation and over-sea sub-path diffraction given by

$$L_{minb0p} = \begin{cases} L_{b0p} + (1-\omega)L_{dp} & for \quad p_t < \beta_0 \\ L_{bd50} + (L_{b0\beta} + (1-\omega)L_{dp} - L_{bd50})F_i & for \quad p_t \geq \beta_0, \end{cases} \tag{5.53}$$

and F_j and F_k are interpolation factors that takes into account the path angular distance and the great circle path distance, described as

$$F_j = 1.0 - 0.5(1.0 + tanh(3.0\xi\frac{(S_{tim} - S_{tr})}{\Theta})), \tag{5.54}$$

$$F_j = 1.0 - 0.5(1.0 + tanh(3.0\kappa\frac{(d - d_{sw})}{d_{sw}}), \tag{5.55}$$

and A_{ht}, A_{hr} are additional losses to account for clutter shielding the transmitter and receiver.

To calculate the overall prediction based in the propagations calculate in the previous sections, we are going to use the follow results

- $Lb0p$ is the notional LoS basic transmission loss not exceeded for p% time, given by Eq. 2.43;

- $Lb0\beta$ is the notional LoS basic transmission loss not exceeded for β% time, given by Eq. 2.44;

-L_{dp} is the diffraction loss not exceeded for p_t% time, calculated using Eq. 2.69;

-L_{ba} is the ducting/layer reflection basic transmission loss not exceeded for p_t% time, calculated using Eq. 2.51;

-L_{bd} is the basic transmission loss for diffraction not exceeded for p% time, calculated using Eq. 2.68;

Finally, the overall prediction calculated varying the frequency from 10GHz to 50GHz and the distance from 0 Km to 100 Km is illustrated in the Figure 5.14.

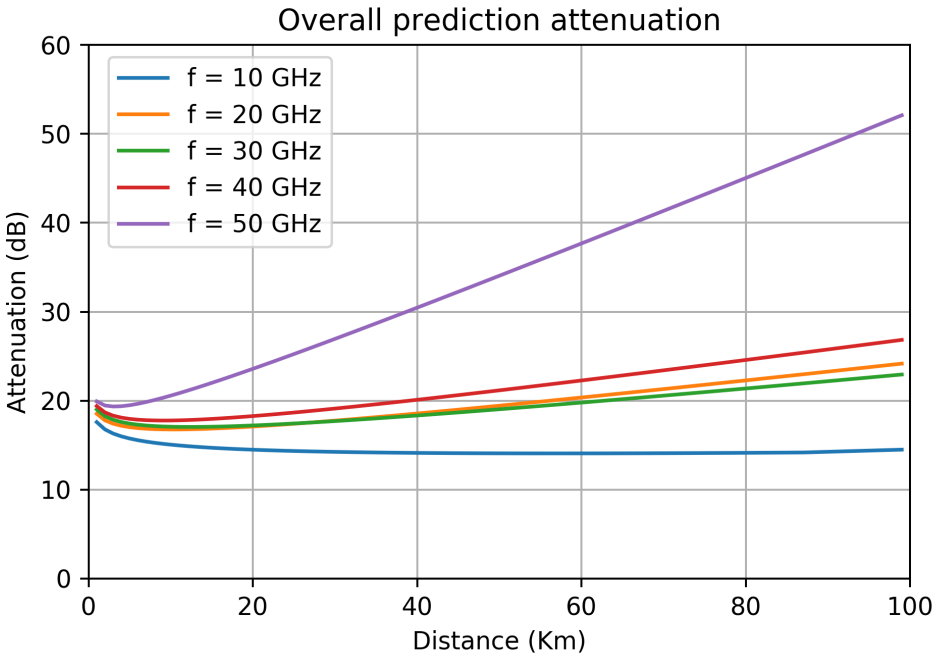

Figure 5.14: Overall prediction attenuation.

5.2 PATH LOSS MODELS

The 3GPP TR 38.900 v14.2.0 document named "Technical Specification Group Radio Access Network; Study on channel model for frequency spectrum above 6 GHz" is a technical report produced by the 3rd Generation Partnership Project that has the propose of properly model and evaluate the performance of physical layer techniques using the above-6GHz channel model(s).

Two of the most important supported scenarios are the urban microcell street canyon and the urban macrocell.

In general, a macrocell is a cell in a mobile phone network that provides radio coverage served by a high power cell site and a microcell is a cell served by a low power cellular base station, covering a limited area such as a mall, a hotel, or a transportation hub. The Figure 5.15 illustrate this scenarios.

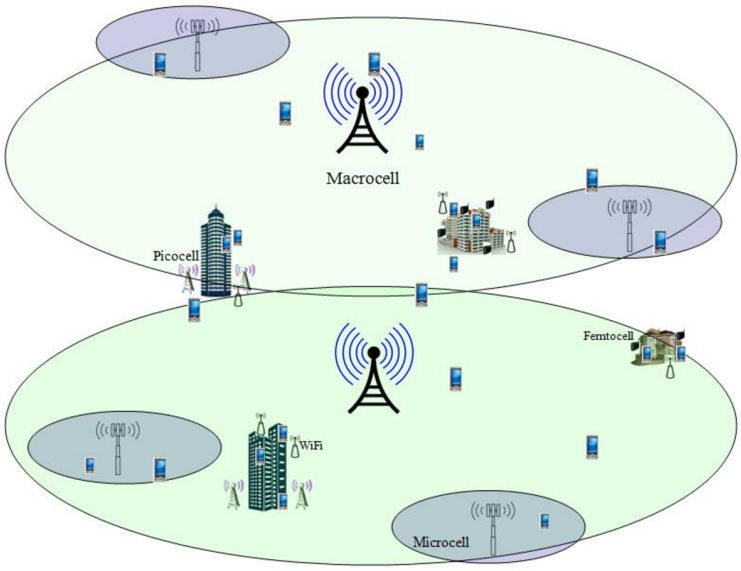

Figure 5.15: Macro and microcells scenarios [40].

Generally, macrocells provide larger coverage than microcell. The antennas for macrocells are mounted on ground-based masts, rooftops and other existing structures, at a height that provides a clear view over the surrounding buildings and terrain. Macrocell base stations have power outputs of typically tens of watts while microcell uses power control to limit the radius of its coverage area.

Typically the range of a microcell is less than two kilometers wide, whereas standard base stations may have ranges of up to 35 kilometres. In general, microcellls are used by mobile carriers to either offload traffic from the macro network in a high density short range environment or to strengthen the range and efficiency of a mobile network.

The next two sections will show how some pathloss models were implemented using the scheme from the Figure 5.16.

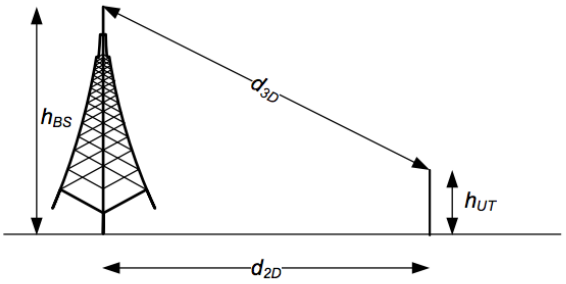

Figure 5.16: Schema and variable definitions [40].

5.2.1 Urban Macro pathloss model

The urban macrocell pathloss model is described in the technical report 3GPP TR 38.900 [40] as two different blocks of equations depending on the existence or not of line-of-sight. In this way, the first step is to calculate the line-of-sight (LOS) probability of the scenario.

$$P_{LOS} = \begin{cases} 1 & d_{2D} < 18m \\ [\frac{18}{d_{2D}} + \exp(\frac{-d_{2D}}{63})(1 - \frac{18}{d_{2D}})](1 + C'(h_{UT})\frac{5}{4}(\frac{d_{2D}}{100})^3 \exp(\frac{-d_{2D}}{150})) & 18 < d_{2D}, \end{cases} \tag{5.56}$$

in which

$$C'(h_{UT}) = \begin{cases} 0 & h_{UT} \leq 13m \\ (\frac{h_{UT}-13}{10})^{1.5} & 13 < h_{UT} \leq 23m. \end{cases} \tag{5.57}$$

Then, the pathloss for a LOS scenario can be modeleted as

$$PL_{UMa-LOS} = \begin{cases} PL_1 & 10m \leq d_{2D} < d'_{BP} \\ PL_2 & d'_{BP} \leq d_{2D} < 5Km, \end{cases} \tag{5.58}$$

in which PL_1 and PL_2 are given by

$$PL_1 = 32.4 + 20log_{10}(d_{3D}) + 20log_{10}(f_c), \tag{5.59}$$

$$PL_2 = 32.4 + 40log_{10}(d_{3D}) + 20log_{10}(f_c) - 10log_{10}((d'_{BP})^2 + (h_{BS} - h_{UT})^2), \tag{5.60}$$

with a shadowing factor (σ_{SF}) of 4.

For a NLOS scenario, the pathloss is calculated as

$$PL_{UMa-NLOS} = max(PL_{UMa-LOS}, PL_{UMa-NLOS}) \qquad for \;\; 10m \leq d_{2D} < 5Km, \quad (5.61)$$

in which

$$PL_{UMa-LOS} = 13.54 + 39.08log_{10}(d_{3D}) + 20log_{10}(f_c) - 0.6(h_{UT-1.5}), \quad (5.62)$$

with a shadowing factor (σ_{SF}) of 6.

The Urban Macro model was here implemented using the shadowing factor as a normal (Gaussian) distribution with σ_{SF} as standard deviation.

The Figures 5.17 and 5.18 shows the urban macro LOS probability versus distance and the urban macro path loss versus distance for the frequency of 27 GHz.

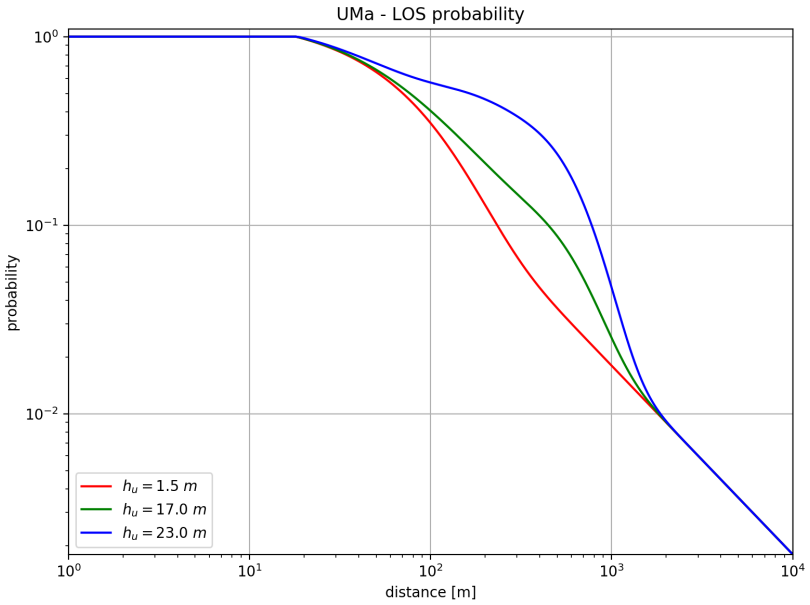

Figure 5.17: Urban macro LOS probability.

It's possible to observe, from the above curves, that the distance has a great importance in the path loss as well as the type of simulated environment. The NLOS scenario is the most aggressive and the free loss scenario the softest, as expected. It is interesting to observe the LOS probability curves as it depends on the UT height.

5.2.2 Urban Micro pathloss model

Then, the Urban Micro (Street Canyon) path loss model is presented. As the Urban macro scenario, we start by calculating the LOS probability given by

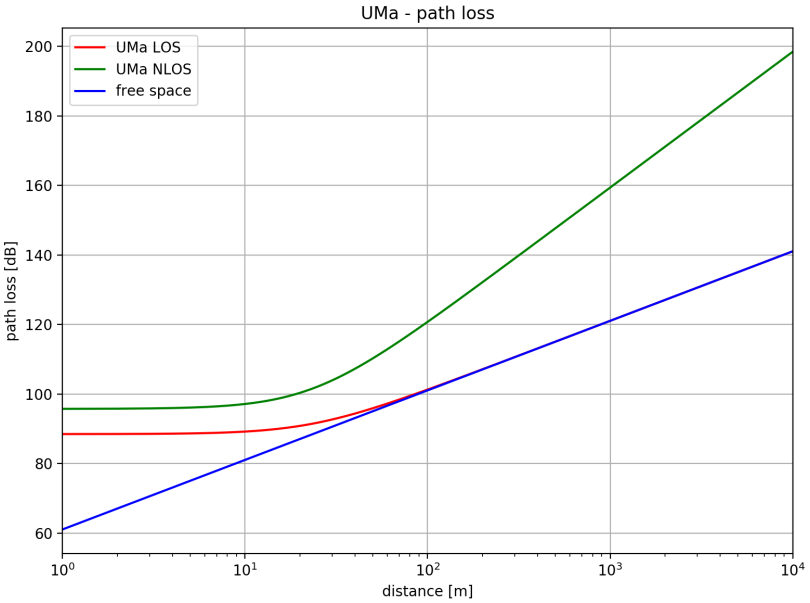

Figure 5.18: Urban macro path loss.

$$P_{LOS} = \begin{cases} 1 & d_{2D} < 18m \\ \frac{18}{d_{2D}} + \exp(\frac{-d_{2D}}{63})(1 - \frac{18}{d_{2D}}) & 18 < d_{2D}. \end{cases} \tag{5.63}$$

The pathloss for a LOS scenario is given by

$$PL_{UMi-LOS} = \begin{cases} PL_1 & 10m \leq d_{2D} < d'_{BP} \\ PL_2 & d'_{BP} \leq d_{2D} < 5Km, \end{cases} \tag{5.64}$$

in which PL_1 and PL_2 are given by

$$PL_1 = 32.4 + 21log_{10}(d_{3D}) + 20log_{10}(f_c), \tag{5.65}$$

$$PL_2 = 32.4 + 40log_{10}(d_{3D}) + 20log_{10}(f_c) - 9.5log_{10}((d'_{BP})^2 + (h_{BS} - h_{UT})^2), \tag{5.66}$$

with a shadowing factor (σ_{SF}) of 4.

For a NLOS scenario, the pathloss is calculated as

$$PL_{UMi-NLOS} = max(PL_{UMi-LOS}, PL_{UMi-NLOS}) \qquad for \;\; 10m \leq d_{2D} < 5Km, \tag{5.67}$$

in which

$$PL_{UMa-LOS} = 22.4 + 35.3log_{10}(d_{3D}) + 21.3log_{10}(f_c) - 0.3(h_{UT-1.5}), \tag{5.68}$$

with a shadowing factor (σ_{SF}) of 7.82.

This time, the UMi LOS probability and the UMi pathloss values using the frequency of 27 GHz were calculated and are show in Figures 5.19 and 5.20.

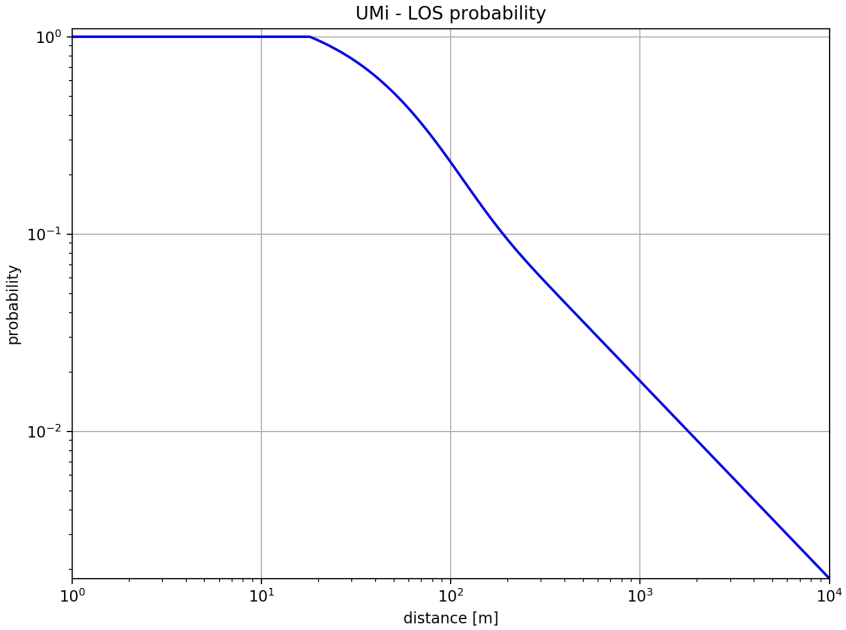

Figure 5.19: Urban micro LOS probability.

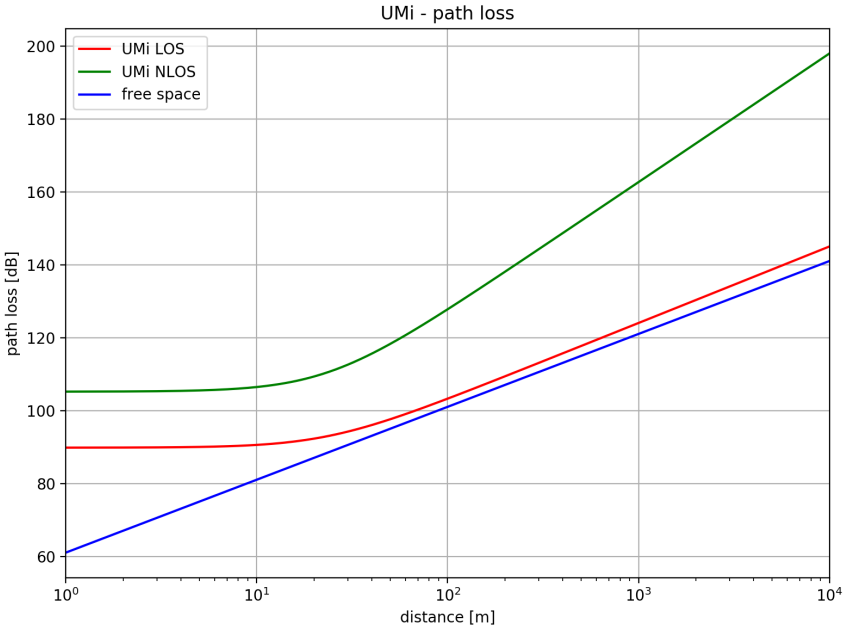

Figure 5.20: Urban micro path loss.

The curves indicates higher pathloss values for the micro urban area both in LOS and NLOS situations, what is expected. As the LOS probability no longer depends on the UT high but only on distance, the Figure 5.19 shows only one curve that decreases with distance, since several meters away from the transmitter the probability of LOS is practically zero.

5.2.3 ABG path loss models

The ABG path loss model is a generic all frequency model that describe large-scale propagation pathloss at all relevant frequencies in a certain scenario. In this model, there are three optimization parameters which need to be set in order to minimize the standard deviation (SF) over the data set.

Each group of parameters define a different scenario, as is show in the Table 8. This is a very flexible path loss model that can model different situation only by changing its parameters

Table 5.3: ABG model parameters for different scenarios.

Scenario	**ABG Model Parameters**
UMa- nLoS	α=3.4, β =19.2, γ=2.3, SF = 6.5 dB
UMi-Street Canyon-nLoS	α=3.48, β =21.02, γ=2.34, SF = 7.8 dB
UMi-Open Square-nLoS	α=4.14, β=3.66, γ=2.43, SF = 7.0 dB
InH-Indoor-nLoS single slope (FFS)	α=3.83, β=17.30, γ=2.49, SF = 8.03 dB
InH-Shopping Malls-nLoS single slope (FFS)	α=3.21, β=18.09, γ=2.24, SF = 6.97 dB

In this context, the path loss equation for the ABG model is given by

$$PL^{ABG}(f,d) = 10\alpha \log_{10}(d) + \beta + 10\gamma \log_{10}(f) + X_{\sigma}^{ABG}, \tag{5.69}$$

in which α captures how the PL increase as the transmit-receive in distance (in meters) increases, β is a floating offset value in dB, γ captures the PL variation over the frequency f in GHz, and X_{σ}^{ABG} is the SF term in dB.

The interesting of this model in the context of the SHARC simulator, besides the flexibility of the model, is that it was the path loss model utilized in the document " Example implementations of the methodology contained in recommendation ITU-R M.2101" made by Intel Corporation, Telefon AB-LM Ericsson, Nokia Corporation and Samsung Electronics in June 2017. It is important to add this model to the group of available path loss models.

The Figure 5.21 shows the curves for the UMa NLOS, UMi Street Canyon NLOS and free space scenarios using the frequency of 27 GHz.

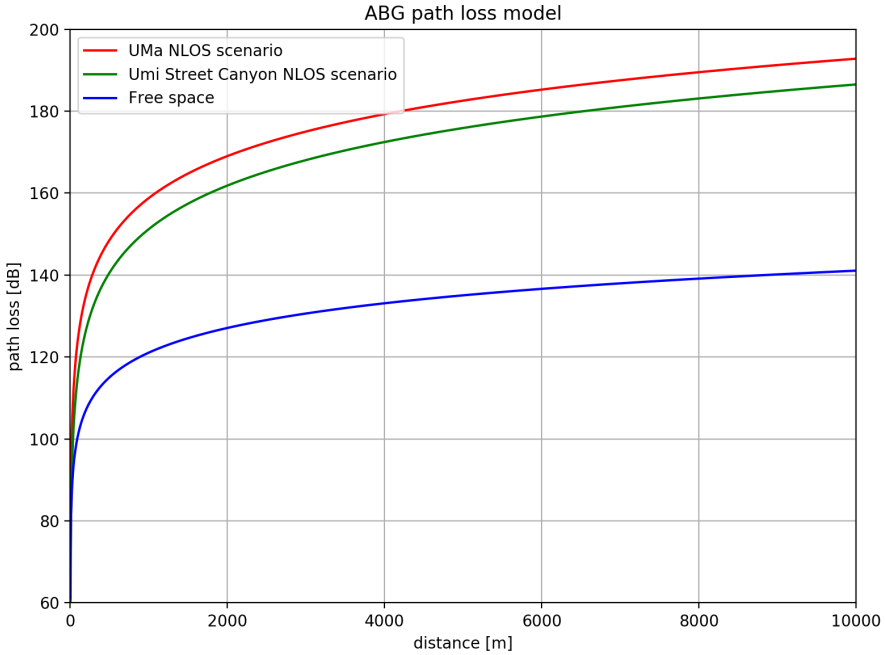

Figure 5.21: ABG path loss model.

The curves corroborate the result of the section 5.3 in relation to the values obtained for the path loss and position of the curves for micro and macro urban loss, validating the ABG model.

5.3 SHARING AND COMPATIBILITY STUDIES BETWEEN 5G AND OTHER RADIO-COMMUNICATION SYSTEMS

The main objective in developing the SHARC simulator is the realization of sharing and compatibility studies between the future 5G networks and the current systems already implemented for the identification of frequency bands for the 5G in Brazil. At the time of delivery of this report, the simulator had its main modules developed and a first study had been carried out. This study was made in the format of an article and was accepted in the SBMO/IEEE MTT-S International Microwave and Optoelectronics Conference(IMOC 2017).

In this study, the considered deployment scenario is micro urban, with an outdoor small area coverage in a heterogeneous network, which means that small hotspots are uniformly distributed in a macro-cell network, as shown in Figure 5.22. The macro-cell BSs operate in current mobile communications bands, while the hotspots operate in the 5G band. Furthermore, hotspot BSs have elevation angles of -10 and azimuth angles of either 0, 90, 180 and 270, chosen with equal probability.

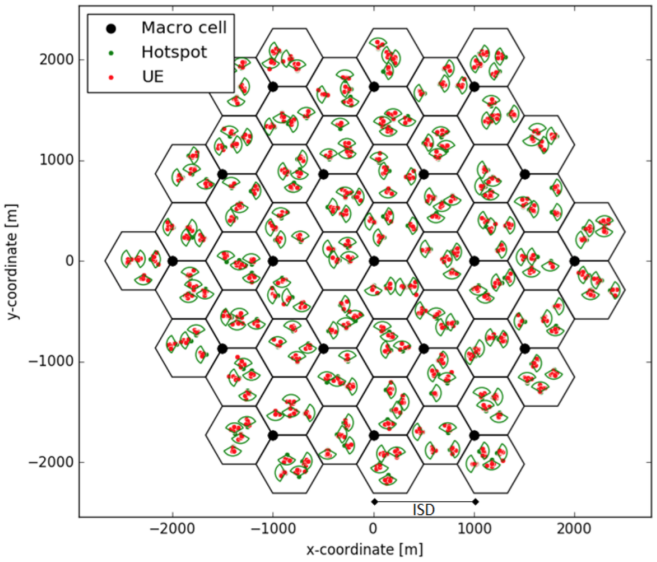

Figure 5.22: Deployment scenario of 5G network.

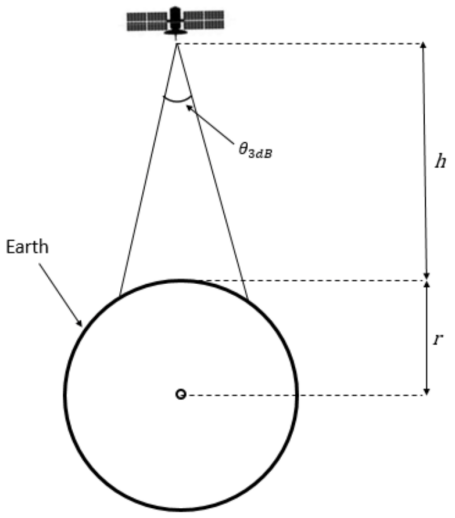

Figure 5.23: Geometry for the aggregate interference analysis.

The user equipment devices (UEs) are distributed within the hotspot coverage area, with a Rayleigh distribution and are considered to have two antenna panels on opposite sides of the device.

The simulation scenario that is used in this sharing study is between 5G systems and fixed satellite service, both operating in the 27-27.5 GHz frequency range. The evaluation of the aggregated interference generated by 5G hotspots is focused on a geostationary satellite, assuming that hotspots are deployed in a relatively large area. Figure 5.23 illustrates the geometry for the aggregate interference analysis

In this scenario, coupling loss (CL) of the k-th link is defined as

$$CL_k = PL_k - G_{tx} - G_{rx}, \tag{5.70}$$

in which CL_k is the path coupling loss, PL_k is the path loss between stations and G_{tx} and G_{rx} are the transmission and reception antenna gains, respectively. For path coupling loss between hotspots and UE's, path loss is calculated using the Urban Micro propagation model described in section 5.3.1 of this report and the beamforming model developed. In the SHARC simulations, every station creates a beam pointed towards all the stations to which it is connected. Besides the use of beamforming, it was developed a power control mechanism in order to equally allocate the resource blocks between active stations, so that the available band is evenly divided among them.

The most important metric in this coexistence study in the protection criteria of the satellite. The protection criteria of a satellite must be met in order to protect the satellite service from harmful interference. This criteria is defined as a function of the interference-to-noise ratio (I/N) and its value must be below a certain threshold. The ratio I/N is calculated as follows

$$\frac{I}{N} = \frac{I_{aggr}}{N_{floor}}, \tag{5.71}$$

in which I_{aggr} is the total aggregated interference from 5G systems that depends on the transmit power of a 5G station and on the coupling loss of the k-th interfering link (CL_k) and N_{floor} is the satellite's noise floor. In this study, the path loss between 5G devices and satellite is given by the well known free space model with additional 1 dB loss to account for atmospheric loss, 3 dB for polarization loss and clutter loss modeled in the section 5.2.5 of this report.

In order to calculate the aggregate interference from several 5G devices into the geostationary satellite, it is necessary to setup a simulation with a very large amount of stations and this requires high computational capabilities. Instead, we model a representatively large segment of the 5G network, collect the statistics of this segment and then calculate the aggregated interference generated by multiple segments that have similar characteristics.

A simulation result is shown in Figure 5.24, where we can analyze the cumulative distribution of antenna gains of 5G stations for different satellite elevation angles. All stations use beamforming to achieve higher antenna gains in the their respective link direction and lower gains in other directions. Assuming the simulation scenario, it can be seen that the gains of 5G stations towards satellite increase as the satellite elevation angle decreases. Hence, 5G user equipments would potentially generate more interference into lower elevation angle satellites. In general, the gains of the base stations (indicated as 'DL' in the figure) are lower than the ones of the user equipments (indicated as 'DL' in the figure) mainly due to the fact that antennas at base stations are downtilted and have more elements, which provides higher attenuation in sidelobes.

In Figure 5.25 it is possible to analyze the combined effect of clutter losses and antenna gains of 5G stations into the aggregate interference at the satellite. The figure shows the CDF of interference-to-noise ratio (I/N) at the satellite. Regarding the user equipments, I/N is lower when elevation angles are higher mainly due to the lower user equipment antenna gains towards the satellite. In low elevation angles, clutter losses attenuate interference at the satellite. Actually, the worst scenario (higher I/N values) is found for inter- mediate elevation angles, when clutter losses do not serve as a counterbalance to the higher UE antenna gains. Anyway, the achieved I/N values are much lower than the -12.2 dB protection criteria of the satellite. For the case of interfering base stations, interference would be even higher than the one generated by user equipments, but I/N would be still lower than protection criteria.

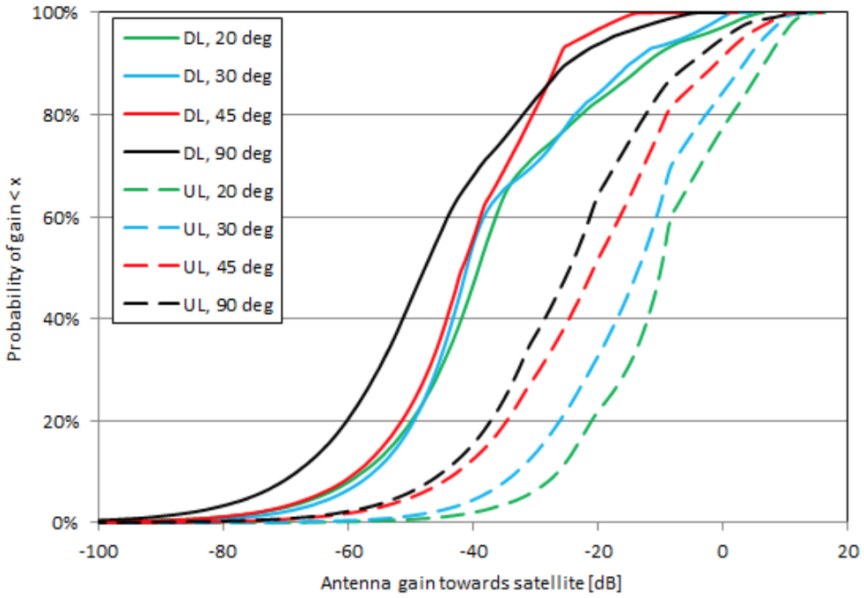

Figure 5.24: CDF of UE antenna gains towards satellite for different satellite elevation angles.

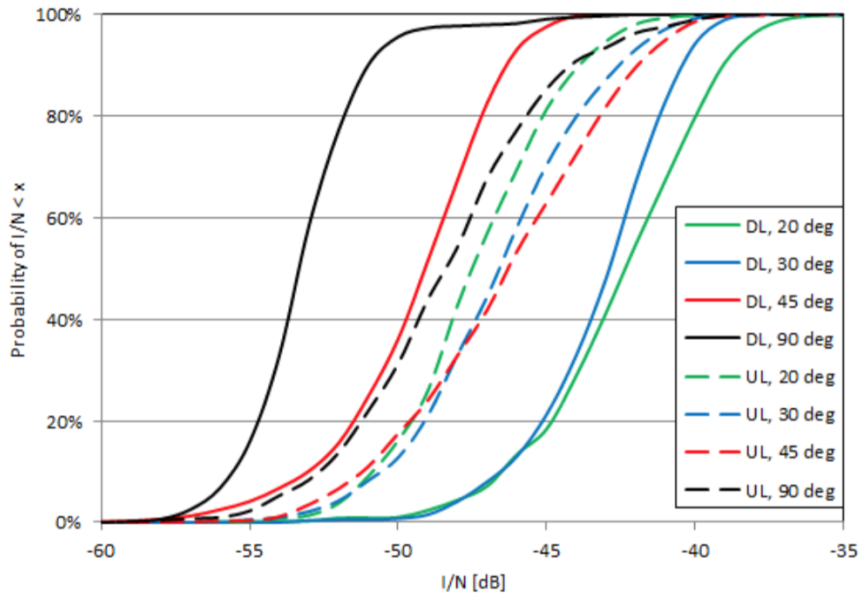

Figure 5.25: CDF of INR at the satellite for different satellite elevation angles.

Simulation outputs indicate that satellite's protection criteria is met for the modelled network with a large safety margin when using the 5G deployment parameters proposed in TG 5/1.

Complete information about this study like used parameters and some others definitions are found in the article "An Open Source Simulation Tool for Sharing and Compatibility Studies between 5G and Other Radiocommunication Systems" [41].

5.4 CONCLUSION

This section presented the open-source simulation tool called SHARC. It is designed by the University of Brasília and by the Brazilian National Telecommunications Agency (ANATEL) to support sharing and coexistence studies between 5G and other radiocommunication systems in the context of Agenda Item 1.13 of WRC-19, which considers identification of frequency bands for the future development of IMT. Throughout the internship period, it was developed propagation mechanisms for terrestrial communications and path loss models for use in the simulator.

Then, a preliminary study was presented, where a geostationary satellite was subject to aggregated interference generated by 5G systems. Based on this first study, we aimed to carry out several other studies with other services and in other frequency bands to continue the identification of frequency bands for 5G.

6 CONCLUSION AND FUTURE PERSPECTIVES

The work presented in this report describes the results of four distinct projects performed during the months of march to august 2017. In this report, it was presented different contributions to radio communication systems through modeling a realistic composite distribution that models mobile radio channels, simulating coexistence studies and designing practical tests for verifying the level of interference between systems and the quality of the signal that mobile carriers delivers to clients.

As a result, for the α-μ/Γ *generalized* distribution, it was found an excellent visual agreement and low mean error deviation between the experimental and the theoretical data, showing that the distribution is a great choice for modeling real environments that suffers from composite fading. In addition, the network quality analyzer shows the coverage map of a given region based on users measured data and can returns statistics analysis about the channel characterization and practical investigation of fading distributions, helping users to choose their network operators and helping the mobile carriers to optimize their networks and even improve signal coverage in critical areas. Regarding the LTE 700 MHz and digital TV, the results found that in the scenario of the neighborhood of Asa Norte and taking into account the urban morphology and the RF characteristics used in the test, the users will not have problems with the TV signal due to interference from the 700MHz LTE signal, allowing both technologies to coexist in adjacent frequency bands. Finally, SHARC simulator was developed and a first sharing and coexistence study was realized. The contributions of this internship allowed the calculation of the link coupling loss (CL) and consequently the calculation of the total aggregated interference from 5G systems used in the protection ratio formula. For this study, simulation outputs indicate that satellite's protection criteria is met for the modelled network with a large safety margin when using the 5G deployment parameters proposed in TG 5/1, allowing the coexistence between the IMT-2020 and the fixed satellite service in this frequency range.

Once the internship is finished, we propose some perspectives that could be implemented in the next months. First of all, for the study of coexistence between LTE cellular networks and ISDB-T in 700MHz band, it is planned to continue the practical tests at the university of Brasilia with the support of a TV broadcaster using software-defined radio (SDR), where it will be used more modern equipment for the tests. Regarding the SHARC project, once the source code has been developed, it is necessary to improve it over time with the goal of making the code more efficient and to carry out others studies of coexistence in other frequency bands and with other services. These studies will serve as a contribution to the Working Party 5D (WP 5D) and/or Task Group 5/1 regarding the identification of new

bands for IMT-2020, showing frequencies ranges where the coexistence between IMT-2020 and other services is possible. About the system of measurement and analyze of mobile networks' quality, it is expected to carry out more practical tests for the detection of errors in the mobile application, for the evaluation of the performance of the application and to store the data on the project's database. Finally, for the $\alpha - \mu/\Gamma$ Generalized composite distribution project, it is expected to continue testing the function with more field data in order to better validate the proposed function. All results will be subject of article submission in the future.

To finish, the accomplishment of this internship was a great opportunity to work with interesting projects of my area of activity enabling a direct contact with people and corporations in telecommunication systems field.

REFERENCES

1 GOLDSMITH, A. *Wireless Communications*. Cambridge University, United Kingdom: Cambridge University Press, 2005.

2 ABDI, A.; KAVEH, M. On the utility of gamma pdf in modeling shadow fading (slow fading). *IEE Vehicular Technology Conference*, vol. 49, 1999.

3 YACOUB, M. D. The α - μ distribution: A physical fading model for the stacy distribution. *IEE Transactions on Vehicular Technology*, vol. 56, p. 27 – 34, 2007.

4 STACY, E. W. A generalization of the gamma distribution. *The Annals of Mathematical Statistics*, vol. 33, p. 1187–1192, 1962.

5 PARSONS, J. D. *The Mobile Radio Propagation Channel. Second Edition.* [S.l.]: JOHN WILEY SONS, INC, 2000.

6 SAUNDERS, S. R.; ARAGÓN-ZAVALA, A. A. *Antennas and Propagation for Wireless Communication Systems*. [S.l.]: Wiley, 2007.

7 NEGUS, K.; STEPHENS, A.; LANSFORD, J. Home rf: wireless networking for the connected home. *IEEE Pers. Commun. Mag*, vol. 7, p. 20 – 27, 2000.

8 SIMON, M. K.; ALOUINI, M.-S. *Digital Communication over fading channels: A Unified Approach to Performance Analysis*. [S.l.]: JOHN WILEY SONS, INC, 2000.

9 TSE, D.; VISWANATH, P. *Fundamentals of Wireless Communication*. [S.l.]: Cambridge University Press, 2005.

10 KOSTIC, I. Analytical approach to performance analysis for channel subject to shadowing and fading. *IEE Proceedings - Communications*, vol. 152, p. 821 – 827, 2005.

11 SHANKAR, M. *Fading and Shadowing in Wireless Systems*. [S.l.]: Springer, 2007.

12 ABDI, A.; TEPEDELENLIOGLU, C.; KAVEH, M.; GIANNAKIS, G. On the estimation of the k parameter for the rice fading distribution. *IEEE Communications Letters*, vol. 5, p. 92 – 94, 2001.

13 SAGIAS, N.; KARAGIANNIDIS, G. Gaussian class multivariate weibull distributions: theory and applications in fading channels. *IEEE Information Theory Society*, vol. 51, p. 3608 – 3619, 2005.

14 STEIN, S. Fading channel issues in system engineering. *IEEE J. Selected Areas in Commun*, vol. 5, p. 68 – 69, 1987.

15 YACOUB, M. D. The κ - μ distribution and the η - μ distribution. *IEEE Antennas and Propagation Magazine*, vol. 49, p. 68 – 81, 2007.

16 WOLFRAM. *Wolfram Mathematica*. 2017. Available from Internet: <https://www.wolfram.com/mathematica/>. Cited: October 14, 2017.

17 JUSTIçA, M. da. *consumidor.gov.br plataform*. 2017. Available from Internet: <https://www.consumidor.gov.br/>. Cited: October 25, 2017.

18 CONSUMIDOR.COM.GOV. Consumidor.gov.br : Balanço 2016. 03 2016.

19 EULA. *Anaconda's description*. 2017. Available from Internet: <https://anaconda.org/anaconda/anaconda-navigator>. Cited: October 14, 2017.

20 EULA. *Spyder's description*. 2017. Available from Internet: <https://anaconda.org/anaconda/spyder>. Cited: October 14, 2017.

21 AGENCY, N. telecommunications. Resolution cd/anatel nº 544. 2010.

22 AGENCY, N. telecommunications. Relatório do teste em campo sobre a convivência do lte na faixa de 700 mhz com isdb-t. 2014.

23 3GPP. *What are the spectrum band designators and bandwidths?* 2017. Available from Internet: <https://www.nasa.gov/directorates/heo/scan/communications/outreach/funfacts/txt_band_designators.html>. Cited: October 14, 2017.

24 3GPP. *LTE*. 2017. Available from Internet: <http://www.3gpp.org/technologies/keywords-acronyms/98-lte>. Cited: October 14, 2017.

25 OPENSIGNAL. *State of Mobile Networks: Brazil (January 2017)*. 2017. Available from Internet: <https://opensignal.com/reports/2017/01/brazil/state-of-the-mobile-network>. Cited: October 14, 2017.

26 WORLD, R. W. *LTE Tutorial*.

27 KITANA, A.; TRAORE, I.; WOUNGANG, I. Impact study of a mobile botnet over lte networks. 05 2016.

28 TECHINBRAZIL. *The State of 4G in Brazil*. 2017. Available from Internet: <https://techinbrazil.com/the-state-of-4g-in-brazil>. Cited: October 14, 2017.

29 TELECO. *4G may surpass 3G in Brazil in 2017*. 2017. Available from Internet: <http://www.teleco.com.br/en/en_comentario/en_com714.asp>. Cited: October 14, 2017.

30 TELECO. *Launch of Digital TV in Brazil*. 2017. Available from Internet: <http://www.teleco.com.br/en/en_tvdigital.asp>. Cited: October 14, 2017.

31 GINGA. *About Ginga*. 2017. Available from Internet: <http://www.ginga.org.br/en/sobre>. Cited: October 14, 2017.

32 IDEAON. *CelPlanner*. 2017. Available from Internet: <http://www.celplan.com.br/RepeatDetail.asp?IDMenu=3&idRepCat=3&IDRep=13>. Cited: October 14, 2017.

33 PAHL, J. *Interference Analysis: Modelling Radio Systems for Spectrum Management*. [S.l.]: John Wiley Sons, 2016.

34 ITU, C. Itu p.676: Attenuation by atmospheric gases. *ITU Recommendations*, vol. 11, 2016.

35 ITU, C. Itu p.836: Water vapour: surface density and total columnar content. *ITU Recommendations*, vol. 5, 2013.

36 ITU, C. Itu p.453: The radio refractive index: its formula and refractivity data. *ITU Recommendations*, vol. 12, 2016.

37 BARCLAY, L. *PROPAGATION OF RADIOWAVES*. [S.l.]: INSPEC/IEE, 2002.

38 ITU, C. Draft new recommendation itu-r p.[clutter]. *ITU Recommendations*, vol. 1, 2017.

39 ITU, C. "draft new recommendation itu-r p.[bel : Prediction of building entry loss. *ITU Recommendations*, vol. 1, 2017.

40 3GPP. 3rd generation partnership project; technical specification group radio access network; study on channel model for frequency spectrum above 6 ghz (release 14). *Technical Report*, vol. 14, 2016.

41 SOUZA, E.; LINHARES, A.; QUEIROZ, C.; VALLE, L.; DIAS, U.; BARRETO, A. N. An open source simulation tool for sharing and compatibility studies between 5g and other radiocommunication systems. 08 2017.